



HAL
open science

supramolecular chirality induction: toward new hybrid chiroptical nano-objects

Antoine Scalabre

► **To cite this version:**

Antoine Scalabre. supramolecular chirality induction: toward new hybrid chiroptical nano-objects. Other. Université de Bordeaux, 2019. English. NNT: 2019BORD0157 . tel-02370638

HAL Id: tel-02370638

<https://theses.hal.science/tel-02370638>

Submitted on 19 Nov 2019

HAL is a multi-disciplinary open access archive for the deposit and dissemination of scientific research documents, whether they are published or not. The documents may come from teaching and research institutions in France or abroad, or from public or private research centers.

L'archive ouverte pluridisciplinaire **HAL**, est destinée au dépôt et à la diffusion de documents scientifiques de niveau recherche, publiés ou non, émanant des établissements d'enseignement et de recherche français ou étrangers, des laboratoires publics ou privés.

PHILOSOPHIAE DOCTOR

PRESENTED IN



DOCTORAL SCHOOL OF CHEMICAL SCIENCES

BY **ANTOINE SCALABRE**

TO OBTAIN THE STATUS OF

DOCTOR

SPECIALTY: PHYSICAL-CHEMISTRY

**Supramolecular chirality induction:
Toward new hybrid chiroptical nano-objects**

**Induction de chiralité supramoléculaire :
Vers de nouveaux nano-objets chiro-optiques hybrides**

Defended on: 1st October 2019

After review of:

Mrs.	J. CRASSOUS	Director of research, ISCR, Rennes University	Reviewer
Mr.	H. IHARA	Professor, DACB, Kumamoto University	Reviewer

In front of the exam commission form by:

Mrs.	Á. SASTRE-SANTOS	Professor, IB, University Miguel Hernández	President
Mrs.	C. OLIVIER	CNRS researcher, ISM, Bordeaux University	Examiner
Mrs.	R. ODA	Director of research, CBMN, Bordeaux University	Supervisor
Mr.	D. M. BASSANI	Director of research, ISM, Bordeaux University	Supervisor

*Ce mémoire est dédié à mon père,
Il m'a toujours poussé vers l'avant
Puisse-t-il reposer en paix*

ACKNOWLEDGEMENTS – REMERCIEMENTS

Ce travail est le fruit d'une collaboration entre les équipes Chiral Molecular Assemblies (CMA) de l'Institut de Chimie et Biologie des Membranes et des Nano-objets (CBMN) et Nano-structures Organiques (NEO) de l'Institut des Sciences Moléculaires (ISM). Cette collaboration est faite dans le cadre du Laboratoire International Associé portant sur les Nano-structures Chirales pour des Application Photoniques (LIA-CNPA) et je tiens à remercier les membres de chacun des laboratoires participant à cette aventure, aussi bien au sein de l'Université de Bordeaux que de l'Université de Kumamoto et de l'Université de Kyoto, pour les discussions durant nos réunions régulières.

Je tiens à remercier personnellement Dr. **Reiko ODA** et Dr. **Dario BASSANI**, directeurs de recherches des équipes CMA et NEO, pour m'avoir accueilli dans leurs équipes durant ces trois ans. Vous avez tous deux été les meilleurs directeurs de thèse que j'aurais pu avoir, stricts quand il en est besoin, mais jamais dans l'excès et d'une bonté sans limite. Vos conseils, encouragements et reproches m'ont guidés tout au long de ces 3 ans et me suivront tout au long de ma vie.

Mes plus sincères remerciements aux membres de mon jury, Dr. **Céline OLIVIER**, Prof. **Angela SASTRE-SANTOS** et tout particulièrement les rapporteurs Dr. **Jeanne CRASSOUS** et Prof. **Hiroataka IHARA** d'avoir accepté de juger la qualité de ce travail.

Mes remerciements les plus profonds au Dr. **Emilie POUGET**, chargée de recherche au sein du groupe CMA, qui m'a suivi tout au long de ma thèse avec une patience et une bienveillance exemplaire. Merci pour toutes les connaissances que tu m'as transmises, toute l'aide et le support que tu m'as apporté, et l'immense quantité de travail de l'ombre que tu fais pour que les recherches se passent au mieux dans notre équipe.

Je remercie également **Damien JARDEL**, **Pascale GODARD** et **Clotilde DAVIS**, techniciens au sein de l'équipe NEO, pour leur aide au quotidien et leur amitié vis-à-vis de tous les membres de l'équipe. Merci d'être là, toujours attentifs et bienveillants, jamais sarcastiques et toujours prêts à tout pour rendre notre quotidien plus agréable.

Je remercie une fois encore Prof. **Angela SASTRE-SANTOS** et le groupe DYSMOL pour m'avoir fournis des dérivés peryléniques dépassant de loin mes compétences de synthèse organique.

Je tiens également à remercier les personnes ayant contribué à ce projet, **Sisareuth TAN** et **Marion DESOSSA-MENDOZA**, pour leur formation et support de tous les instants sur le TEM ; **Laëtitia MINDER**, de m'avoir tout appris sur le CD ; **Estelle MORVAN**, **Axelle GRELARD** et **Yannick CHOLLET**, pour leur aide précieuse sur la spectroscopie RMN ; **Loïc KLINGER**, **Christelle ABSALON**, **Patricia CASTEL** et **Claire MOUCHE**, pour les spectrométries de masse.

Je remercie également toutes les personnes m'ayant permis de collaborer sur leurs projets, Dr. **Irene PAPAGIANNOULI**, Dr. **Valérie BLANCHET**, **Jerome GAUDIN**, Dr. **Brigitte BIBAL**, **Dorian SONET**, **Zhen CAO**, **Satya RAMALINGAM**, Dr. **Adeline PERRO**, Dr. **Fabien DUROLA** et Dr. **Yoann COQUEREL** apportant un vent de fraîcheur dans les moments parfois difficiles de la thèse.

Je remercie également très vivement tous les doctorants, post-doctorants et anciens membres des équipes CMA et NEO, en particulier **Antoine AMESTOY**, Dr. **Mariam ATTOUI**, Dr. **Jiaji CHENG**, Dr. **Jie GAO**, **Jian-Qiao JIANG**, Dr. **Balamurugan KUPPAN**, Dr. **Marcello LA ROSSA**, **Peizhao LIU**, Dr. **Yutaka OKAZAKI**, Dr. **Shaheen PATHAN**, Dr. **Luca PISCIOTTANI**, Dr. **Naoya RYU**, Dr. **Kyohei YOSHIDA** et **Wijak YOSPANYA** qui m'ont tous beaucoup aidé et grâce à qui j'ai eu l'opportunité de travailler dans la meilleure atmosphère possible.

Un grand merci à tous les amis qui m'ont soutenu tout au long de ma thèse, **Julien**, **Alexis**, **Claude**, **Sylvain**, **Valentin** et **Vincent** votre support m'a aidé au-delà de ce que je ne saurais le dire. Je remercie aussi ceux que je ne rencontre qu'en ligne, **JB**, **Sev**, **Joe**, **Braska**, **Wed**, **Crosh**, **Dova** et tous les autres quaggans et pandas que j'oublie... Aucun de vous ne s'en rend compte mais vous avez toujours su me rendre le sourire dans les moments où j'étais au plus bas. Merci à tous !

Je ne peux décrire à quel point ma famille m'a supporté ces trois dernières années... **Anne-Marie**, **Aurélie**, **JC**, **Maryline**, **Philippe**, **Elise**, **Anaïs**, **Nicolas**, **Mélina**, **Clément**, **Anaëlle**, **Maëlla** vous êtes une famille en or.

Enfin, **Evelyne**, ma maman adorée, qui ne sais pas venir me rendre visite sans faire toutes mes corvées avant de partir. Merci pour ton support infini et inconditionnel, je t'aime.

RESUME

La polarisation de la lumière, bien que connue depuis fort longtemps, pourrait être plus exploitée. Cependant, de plus en plus d'entreprises de pointe dans les domaines de la sécurité et la transmission d'information commencent à l'utiliser. Une raison de la sous-exploitation actuelle de la polarisation vient des méthodes de polarisation, qui ont une transmission de la lumière limitée (généralement jusqu'à 45%). Afin d'outrepasser cette limite physique, un moyen est d'utiliser des matériaux fluorescents émettant une lumière polarisée. Cependant, la synthèse et la purification de tels matériaux sont compliquées et obtenir les deux énantiomères n'est pas toujours possible. Ce travail se concentre sur une nouvelle méthode de synthèse, plus simple, utilisant des nano-structures hybrides ou inorganiques hélicoïdale, et des luminophores organiques pouvant interagir ensemble. L'agrégation chirale des chromophores autour des structures formera ainsi des nano-objets fluorescents chiraux.

Le premier chapitre explique comment la chiralité est aujourd'hui présente dans tous les domaines et à toutes les échelles, des molécules aux objets du quotidien. Nous y étudierons également l'induction de la chiralité à différentes échelles. Le second aspect de ce travail, l'interaction lumière-matière, sera également mis en avant, aussi bien concernant l'absorption que l'émission lumineuse, mais aussi en quoi l'assemblage des molécules peut affecter ces propriétés. Nous nous pencherons également sur les cas très particuliers du dichroïsme circulaire et de la luminescence circulairement polarisée. Pour finir, nous verrons quels sont les matériaux actuels existant pour obtenir ces propriétés et quels sont leurs inconvénients.

Afin d'outrepasser ces défauts, nous avons choisi d'utiliser deux systèmes. Le premier, constitué de nano-hélices organiques dans une coque de silice a pour avantage d'utiliser à la fois une induction de chiralité par assemblage des chromophores organiques, mais aussi une seconde induction de la chiralité à l'échelle moléculaire. L'inconvénient étant que ce système n'est pas très robuste à un changement d'environnement. Pour résoudre cet inconvénient, nous n'avons conservé, dans un second temps, que la coque de silice afin de l'utiliser comme patron pour supporter le greffage covalent de luminophores à sa surface.

Dans le second chapitre, la méthode de synthèse des nano-structures sera présentée. De même le choix des différents luminophores utilisés dans ces travaux sera justifié, et leur voie de synthèse, expliquée. Enfin, les différentes méthodes de caractérisation seront détaillées.

Le troisième chapitre portera sur les résultats obtenus lors de l'intégration de chromophores non-chiraux dans les hélices hybrides, ou leur greffage sur les structures inorganiques. Nous y verrons l'importance à la fois de l'assemblage intermoléculaire, mais aussi de l'interaction avec un environnement chiral, pour l'induction de chiralité dans le but d'obtenir dichroïsme circulaire et luminescence circulairement polarisée. Les différents chromophores utilisés y sont présentés et comparés permettant la mise en évidence des principaux facteurs aidant à l'induction de chiralité pour chaque type de structure.

Enfin, un dernier chapitre s'intéressera à des systèmes plus complexes utilisant des molécules présentant en solution des propriétés chiro-optiques, ou ayant la capacité de s'agréger en nano-structures ayant de telles propriétés, et ce afin de savoir si leurs propriétés sont ajustables grâce à l'utilisation des hélices hybrides pour leur imposer une agrégation spécifique. Une dernière approche a également été étudiée, en synthétisant des quantum-dots carbonés fluorescents à partir des nano-structures hybrides. Ces quantum-dots, s'ils conservent la forme de la structure initiale, pourraient posséder un dichroïsme circulaire et une luminescence circulairement polarisée sans besoin de les complexer avec une molécule chirale.

SUMMARY

The polarization of light, despite being known since long time, is recently at the center of renewed interest. More and more high technology companies in the fields of safety and information transmission are starting to exploit this property. One bottleneck for their use comes from the limitation in the light transmission of current methods of polarization (typically up to 45%). In order to overpass this physical limitation, one possible approach would be to use fluorescent materials emitting polarized light. However, the synthesis and purification of such materials is complex and obtaining both enantiomers is not always possible. The current work focus on a new synthetic pathway, possibly simpler and more versatile, using chiral hybrid or inorganic nano-helices and organic fluorophores interacting together. The aggregation of chromophores around the template will form chiral fluorescent nano-objects.

The first chapter explains how chirality is present in many fields and at every scale, from molecules to daily objects. We will discuss the way of inducting or transferring chirality. The second facet of this work, light-matter interactions, will also be explained, concerning both absorption and emission of light, but also on how molecular assembly can affect these properties. We will study into detail the very particular case of circular dichroism and circularly polarized luminescence. Finally, we will see the existing systems that are used to obtain these properties and the drawback of these materials.

In this work, we chose to use two systems. The first, constituted of organic nano-helices in a silica shell, has the advantage of using the organic template confined in chiral nano-space to induce chirality to the organic chromophores in interaction with them molecularly, but also through aggregation due to the confinement. The disadvantage being that this system is not robust toward environmental changes. The alternative approach is to use the silica shell as an inorganic template for the covalent grafting of fluorophores onto its surface.

In the second chapter, the method for the synthesis of nano-structures is described, along with an explanation on the choice and synthesis of the chromophores used in this study. Finally, the characterization processes used are detailed.

The third chapter will focus on the results we obtained when integrating achiral chromophores into hybrid helices or by grafting them onto the silica surface. We will see the importance of the intermolecular assembly and of the interaction with a chiral environment to obtain circular dichroism and circularly polarized luminescence through chiral induction. Various fluorophores are presented and compared allowing the understanding of the key parameters for chirality induction of each type of structure.

In the last chapter, more complex systems are studied using molecules presenting chiroptical properties in solution state or having the ability to form self-assemblies showing such properties. The objective will be to tune the chiroptical properties of these chromophores, by the use of hybrid helices to force a specific organization. The last part will focus on the synthesis of fluorescent carbon based quantum dots using hybrid structures. These quantum dots, can retain the shape of the original structure and show circular dichroism or circularly polarized luminescence without needing to form a complex with an external source of molecular chirality.

OUTLINE

CHAPTER I: CHIRALITY INDUCTION FROM MOLECULES TO LIGHT	1
1. Chiral objects.....	2
1-a. What is chirality?	2
1-b. Induction of chirality between objects of similar size	4
1-c. Chiral supramolecular objects: molecules inducing chirality at nano-scale	6
1-d. Chirality induction from nano-object to small molecules.....	9
2. Light – matter interaction	10
2-a. Light absorption	10
2-b. The excited state and relaxation processes	12
2-c. The complex case of circularly polarized light.....	15
3. Chiroptical properties from achiral chromophores	17
3-a. Previously reported systems.....	17
3-b. Use of helical nano-structures.....	18
4. Conclusion and objective of this work	20
CHAPTER II: FORMATION OF HELICAL ARCHITECTURES, ORGANIC CHROMOPHORES AND THEIR CHARACTERIZATION	21
1. Formation of twisted and helical nano-objects.....	22
1-a. Synthesis of 16-2-16 tartrate	23
1-b. Formation of silica coated chiral nano-structures	25
1-c. Purification and final steps.....	27
2. Organic fluorophores.....	30

2-a.	Chromophores used without further synthesis	30
2-b.	Synthesis of perylene and acridine derivatives.....	31
2-c.	Covalent surface grafting.....	33
3.	Characterization techniques	35
3-a.	Structural characterization.....	35
3-b.	Transmission Electron Microscopy (TEM).....	36
3-c.	Photophysical properties: Absorption and Fluorescence.....	36
3-d.	Quantification of amine groups on the silica helices.....	36
3-e.	Chiroptical properties	39
 CHAPTER III: INDUCTION OF CHIROPTICAL PROPERTIES TO NON-CHIRAL CHROMOPHORES		43
1.	Chirality induction from hybrid helices	45
1-a.	Interaction between chromophores and hybrid helices (previous studies).....	45
1-b.	Interaction between organic fluorophore and hybrid helices (new study)	48
2.	Chirality induction using silica template.....	62
2-a.	Covalent grafting on silica surfaces.....	62
2-b.	Chirality induction on polyoxometalates ⁶²	62
2-c.	Grafting by acridine derivatives	63
2-d.	Grafting by pyreneacetic acid.....	67
2-e.	Grafting by perylene derivatives	70
3.	Conclusion	77
 CHAPTER IV: TOWARD MORE COMPLEX SYSTEMS		79
1.	Chiral chromophores	80

1-a.	Optically active chiral center	80
1-b.	Chiral aggregates.....	86
2.	Formation of carbon dots from the organic template	91
3.	Conclusion.....	98
CHAPTER V: CONCLUSION AND PERSPECTIVES.....		99
1.	General conclusion.....	100
2.	Perspectives for futures studies	102
CHAPTER VI: ADDITIONAL INFORMATION.....		103
1.	Experimental section.....	104
1-a.	Synthesis of 16-2-16 tartrate	104
1-b.	Formation of silica coated chiral nano-structures	106
1-c.	Purification and final steps.....	108
1-d.	Synthesis of perylene and acridine derivatives	109
1-e.	Carboxylic acid activation and surface reaction	114
2.	Details on the self-assembly of 16-2-16 tartrate^{55,89}	115
2-a.	Molecular conformation.....	115
2-b.	Multiples bilayers structure.....	116
2-c.	Supramolecular morphology	116
3.	NMR spectra.....	118
3-a.	Gemini molecules	118
3-b.	Organic chromophores	119

CHAPTER I: CHIRALITY INDUCTION FROM MOLECULES TO LIGHT

1. Chiral objects

1-a. What is chirality?

1-a.i General definition

Chirality was defined in 1893 by Sir William Thomson Lord KELVIN at the Oxford University Junior Scientific Club as “I call any geometrical figure, or group of points, 'chiral', and say that it has chirality if its image in a plane mirror, ideally realized, cannot be brought to coincide with itself.”¹ The two forms of a chiral object are called enantiomorphs. In opposition, an object which is isomorph by mirror symmetry is called achiral.

This first definition is very general, and was adopted in many fields, particularly in science where almost every domain adopted the concept of chirality, from mathematics² to chemistry, but also astronomy, meteorology or biology. This is because chirality can be found at every scale, as represented in Figure I-1, from galaxies to molecules and, according to recent studies, even at the atomic level.^{3,4}

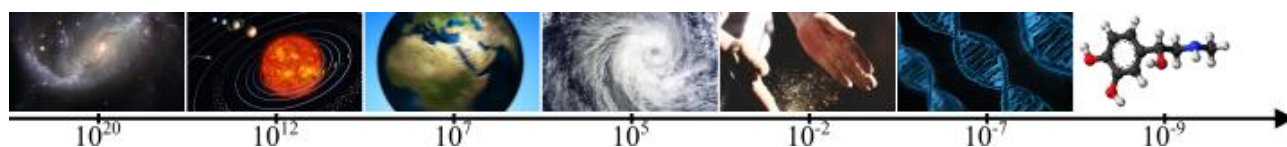


Figure I-1: Examples of chirality at every scale (scale in meter)

1-a.ii Chirality in physic

Polarization is a property of electromagnetic waves specifying the geometrical orientation of its oscillations. There are two types of wave polarization: linear polarization, discovered in 1808 by E.-L. MALUS, and circular polarization, discovered in 1822 by A. FRESNEL⁵. In case of linear polarization, the polarization plane does not change along the direction of propagation of the wave while, in the case of circular polarization, there is a rotation of the polarization plane (Figure I-2). This rotation can be right-handed or left-handed, making circular polarization an example of chirality in physics.

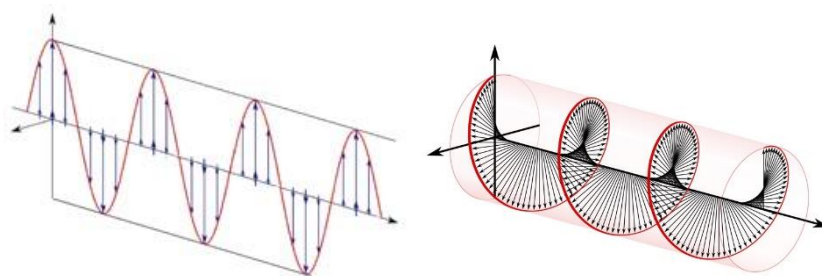


Figure I-2: Scheme of linearly and circularly polarized waves

We can note that a circularly polarized (CP) wave can be considered as the sum of two perpendicular linearly polarized (LP) waves with the same wavelength and in phase opposition. Conversely, an LP wave can also be considered as the sum of two CP waves with same wavelength and in phase, but with opposite handedness. This property can be applied to any electromagnetic wave and will be used in this work for ultra-violet and visible light. Light sources such as a tungsten lamps or the sun are non-polarized. But, it has been shown that in some cases, astrophysical phenomena such as star formation can show emission of circularly polarized light.⁶ We can also find CP light in nature. For example, it has been shown that some species are able to detect (mantis shrimp⁷) or emit (firefly⁸) CP light.

1-a.iii Chirality in chemistry

In chemistry, enantiomorphs are termed enantiomers,⁹ and we define the enantiomeric excess (*ee*) by the following equation, where $[R]$ and $[S]$ are the concentrations in the R and S enantiomer, respectively.

$$ee = \frac{[R] - [S]}{[R] + [S]} \quad (1)$$

The value of enantiomeric excess varies from -1 to 1. An *ee* of 0 means that both enantiomers are in equal concentrations and such mixtures are called “racemic”.⁹ A sample containing only one enantiomer gives an *ee* of -1 or 1 and is called “enantiomerically pure”.

Although the origin of chirality in Nature is still unclear, we can now control the chirality of chemical products by synthesizing specifically one enantiomer or by separating a racemic mixture after a reaction. Obtaining one specific enantiomer is crucial in medicine as two opposite enantiomers

can possess totally different functions. For example, R-methamphetamine enters into the composition of several drugs, both as a vasoconstrictor or to affect the central nervous system in selegiline (an anti-Parkinson's drug) but does not cause euphoria or addiction, whereas S-methamphetamine is one of the most powerful recreational drug causing a high addiction and euphoria in addition to a much higher effect on the central nervous system (Figure I-3).

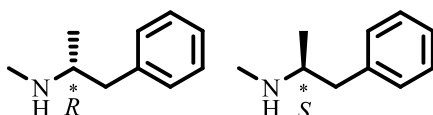


Figure I-3: R- and S-methamphetamine

In order to differentiate two enantiomers, chemists use the “sequence rule procedure” (also known as CAHN, INGOLD and PRELOG rule). In order to explain it, we consider the molecule CHFCIBr (represented in Figure I-4). We arrange the ligands in order of decreasing atomic number, here $\text{Br} > \text{Cl} > \text{F} > \text{H}$. Then, we look at the model from the side, remote from the last element, then trace a path from first to third element. If that path turns clockwise, the molecule is R (right, Latin: *rectus*). If it turn counter-clockwise, the molecule is S (left, Latin: *sinister*).^{9,10} Returning to the previous example of methamphetamine, LEVO-methamphetamine is R and DEXTRO-methamphetamine is S.



Figure I-4: Example of R and S molecules

It is also assumed that every chiral molecule shows optical activities, and that any molecule showing optical activity is chiral.⁹

1-b. Induction of chirality between objects of similar size

Chirality is not a property that is inherently localized onto a single molecule or species, but that can be induced from a molecule to another by intermolecular interactions such as H-bonding or host-

guest complexation.¹¹ Many examples can be found on this topic such as the induction of chirality onto a calixarene host by a chiral sugar complexed within.^{12,13}

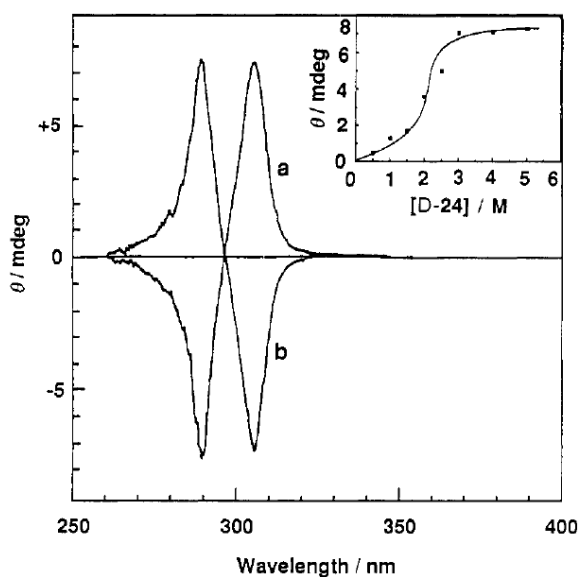


Figure I-5: Induction of optical activity from fructose to calix[4]arene (Reprinted with permission from Kikuchi Y. et al., *J. Am. Chem. Soc.*, **1992**, 114, 1351-1358. Copyright (1992) American Chemical Society)

As we can see in Figure I-5, a chiral sugar interacting with an achiral calix[4]arene induces chiroptical properties to the latter.¹² This phenomena can also be found in other systems such as the one presented in Figure I-6 in which the chiral guest molecule **4** induces chirality to the host **1** by both H-bonding and steric interactions, thereby resulting into the appearance of optical activity upon mixing.¹³

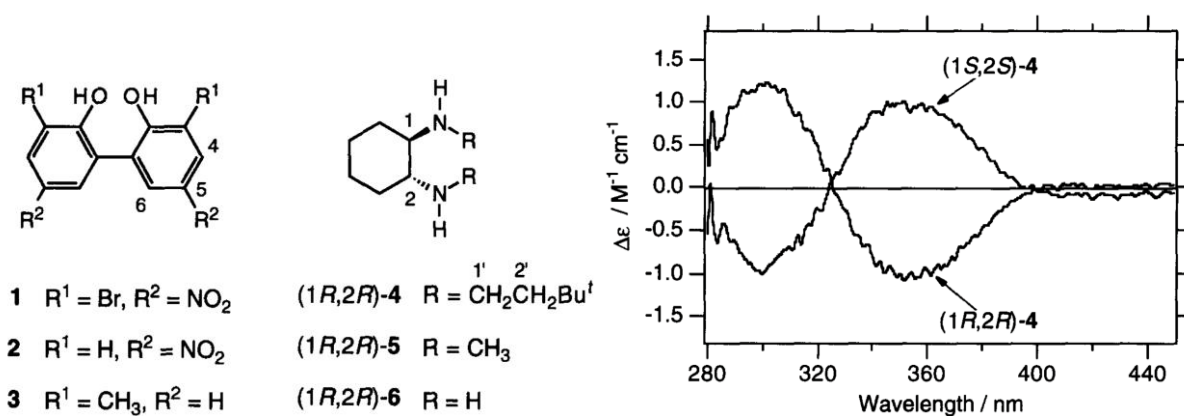


Figure I-6: Structures of used compounds and resulting optical activity (Reprinted with permission from Mizutani T. et al., *Tetrahedron Lett.*, **1997**, 38, 1991-1994. Copyright (1997) Elsevier Science Ltd)

1-c. Chiral supramolecular objects: molecules inducing chirality at nano-scale

1-c.i *Generalities on self-assembled systems*

Some molecules undergo association to form supramolecular assemblies. One of the families of molecules for which this process is common are amphiphilic molecules possessing a hydrophilic and a hydrophobic part. Once dissolved in water, interfacial forces will minimize the contact area between the hydrophobic part and water.

If the concentration of amphiphiles is too low, molecules form small aggregates (pre-micelle) or remain in solution. As the concentration is increased above the critical micellar concentration (CMC) any further addition of free molecules in solution will lead to their assembly to small objects called micelles, in which hydrophilic moieties of the molecule will point outward to water and the hydrophobic part will be confined inward. Further increasing the concentration will lead to the formation of bigger structures such as bilayers containing many more molecules. Bilayers may eventually fold into circular shapes called vesicles. These structures are schematized in the Figure I-7 below.

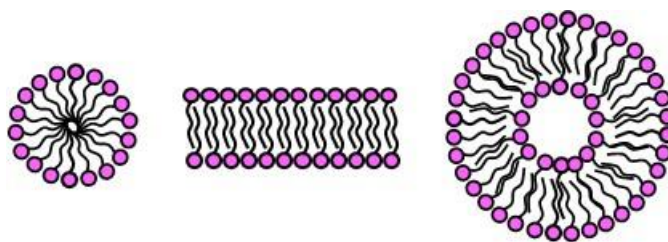


Figure I-7: Different types of self-assembled structures (micelle, bilayer and vesicle) hydrophilic part represented as pink dot and hydrophobic tail by black curve and considering water as solvent

Amphiphilic structures are commonly used for a wide range of applications. For example, soaps are amphiphilic molecules trapping insoluble dirt in the hydrophobic part of micelles and stabilizing its solvation in aqueous medium. Another possible use of such structures would be drug delivery. Recent research show that it is possible to target a specific type of cell with a drug by trapping it in

the center of a vesicle, which attach to the targeted cell membrane and appear to fuse with it, releasing the drug inside the cell.¹⁴

1-c.ii Case of chiral supramolecular objects

Among all supramolecular objects, ribonucleic acid (DNA and RNA) occupies a very special place in scientific research as it is the building block of life form on Earth. DNA is composed of two branches each composed of a phosphate-deoxyribose polymer backbone functionalized by 4 different nucleobases: adenine, cytosine, guanine and thymine (Figure I-8). One of the incredible property of DNA is its ability to form a double helix, this very specific shape come from the chirality of the enantiopure phosphate-deoxyribose forming the backbone and the interactions between the nucleobases.

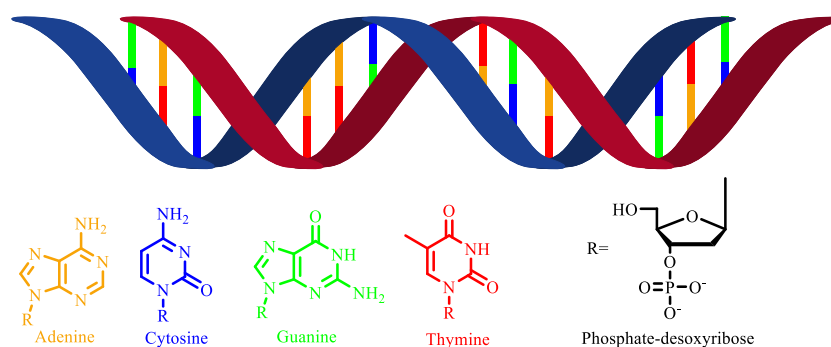


Figure I-8: Structure of DNA with its four components and the backbone molecule

The specific shape of DNA makes it a highly studied subject for templating chirality to molecules that can be attached to its surface. Another Nature-based chiral supramolecular structure can be found in proteins. Proteins are large molecules or macromolecules composed of amino acids. These chiral units forming the protein will strongly interact together by H-bonding and Van der Waals interactions, inducing a supramolecular shape. This is mainly constituted of 2 types of 3D structures, α -helices and β -sheets (represented on Figure I-9).

1-d. Chirality induction from nano-object to small molecules

In general, chirality transfer occurs between objects of similar dimensions or from small component to larger assembly, and less examples are known for chirality transfer from a larger object (10-100nm) to a molecule. This recently became the focus of many research teams around the world. The most widely known examples of chirality transfer from a nano-structure to a molecule are enzymatic reactions. This is the case of the stereospecific isomerization of citrate into (2R,3S)-isocitrate. This 2-step reaction is catalyzed by aconitase (83kDa).²¹

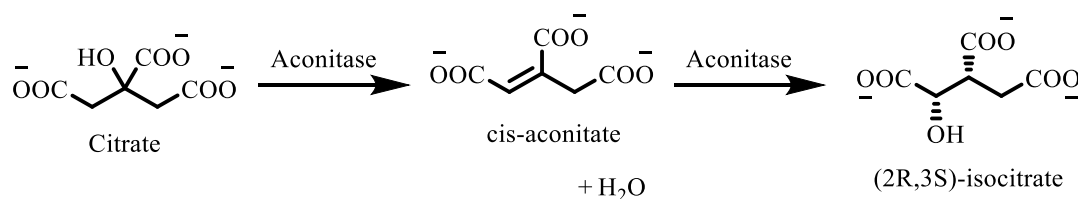


Figure I-11: Stereospecific isomerization of citrate by aconitase²¹

This reaction is a primordial part of the Krebs cycle and relies on the non-chiral [4Fe-4S] site located in the aconitase enzyme. However, the surrounding environment of this site shows a specific configuration and the cis-aconitate can only approach the reaction site in one configuration, leading to an important enantiomeric excess toward (2R,3S)-isocitrate.²²

Another example of chiral recognition can be found with some clay materials.²³ The chiral properties of some clays can be used to conduct asymmetric catalysis by using them as a support for the catalytic site and leading to asymmetric synthesis. Several research teams are now studying the possibility that clay chiral selectivity might also be the reason of homochirality in the living system of our planet.²⁴

2. Light – matter interaction

The second facet explored through this project is the field of photophysics and photochemistry. We all experience these fields during every day of our life when using our eyes. Thanks to the tool Nature provided, the study of visible light (spectrum shown in Figure I-12) and of the interaction it has with matter have always been a hot topic among both physicists and chemists.

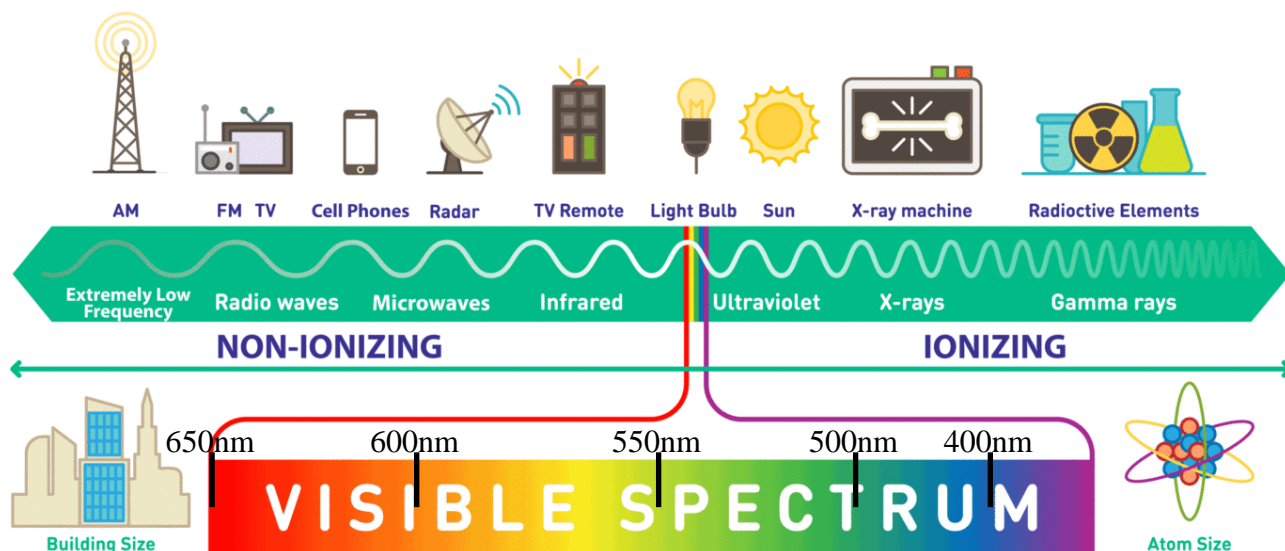


Figure I-12: Electromagnetic spectrum range (picture source: DefenderShield website) with approximative wavelength in visible spectrum

Nowadays, with the evolution of technologies such as 3D screens, security printing and optical fibers (among many others), the number of researchers studying photonic properties is steadily increasing. Within these new technologies, properties such as light polarization receive renewed attention.

2-a. Light absorption

When considering light-matter interactions, the first thing to consider is light absorption, leading a molecule from the electronically stable ground state to an energetically higher excited state. If no light is absorbed, no electronic interaction can occur (principle of photo-activation). There are 2 conditions for absorption to be possible: First, the energy provided by a photon ($h\nu$) should be greater than the energy from the ground state to an excited state (ΔE).

$$\Delta E = h\nu \quad (2)$$

Second, the transition from the ground state to the excited state must be allowed, requiring:

1. Orbital overlap between the two states
2. Conservation of spin
3. No change in the position of nuclei

If the absorption induces a $\sigma\sigma^*$ transition, the bond is no longer stabilized and the molecule may undergo dissociation. However, if the transition is $\pi\pi^*$ the bond stabilization is reduced but still present. There is no dissociation of the molecule, but only an elongation of the bond (Figure I-13).

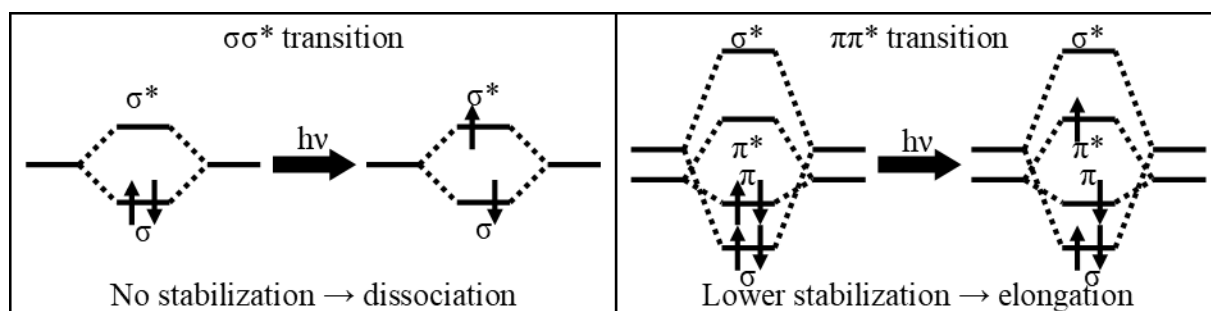


Figure I-13: Schematics representation of $\sigma\sigma^*$ and $\pi\pi^*$ transitions

The absorption of light is described by the BEER-LAMBERT law, which states that the intensity of absorbed light increases proportionally to the sample concentration and thickness.

$$A = -\log(T) = -\log\left(\frac{I_T}{I_0}\right) = \epsilon Cl \quad (3)$$

In this equation, A is the absorption, T the transmittance, I_T and I_0 the transmitted and incident intensity of light, C the concentration of molecule (mol/L), l the length of the sample (cm) and ϵ the molar extinction coefficient (L/mol.cm). We will also note that this law only applies if several conditions are fulfilled:

1. Molecules are independent from each other
2. The solution is homogeneous
3. Incident light rays are parallel

2-b. The excited state and relaxation processes

Once a molecule absorbs light, it is converted into an electronically excited state. Various processes can bring it back to the ground state which are represented in an energy state diagram called a JABONSKI-PERRIN diagram (Figure I-14).

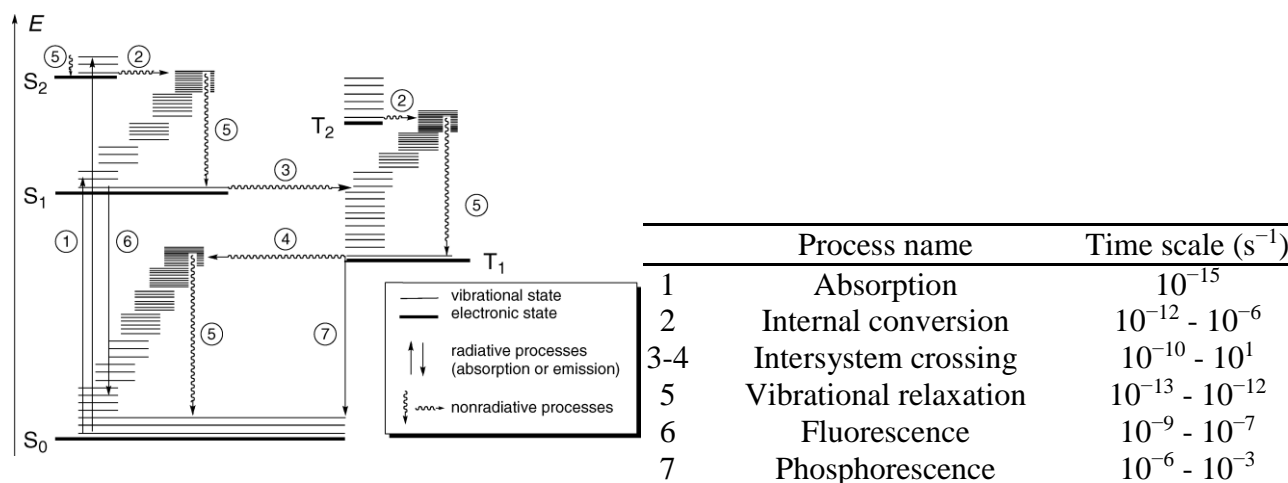


Figure I-14: JABONSKI-PERRIN diagram with name and speed range of represented processes²⁵ (Reprinted with permission from Klan P. and Wirz J., John Wiley & Sons, Ltd, 2009. Copyright 2019 P. Klan and J.

Wirz)

In the ground state, the sum of electron spin is zero and as mentioned above, the spin cannot change during light absorption, meaning that the initially populated excited state must have the same spin. Such states are called singlet states (S_n). However, it is possible through intersystem crossing to invert the spin of an electron leading to the production of a triplet state (T_n), in which the sum of electron spin is 1.

In order to quantify the efficiency of each process, we define the quantum yield (Φ) as follows:

$$\Phi_P = \frac{\text{number of event } P}{\text{number of absorbed photons}} = \frac{k_{\text{observed process}}}{\sum_{\text{every process}} k_P} \quad (4)$$

Where k_i is the rate constant of the process. Determination of quantum yield for luminescence can be done using an integrating sphere²⁶ or using a secondary standard (with a known quantum yield).

2-b.i Fluorescence

Fluorescence was first reported by HERSCHEL in 1845:

“The quinine sulfate... Though perfectly transparent and colorless when held between the eye and the light, or a white object, it yet exhibits in certain aspects, and under certain incidences of the light, an extremely vivid and beautiful celestial blue color...”²⁷

Absorption of light by quinine sulfate in the near UV ($\lambda_{max}=350\text{nm}$) result in emission of blue light ($\lambda_{max}=450\text{nm}$). The difference in energy between absorption and fluorescence is called the STOKES Shift and it is due to the energy lost through vibrational relaxation while the molecule is in the excited state (represented by the process 5 in the JABONSKI-PERRIN diagram).²⁸ We can also note that the more rigid a molecule is, the smaller the Stokes shift.

The spectral distribution of fluorescence emission is, in the case of a rigid aromatic chromophore the mirror-image relationship to the first absorption band. This is because the spacing between the dominant vibronic bands in the excited state is similar to those in the ground state if the potential energy surfaces of the ground and excited state are similar in shape. We can also note that the absorption spectra provides information about vibronic levels of the excited state, whereas the fluorescence spectra gives information about the ground state.²⁵

2-b.ii Phosphorescence

Intersystem crossing is a competitive process to fluorescence and results in the population of the triplet state. This process happens iso-energetically and the de-excitation of the triplet excited state to the ground state is much slower than the one from a singlet excited state due to the spin change of one of the electron (forbidden transition). The emission from triplet state is called phosphorescence, and the slow relaxation kinetic make emission from such states happen with much longer lifetimes. Because of the singlet-triplet energy gap, phosphorescence from T_1 is at longer wavelengths than fluorescence.

Many room-temperature phosphorescent materials are based on heavy-metals, making them toxic and often expensive. In case of phosphorescence from organic compounds, it was reported for the first time in 1930 by BOUDIN from a solution of eosin in glycerol.²⁹ Generally, phosphorescence emission is quenched due to the presence of oxygen in solution and thermal and vibrational relaxation.

Interestingly, these effects may be diminished once the molecules are highly aggregated or in the crystalline state.³⁰

2-b.iii Excimer formation

In the ground state, orbital overlap between molecules is disfavored because of electronic repulsion. However, if one molecule is in the excited state, there is an energetic stabilization due to the intermolecular electronic interaction between the filled and the half-filled orbitals (Figure I-15).

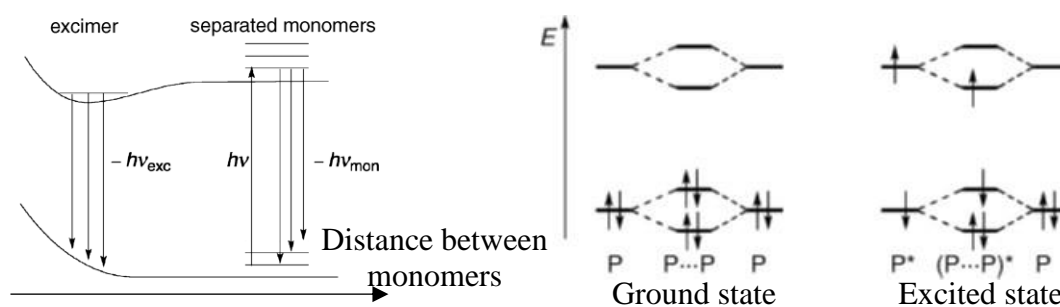


Figure I-15: Left: Potential energy surfaces for excimer formation and relaxation²⁵ / Right: Orbital diagram for the encounter of two molecule (Reprinted with permission from Klan P. and Wirz J., John Wiley & Sons, Ltd, 2009. Copyright 2019 P. Klan and J. Wirz)

Once an excimer (excited dimer) is formed, it can relax to ground state by radiative processes. However, because the ground state potential energy surface is repulsive, no vibronic structure will be observed and the emission is broad and featureless.

2-b.iv Exciton coupling

For certain chromophores presenting strong intermolecular interactions (Van der Waals, H bonding, π - π stacking...), it is possible to observe self-association in the ground state. In such cases, the aggregate may present new electronic transitions compared to those of the monomeric chromophores. The position of these transition depends on the geometrical arrangement of the chromophores as described by exciton theory. Two extreme cases can be pictured, one with a “ladder” and the other with a “staircase” arrangement of the chromophores (Figure I-16).

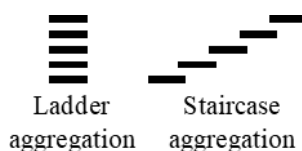


Figure I-16: Illustration of the two extremes aggregation type

The “ladder” type aggregation will lead to anti-parallel arrangement of the electronic transition dipole moments of the $S_0 \rightarrow S_1$ transitions. This coupling result in two new transitions in which the lower energy one is symmetry forbidden. In this case, light absorption will lead to a $S_0 \rightarrow S_2$ transition, with a higher energy compared to the monomeric state thus presenting a hypsochromic shift (toward the blue). Such aggregation is called H-aggregation. On the opposite extreme, a “staircase” type aggregation will lead to a parallel conformation of the electronic transition dipole moment of S_1 . In this case, the lower energy transfer is allowed and results in a bathochromic shift (toward the red) of the $S_0 \rightarrow S_1$ transition. This “staircase” type aggregation is called J-aggregation (named after JELLY, one of the discoverer of this phenomena) (Figure I-17).^{31,32}

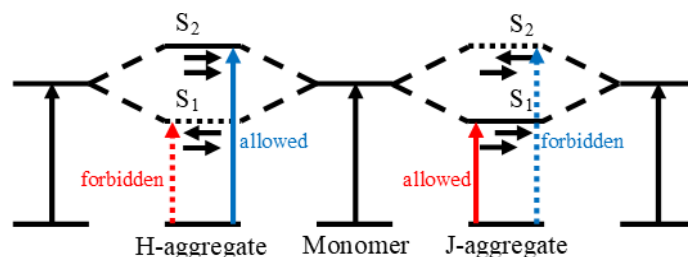


Figure I-17: Schematic representation of absorption difference depending of aggregation type

Of course, these two aggregations types are extreme cases and aggregation may occur through other geometries. We can also note that if J-aggregates usually exhibit a strong luminescence intensity, H-aggregates have a quenching effect since the lowest energy transition is forbidden.

2-c. The complex case of circularly polarized light

2-c.i Circular Dichroism (CD)

When linearly polarized light passes through a chiral medium, a rotation of the polarization plane is observed (birefringence). This phenomena can be explained because of the difference between the refractive indexes of the chiral medium for the left- and right-handed circular components. This

difference causes a phase shift between the two circularly polarized waves composing the light (cf page 2), causing a rotation of the polarization plane for the resulting linearly polarized light.³³

The main parameter explaining the difference between the two refractive indexes is the optical rotation parameter. This parameter also affects slightly the absorption coefficients of both circular component of light. The differential absorption of a material toward left- and right-handed circularly polarized light is called circular dichroism (CD) and result in an amplitude differentiation of both circular component of the linearly polarized light making it acquire a small degree of elliptical polarization.³⁴

2-c.ii Circularly Polarized Luminescence (CPL)

Circularly polarized luminescence (CPL) is the emissive analogue of CD. However, whereas CD originates from a molecule in the ground state, CPL come from a vibrationally relaxed excited state. This explains that, even though CD and CPL can be redundant when the geometry of the molecule is same in the ground and in the excited state, it is possible for a system to show only CD or CPL. In order to measure CPL, it is important to excite the sample with depolarized light as it is known that upon aggregation, a racemic mixture can exhibit CPL due to different excitation probabilities of one of the enantiomers (photoselection).³⁵

CPL recently became the focus of attention for possible technological applications. For example, higher information transmission speeds can be achieved using polarized light, extending information transport compared to non-polarized light (polarization plane or handedness). Linearly polarized light cannot be used in this context, because of its angle dependence: every information would be lost when the polarization plane and the detector are orthogonal. In contrast circularly polarized light does not present any type of blind angle. Also, if the selective polarization of light is intrinsically limited by the use of polarizers (a linear polarizer easing light by around 50%), the emission of CP luminescence is only limited by our current knowledge of such systems.

3. Chiroptical properties from achiral chromophores

The emission of CPL requires high enantiomeric purity of the system, but it can be extremely difficult to make enantiopure synthesis of the molecules. Also the enantio-separation of the racemic mixture maybe very complicated in some cases. Additionally, it is not always possible to produce both enantiomers of the desired molecule. For all of these reasons, there is strong interest in studying the possibility to induce CD and CPL to achiral molecules using a chiral environment.

3-a. Previously reported systems

There are different ways to induce chirality to achiral chromophores. One of them is the co-crystallization of the chromophore with a chiral molecule, as reported by by Dr. IMAI in 2008 with crystals of 1,2-diphenylethylenediamine and 2-anthracenecarboxylic acid. He obtained chiral co-crystals with CD and CPL properties.³⁶ Another way is through chiral aggregation of the chromophore. Using this method, it is possible to design molecules without any chiroptical activity in solution, which instead show CD and CPL upon aggregation (Figure I-18).³⁷ Such kind of aggregates may show twisted shapes, and it is logical that researchers thought about DNA as a medium to force the chiral aggregation of such chromophores.^{38,39} It has also already been shown that it is possible to induce chirality to achiral molecules using an organic chiral macromolecular assembly as a template to force the chromophores into chiral aggregates. This method allows the use of different chromophores (chiral or achiral) to tune the absorption and emission wavelength without changing the template.

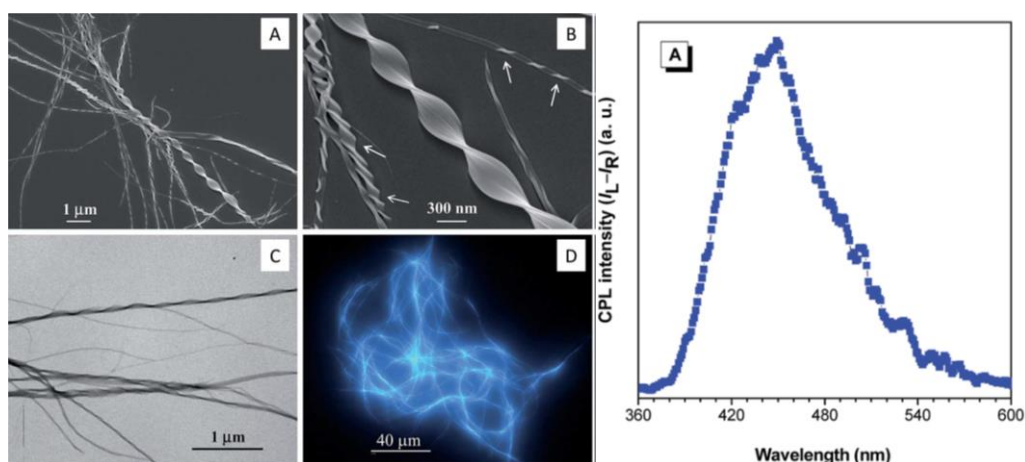


Figure I-18: Chiral aggregation of tetraphenylethylene derivative and associated CPL signal³⁷

(Reprinted with permission from Li H. et al., *J. Matt. Chem. C*, **2015**, 3, 2399-2404. Copyright (2019)

Royal Society of Chemistry)

However, all these methods present several disadvantages. For the aggregation to show chiroptical properties, it should occur at very specific conditions, in a given solvent, with very high purity of the system. Also the handedness is not always switchable as it might not be possible to synthesize both enantiomers of the template. This idea is what brought Dr. ODA and her group, Chiral Molecular Assemblies (CMA), to work on the integration of molecules and nano-particles in the stable chiral inorganic matrices made of silica nano-helices they were already able to synthesize.

3-b. Use of helical nano-structures

In the CMA group, a method for the synthesis of tunable nano-structures has been developed over the last 20 years.⁴⁰ This synthetic process is presented in Chapter II-1 (cf page 22) and extensive details can be found at the end of this manuscript (cf page 115). At the end of the synthesis, we obtain hybrid or inorganic twisted or helical nano-structures. The organic part of the hybrid nano-structures being ionic, it is possible to replace the anion with a chromophore. This has been done in 2016 by Dr. RYU using methyl-orange (**MO**) as a chromophore which is confined in the chiral space of the hybrid helices and leads to chiral induction with the appearance of CD signals from the **MO** (Figure I-19).⁴¹ The idea of changing the environment of an anion by this way was further developed by Dr. OKAZAKI

using monoatomic anions and lead to one of the first examples of induced CD from monoatomic anions.⁴

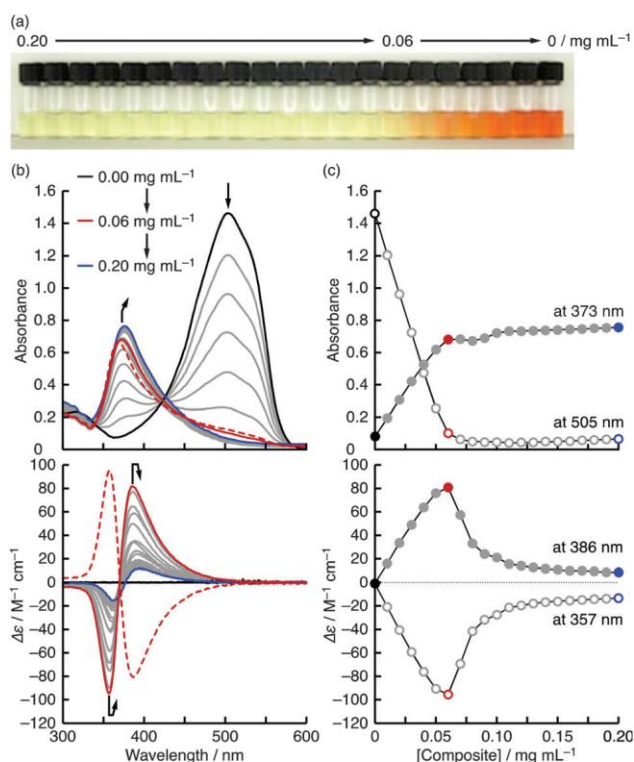


Figure I-19: Evolution of absorbance and CD of methyl orange upon addition of hybrid helices⁴¹
 (Reprinted with permission from Ryu, N. et al., *Chem. Comm.*, **2016**, 52, 5800-5803. Copyright (2019)
 Royal Society of Chemistry)

In the meantime, another study from the group showed that it is also possible to induce CD signals to the plasmon band of spherical gold nano-particles adsorbed/granted around the chiral inorganic nano-helices.⁴²

4. Conclusion and objective of this work

If most of the systems showing chiroptical properties are based on chiral molecules,⁴³ they present several disadvantages. They are difficult to synthesize and/or to purify and both enantiomers may not be available. Also, a small change in the properties may involve a total change of the synthesis without guarantee that the expected properties can be achieved. Despite these difficulties, several systems exist showing induction of the chiroptical properties by assembly of the chromophores into a chiral supramolecular structure.³⁷ However, such systems still present problems concerning the synthetic difficulty for the both enantiomers.

In order to reduce this difficulty, systems based on the induction of chirality from a common chiral template to an achiral chromophore are being developed.^{36,44} However, if such systems solve the synthetic difficulty, they induce new limitations, as the chiral template needs to be stable in the right solvent and under the right conditions. The hybrid and inorganic nano-structures proposed by the CMA group offer interesting alternatives to achieve versatile chiroptical materials. Two approaches are taken in order to reach such objectives. First, the use of hybrid system to induce the chiroptical properties to achiral organic chromophores,^{4,41} second the use of silica helices to chirally align nanoparticles.⁴²

These two ideas are the starting points of this project, in which we propose to use the hybrid nano-structures with organics fluorophores in order to obtain CPL over a wide range of wavelength, but also to use chiral silica templates in order to assemble and graft chromophores on their surface and to induce CD and CPL aiming at creating stable chiroptical systems against external perturbations.

**CHAPTER II: FORMATION OF HELICAL
ARCHITECTURES, ORGANIC CHROMOPHORES
AND THEIR CHARACTERIZATION**

1. Formation of twisted and helical nano-objects

The first step of this project focused on making chiral nano-objects. The story behind these objects is described in details in Chapter I:3-b (page 18), but the process can be schematized as shown in Figure II-1, from the synthesis of the organic molecules, followed by their self-assembly process and silica transcription, to the final steps of preparation.

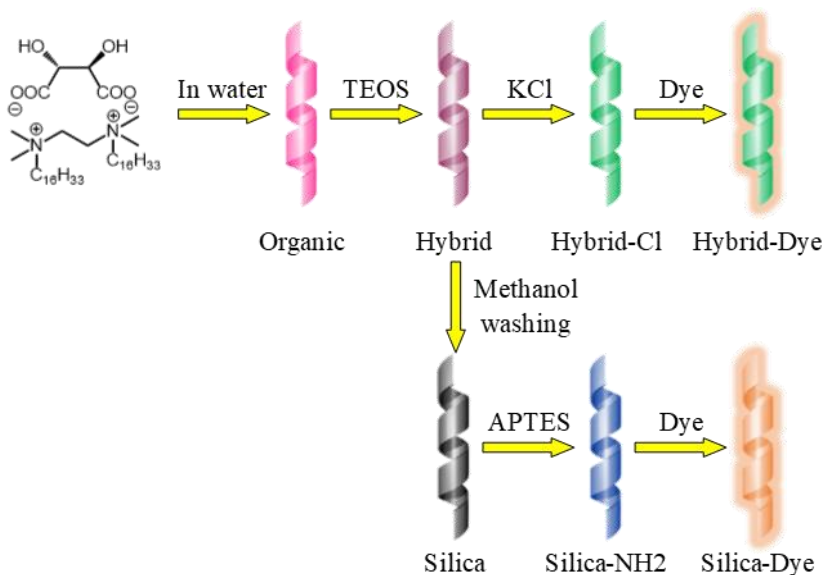


Figure II-1: Simplified scheme of the synthetic pathway toward helical nano-structures used in this study

In this project, a family of di-cationic surfactant molecules, 1,2-ethane bis(dimethylhexadecylammonium) (16-2-16), with various counter-ions (X), were used (Figure II-2). In particular, the nano-helices were formed from the molecular self-assemblies of 16-2-16 with di-anionic tartrate (16-2-16 tartrate).

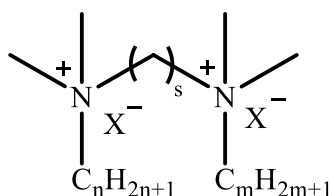


Figure II-2: Schematic model of gemini n - s - m X (in this project $n=m=16$ and $s=2$)

1-a. Synthesis of 16-2-16 tartrate

The synthesis of 16-2-16 tartrate is divided into 3 steps: the synthesis of the gemini moieties having bromide counter ions (16-2-16 Br), then the exchange from bromide to acetate, followed by another ion exchange from acetate to tartrate. Experimental details and NMR results can be found in Chapter VI:1-a (page 104).

1-a.i Synthesis of 16-2-16 bromide

The synthetic pathway to prepare the organic molecule has been described in precedent articles.⁴⁵ *N,N,N',N'*-tetramethylethylenediamine reacting with 1-bromohexadecane forms the desired compound (Figure II-3).

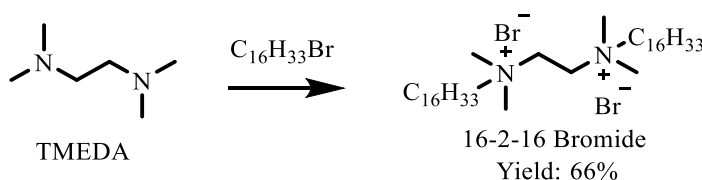


Figure II-3: Synthetic pathway leading to 16-2-16 bromide

This reaction leads to the formation of the amphiphilic part of the molecule. The product is verified by NMR spectroscopy.

1-a.ii Ion exchange to acetate

Once 16-2-16 Br is isolated, the bromide counter ion is exchanged by tartrate. However, the affinity between bromide and the gemini surfactant is too strong, and mixing 16-2-16 Br with tartaric acid does not lead to 16-2-16 tartrate. In order to increase the efficiency of the exchange, a first ion exchange is performed using silver acetate. In this approach, the silver bromide salt precipitates in methanol, shifting the equilibrium according to LE CHATELIER principle (Figure II-4). The ion exchange is verified using NMR spectroscopy.

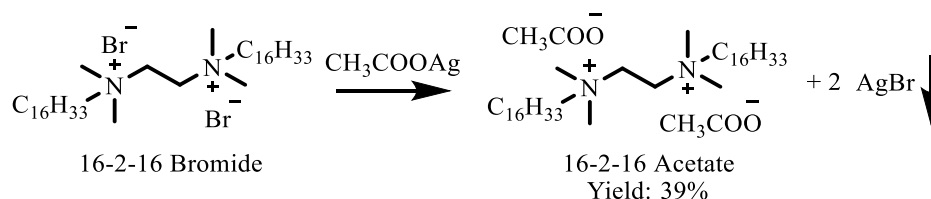


Figure II-4: Synthetic pathway to form 16-2-16 acetate

1-a.iii Ion exchange to tartrate

The final step in the synthesis of the molecule is a second ion exchange from acetate to tartrate. Slow addition of the 16-2-16 acetate solution in a mixture of methanol and acetone (with 1:9 ratio) into a tartaric acid solution is performed and followed by a 2h rest at room temperature (Figure II-5). After that, the product is precipitated in acetone, dried under vacuum and checked by NMR spectroscopy.

The purity of the product is essential for the reproducibility of the nano-structure formation, and a very small quantity of impurities (for example remaining 16-2-16 Br) may prevent a well-formed assembly. As the presence of Br^- cannot be detected by NMR, we mix a small amount of the product with some silver acetate in methanol. If the precipitate turn black after some time, it means that 16-2-16 Br is still present in the product.

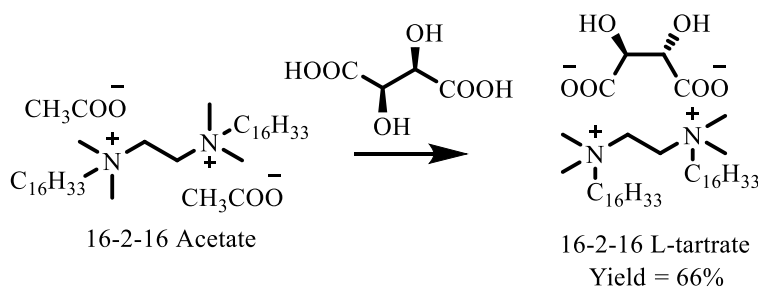


Figure II-5: Synthetic pathway to form 16-2-16 L-tartrate

1-a.iv Powder aging and purification

We observed that after several months on the shelf, samples of 16-2-16 tartrate will evolve and may not form the desired nano-helices once solubilized. To solve this problem, the powder is

dissolved in methanol, filtered through a membrane (200nm) and precipitated in acetone before drying.

1-b. Formation of silica coated chiral nano-structures

The formation of chiral silica nano-structures is done by coating organic nano-helices with a silica shell by sol-gel polycondensation.^{46,47}

1-b.i Preparation of nano-helices organic gel

The self-assembly of 16-2-16 tartrate is triggered by suspending 16-2-16 tartrate in ultrapure water and raising its temperature above the Kraft temperature (43°C for a 10mM solution) at a concentration of 1mM. Once the solid is fully dissolved, the temperature of the solution is lowered to 20°C. At this temperature, the molecules form self-assemblies into twisted or helical ribbons. The solutions are aged for 4 days. The detailed structure of the self-assembled structures thus obtained is described in Chapter VI:2 (page 115).

It is important to note that the morphology of these organic nano-structures evolves with time. After 2h, twisted nano-ribbons are obtained, whereas after 3-4 days the shape changes into nano-helices. At each stage of this evolution, those structures can be replicated into silica by starting the step of silica transcription at the desired time.

The morphology of the organic templates can be checked by transmission electron microscopy (TEM). However, due to the poor contrast of the molecules containing only carbon, nitrogen, oxygen and hydrogen, it is necessary to use a contrast agent as shown in Figure II-6. The alternative is to first let the nano-structures go through sol-gel transcription, then check them with TEM which allows us to avoid using the contrast agent because of the high electronic density of silica.

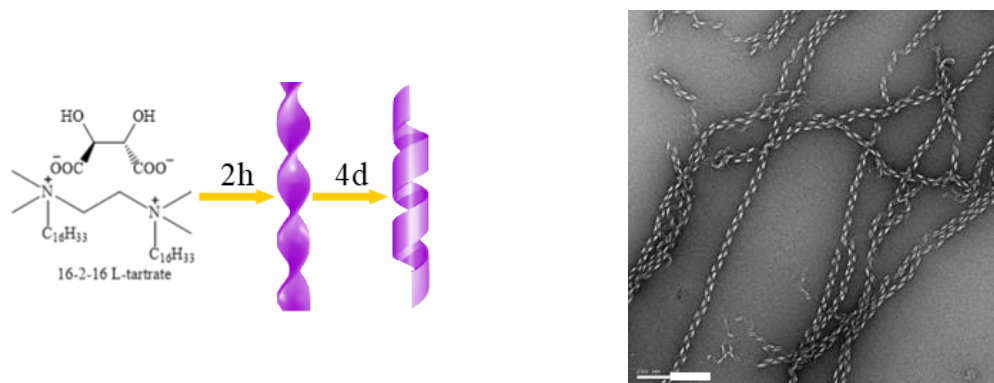


Figure II-6: Left: Scheme of the aging effect on the formation of nano-structures / Right: TEM picture of nano-helices formed after self-assembly of 16-2-16 D-tartrate using uranyl acetate as contrasting agent (120kV / scale bar: 200nm)

1-b.ii Polycondensation of the silica shell

This method allows to “freeze” the shape of self-assembled nano-structures by forming of a silica shell around the organic template. In other word, this shell will prevent the organic template to evolve with time by mechanically keeping it into a fixed shape.

The silica shell is achieved through polycondensation of tetraethylorthosilicate (TEOS), the method which has been optimized in the group since their first publication in 2002.⁴⁶ The method which was used during this thesis was published in 2014.⁴⁸ TEOS is first hydrolyzed in a 100 μ M solution of tartaric acid for 6-7h. After this hydrolysis, the TEOS solution is added to a tube containing the organic template (using the same enantiomer of tartaric acid in both solutions). The polycondensation takes place overnight at 20°C. Note that the reaction occurs exclusively around the helices because the quaternary ammonium of the template catalyzes silica condensation, thereby accelerating the reaction only at the surface of the organic helices. (Figure II-7).

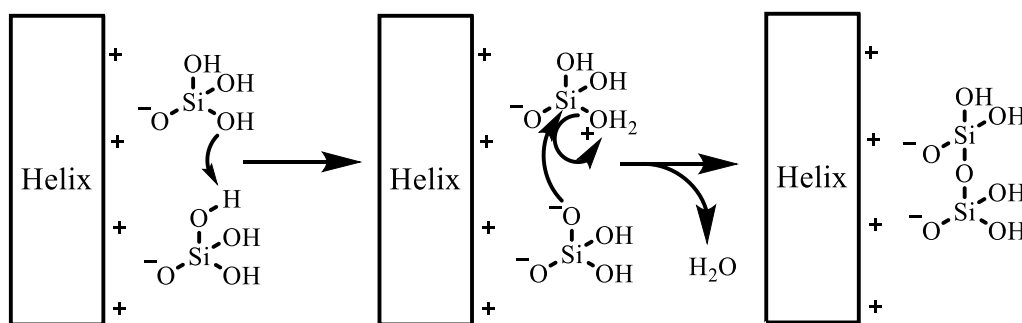


Figure II-7: Polycondensation reaction, negatively charged part of the molecule interact with gemini part of 16-2-16 tartrate

1-c. Purification and final steps

During the polycondensation reaction, the quantity of the TEOS is in large excess with respect to the organic template, as only less than 1 percent of TEOS is used to form the silica shell. The previous study showed that this excess was necessary for the good formation of the silica shell around the nano-helices. This means that after the polycondensation, there will be a large amount of non-reacted TEOS present along the silica nano-helices which needs to be washed away. After the washing, a tip sonication can be done to disperse the helices (20 pulses of 1s at 130W). Then the morphology of the structures is controlled using TEM (Figure II-8).

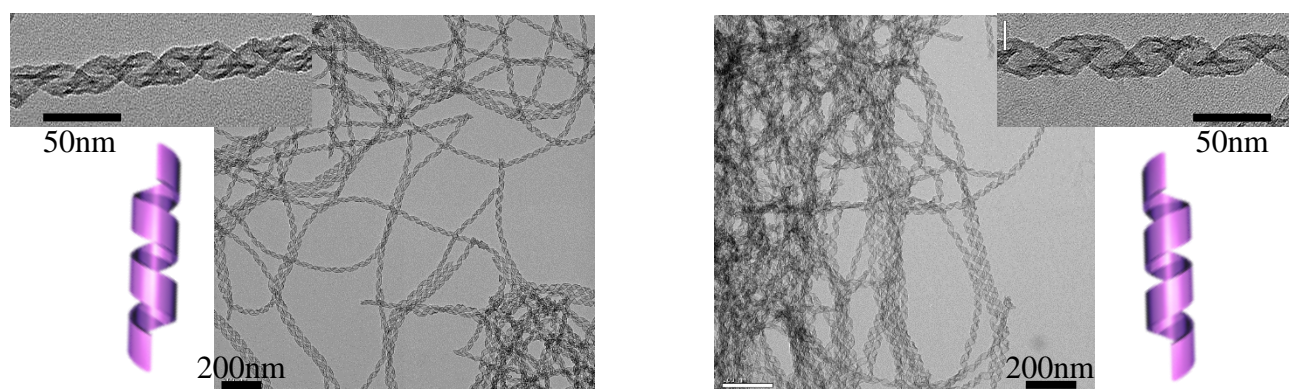


Figure II-8: TEM pictures of left and right handed silica nano-helices without staining (120kV)

The washing and dispersion processes were optimized to keep the organic template inside the silica helices (hybrid structures) or to remove it and retain only the silica nano-helices.

1-c.i Case of hybrids structures

In order to obtain hybrid helices, the mixture of TEOS and helices after the sol-gel reaction is washed using cold ultrapure water (4°C), in which the organic template has a very poor solubility in cold water, followed by short sonication (less than 10 sec). The washing is repeated at least 5 times (until pH > 5). *NB:* Afterward, hybrid samples are stored at 2°C until used.

At the end of this process, well dispersed hybrid structures are obtained. At this stage, the gemini confined inside the silica helices still has tartrate counter-ion. In some studies, it was necessary to replace tartrate by chloride in order to remove all molecular chirality from the sample. This was performed by washing the sample 5 to 8 times using a cold potassium chloride solution, followed by washing with cold water 8 times in order to remove the excess of potassium chloride. It is possible to check the total exchange (i.e. the absence of tartrate) by CD spectroscopy (Figure II-9).

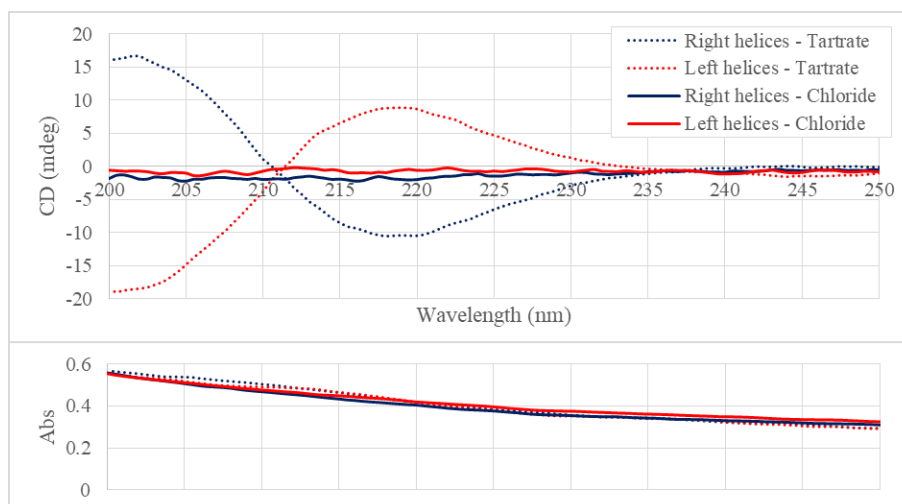


Figure II-9: CD (top) and absorption (bottom) spectra of hybrid nano-helices before and after ion-exchange to chloride ($C_{16-2-16X}=100\mu M$)

In Figure II-9, the CD spectra of gemini tartrate which are confined in the silica helices are compared with gemini for which the counter-ions are exchanged by chloride. L-tartrate shows a positive CD peak at 201nm and a negative CD peak at 219nm, while chloride does not show any signal. As we can see, both tartrate peaks (201nm and 219nm) disappeared after the exchange. Also note that the absorption of those peaks is extremely weak, making them difficult to see especially with light scattering due to the helices aggregates.

It is important to quantify the concentration of the colloidal suspension of the silica helices. To do so, 200 μ L of solution are lyophilized overnight and the powder is weighed. Later, we calibrate the volume of the tested sample to have a mass to volume ratio of 2mg/mL. However, it is important to note here that these dried helices cannot be re-dispersed into suspension because they aggregate strongly during the freeze-drying process.

1-c.ii Case of inorganic structures

In the case of inorganic helices, the purification process is similar except centrifugations are done at room temperature, methanol is used in place of water and the sample is heated up to 70°C to increase the solubility of 16-2-16 tartrate.

In order to make the silica surface reactive toward the chosen chromophores, functionalization of the surface is performed using (3-aminopropyl)triethoxysilane (APTES). This reaction is performed in methanol. Once this reaction is done, the samples are washed with methanol and the grafting is repeated again. After this reaction, we quantify the number of APTES on the surface of helices using NMR. The method for this quantification is described in 3-d (page 36).

2. Organic fluorophores

This section is dedicated to the description of the synthesis of different emissive chromophores suitable for grafting onto the surface of the helical nano-structures. In order to choose which molecule to use, we selected fluorophores with strong emission intensity, soluble in solvents which preserve the morphology of the nano-structures (such as ethanol or acetone) and endowed with the possibility to attach them to the amine group of the APTES grafted onto the surface. Additionally, we imagined that it would be interesting to have a molecule able to form excimers or J-aggregates, allowing these molecules to interact with each other in the excited state, facilitating the induction of the chiroptical properties.

2-a. Chromophores used without further synthesis

2-a.i *Commercials chromophores*

The synthetic chromophores prepared during this project are presented in the following pages. However, several others were used, including commercially available fluorophores: 1-pyreneacetic acid (**PAA**), 1-pyrenesulfonic acid sodium salt (**PSA**) and both enantiomers of 10-camphorsulfonic acid (**S-** or **R-CSA**) (structures shown in Figure II-10).

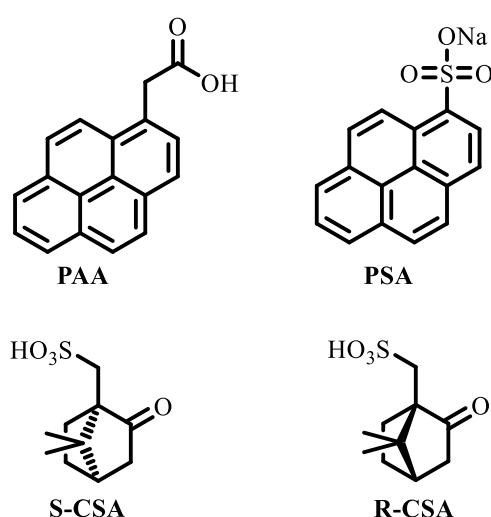


Figure II-10: Commercially available chromophores used during the project

2-a.ii Dissymmetric perylene chromophores

Several perylene derivatives were provided by Professor Angela SASTRE-SANTOS (University Miguel Hernández de Elche, Bioengineering Institute). These are dissymmetric perylene diimide derivatives which possess a carboxylic acid group to graft covalently onto amine functionalized silica surfaces, and others groups to improve their solubility in organic solvents including alcohols (methanol, ethanol) and acetone (structures shown in Figure II-11). Note that these molecules cannot be planer due to the steric hindrance of the R groups in the bay area and adopt twisted conformation that make them chiral.⁴⁹

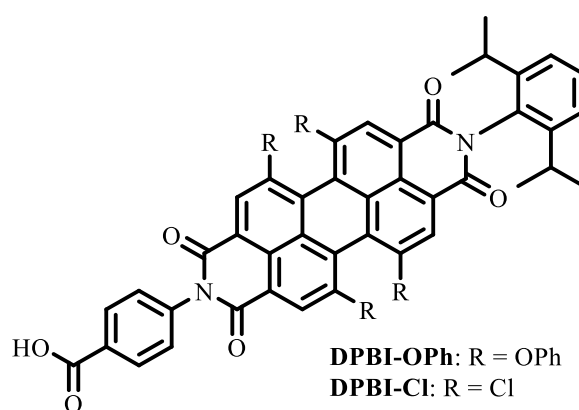


Figure II-11: Perylene derivatives synthesized in DYSMOL group

2-b. Synthesis of perylene and acridine derivatives

2-b.i Perylene

In order to incorporate perylene derivatives within the hybrid helix system, a symmetric derivative was synthesized. It was prepared in one step starting from perylene-3,4,9,10-tetracarboxylic dianhydride through hydration in basic medium and the precipitation of perylene potassium salt (**PTCTK**) which has a high solubility in water (Figure II-12). After reaction, the product is recovered by precipitation in a mix of isopropanol and acetone (1:1), then dried under vacuum.

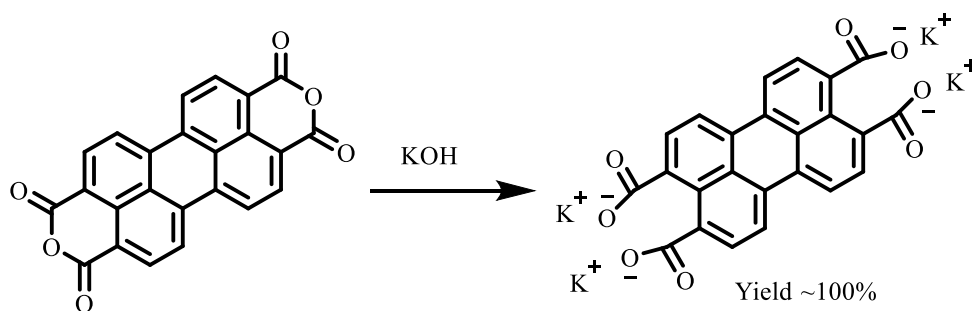


Figure II-12: Synthetic pathway leading to **PTCTK**

A chiral perylene derivative⁵⁰ was also synthesized in order to investigate the interactions between molecules already able to form chiral aggregates and the hybrid helical template. This molecule was prepared by attaching two phenylalanine onto **PTCTK** (Figure II-13) to give perylenebisphenylalanine acid (**PBPA**).

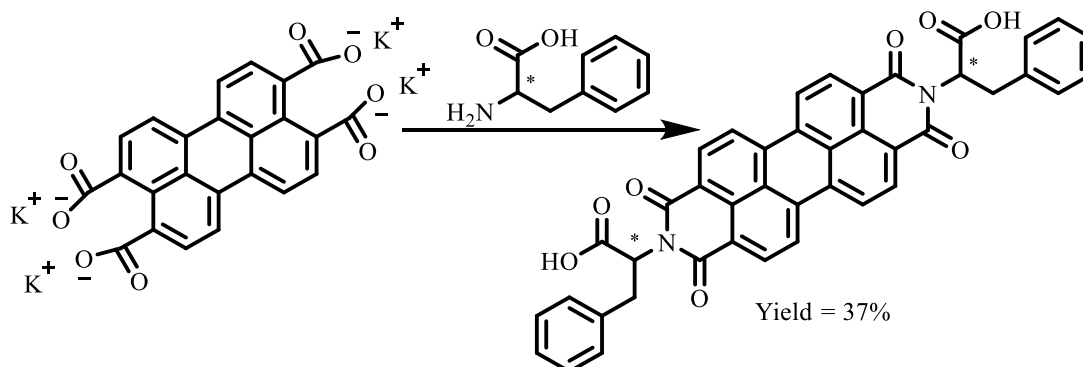


Figure II-13: Synthetic pathway leading to **PBPA**

PBPA has been previously reported to form chiral supramolecular structures upon dissolution in a mixture of dimethyl sulfoxide (DMSO) and water, showing a CD signal, whereas no chiroptical properties were detected before aggregation (in DMSO alone) as shown in Figure II-14 below.⁵⁰

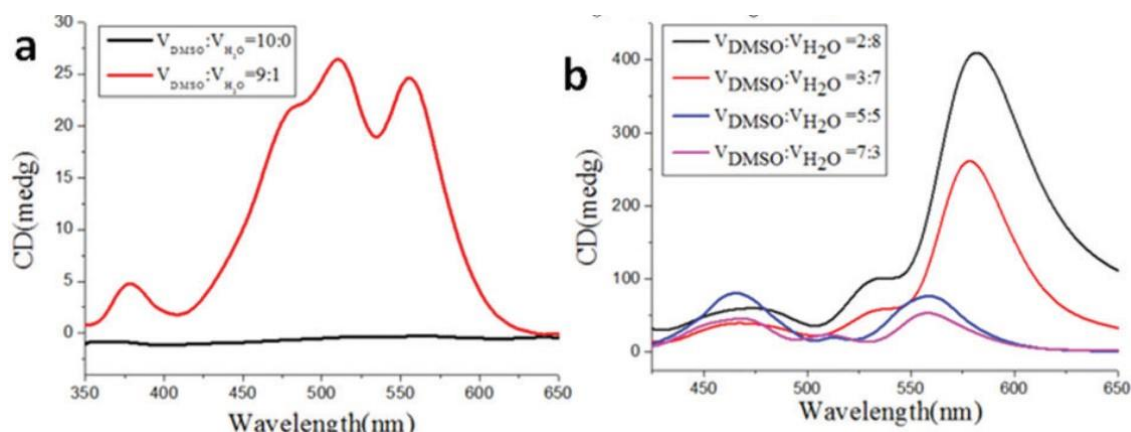


Figure II-14: Chiroptical properties of **PBPA** in various mixtures of DMSO/water⁵⁰ (Reprinted with permission from Chen W. et al., *PCCP*, **2018**, 20, 4144-4148. Copyright (2019) Royal Society of Chemistry)

2-b.ii Acridine

An acridine derivative, 4-(acridin-9-ylamino)butanoic acid (**ABA**) was prepared starting from acridone via 9-chloroacridine (Figure II-15). This molecule is interesting because after grafting, dimer formation could be favored through electrostatic interactions with a di-anionic molecule such as succinic acid.

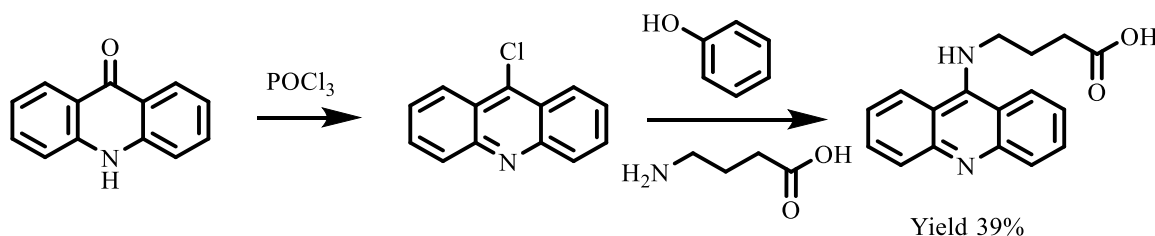


Figure II-15: Synthetic pathway leading to ABA

2-c. Covalent surface grafting

In the case of covalent grafting of the above mentioned chromophores onto inorganic helices, an activation step is necessary to allow formation of an amide bond between the amine group of APTES and the carboxylic acid of the chromophore. The activation of the acid is done through reaction with

ethyl chloroformate to form the corresponding mixed anhydride (Figure II-16). Other activation procedures have been tried using 1-ethyl-3-(3-dimethylaminopropyl) carbodiimide and *N*-hydrosuccinimide, but the reactivity of the anhydride leads to more efficient grafting.

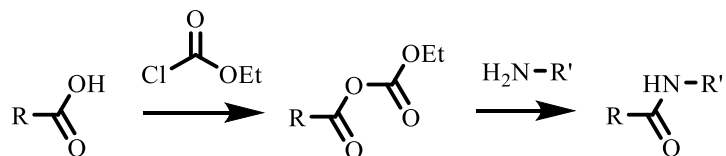


Figure II-16: Activation using ethyl chloroformate and reaction with amine group (*R* is the chromophore and *R'* is attached to the helix)

On the other hand, due to the reactivity of anhydride, we need to use an anhydrous non-nucleophilic solvents to prevent any side reaction. The grafting was conducted in freshly dried acetone in which APTES-helices were washed 5 times.

3. Characterization techniques

Three broad types of characterization technique were used during this study: molecular properties, electron microscopy and photophysical properties. The chemical structure of molecules used was verified using nuclear magnetic resonance (NMR) spectroscopy and mass spectrometry (MS). Supramolecular morphology was studied by transmission electron microscopy (TEM). Classical photophysical properties were measured using absorption (UV-Vis) and fluorescence spectroscopies, while the chiroptical properties were investigated using circular dichroism (CD) and circularly polarized luminescence (CPL).

3-a. Structural characterization

3-a.i Nuclear Magnetic Resonance (NMR)

Liquid state ^1H and ^{13}C NMR measurements were performed on a Bruker Avance I, II and III 300MHz SB spectrometer (Wissembourg, France), working at a frequency of 300.18MHz (for ^1H) or 75.48MHz (for ^{13}C), equipped with 5mm broadband BBFO probe. ^{13}C spectra were recorded using a one-pulse sequence with proton decoupling. An average of 256 scans were collected for each spectrum and a Lorentzian filtering function of 1Hz was applied. ^1H and ^{13}C chemical shifts are reported relative TMS using the residual solvent signal as reference. All ^1H spectra were recorded using a one-pulse sequence. An average of 16 scans were collected for each spectrum and a Lorentzian filtering function of 0,3Hz was applied.

3-a.ii Mass Spectrometry (MS)

Mass spectrometry measurement were performed on 3 machines: MALDI-TOF Voyager from ABSciex, ESI-Qtof QStar from ABSciex and GC-TOF FD AccuToFGC from Jeol.

3-b. Transmission Electron Microscopy (TEM)

For the supramolecular structures characterization, two different microscopes were used. The first one, for routine analysis is a LVEM5 from Delong Instruments (Brno, Czech Republic). The instrument is working with a Schottky field emission gun operating at a nominal acceleration voltage of 5kV, and a crystal of yttrium aluminium garnetis (YAG) used to convert the electronic image into a visible image, which is observed using a camera (Zyla 5.5 Scientific CMOS) through a microscope objective (Objectives Olympus M 4x or 40x). The second TEM is a CM120 from Philips, using a LaB6 filament at a working tension of 120kV. Images are collected through a camera CCD Ultra scan 1000.

TEM samples were prepared by deposition of 5-7 μ L of the sample onto a 400 mesh ultrathin carbon film copper grid (Electron Microscopy Sciences CF400-CU). In case of samples dispersed in water, an ozone treatment is performed prior deposition to make the grid hydrophilic (BioForce Nanosciences / UV-Ozone ProCleaner / 15min). 1min after the drop is applied onto the grid, the excess is removed by applying a piece of filter paper on the side of the grid, then the remaining solvent was dried by a gentle air flow until liquid is visible anymore. Note that for organic samples, a drop of uranyl acetate 2%_w solution is deposited on the grid before the drying of the remaining film to contrast the structures, then removed by the same way than before.

3-c. Photophysical properties: Absorption and Fluorescence

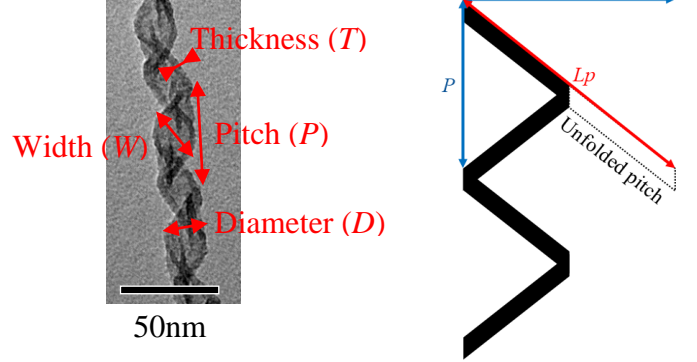
Absorption spectra were collected on a Varian Cary 5000 or on a Varian Cary 300. Fluorescence spectra were measured on a Fluormax-4 or on a Horiba Fluorolog-3 (Jobin Yvon) spectrophotometer.

3-d. Quantification of amine groups on the silica helices

The density of APTES grafted on the silica nano-helices (according to procedure described in Chapter II:1-c.ii on page 29) can be quantified using TEM and NMR spectroscopy by estimation of the surface area of the helices and quantifying the total amine present. This method was developed based on previously published studies and is described below.⁵¹

3-d.i Surface estimation of nano-helices

The surface of the helices is calculated from their pitch (P), diameter (D), width (W) and thickness (T). These parameters can be estimated from the TEM images as shown below. The length of a pitch along the twist (L_P) can be known by considering one unfolded turn, which is a trapeze as shown on right. Once L_P is known, it is easy to determinate the available surface on a turn (S_P) taking into account that the helices are hollow (due to the presence of the organic template during the polycondensation of silica), 4 surfaces are available for grafting. For the calculation of the silica volume in one turn (V_P) it is also necessary to know how many turns we have in a given mass of sample.



$$L_P = \sqrt{P^2 + (\pi D)^2} \quad (5)$$

$$S_P = 4WL_P = 4W\sqrt{P^2 + (\pi D)^2} \quad (6)$$

$$V_P = T \frac{S_P}{2} = 2TW\sqrt{P^2 + (\pi D)^2} \quad (7)$$

A usual sample will give the following values (Table 1):

Parameter	Value	Error
P	60nm	± 0.5 nm
W	30nm	± 0.5 nm
D	30nm	± 0.5 nm
T	3nm	± 0.5 nm
L_P	110nm	± 5 nm
S_P	13000nm ²	± 800 nm ²
V_P	20000nm ³	± 4500 nm ³

Table 1: Typical dimension of the helices used in this study

Considering a density of 2.4 for the silica, the estimated surface area is 280m²/g. Note that this value may be underestimated as all the calculations were done considering the surfaces as flat and non-porous.

3-d.ii Amine quantification

To quantify the total amine concentration, around 1mg of amine functionalized silica material is taken from the sample (around 500 μ L at 2mg/mL). The solvent is exchanged for ultrapure water by centrifugation (9800g / 20min) and washed. Then, the sample is dried by lyophilization and weighted using a micro balance. The powder is dissolved in precisely 2mL of deuterated water containing NaOH (pH>12) to destroy the inorganic structures. A known amount of 2,2,3,3-d(4)-3-(Trimethylsilyl)propionic acid sodium salt (Alfa Aesar / CAS: 24493-21-8) is added as reference (typically 250 μ g).

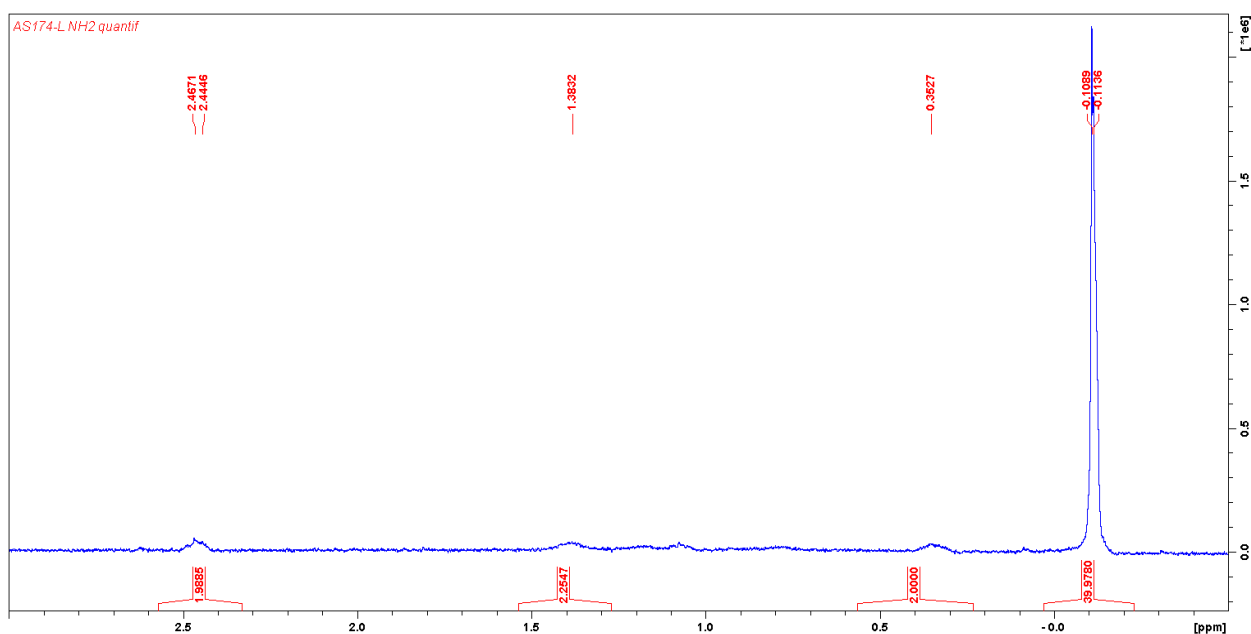


Figure II-17: Typical NMR spectra of APTES-Helices + TMSP ^1H NMR (300MHz, D_2O)

Based on the NMR spectra (Figure II-17) and the silica helix surface area as estimated above, the result of this quantification indicates 0.7-1.3APTES/ nm^2 (average value 1.10) which is consistent with previously established values in the group using ninhydrine quantification (0.7-1APTES/ nm^2).⁴²

3-e. Chiroptical properties

3-e.i Circular Dichroism (CD)

Circular dichroism (CD) spectra were measured on a Jasco J-815 (190-800nm) equipped with a xenon-mercury lamp and running under nitrogen atmosphere. The sample temperature is maintained between 4 and 20°C using a Peltier device (PFD-425S/15). All samples were stirred at 1000rpm during measurements, and every spectra was taken as the average of 4-10 scans.

CD spectrometers are similar in operation to absorption spectrometers. The difference is the addition of a linear polarizer and a photoelastic modulator (PEM) before the sample. The PEM acts as a quarter-wave plate, presenting different optical properties along the 2 axis. The fast axis barely affects the light while the slow axis (orthogonal to the fast axis) induces a delay of $\lambda/4$, thereby changing the linearly polarized (LP) light through the PEM into circularly polarized (CP) light (Figure II-18).

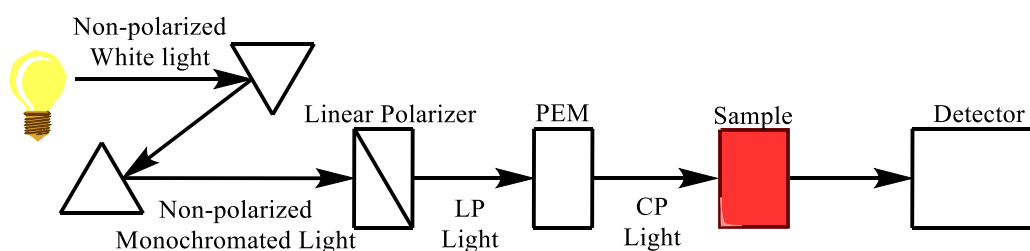


Figure II-18: Schematic representation of a CD spectrometer

The interesting property of a PEM is that it can be switched from a $+\lambda/4$ plate to a $-\lambda/4$, depending on the potential applied, making possible the generation of both left and right handed CP light. If the sample shows CD, its absorbance toward one of the polarizations will be higher than the other, which is detected. Note that the CD spectrometer gives the measurement of the ellipticity (θ_{abs} in millidegree) that the light would have after the sample upon linearly polarized excitation, as represented in the Figure II-19 below.

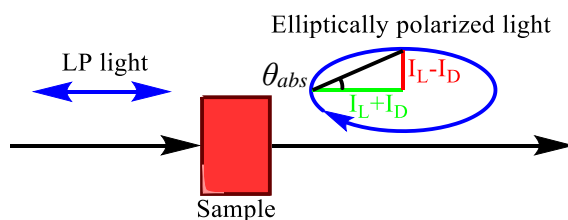


Figure II-19: Illustration of ellipticity due to CD

$$\tan(\theta_{abs}) = \frac{I_L - I_D}{I_L + I_D} \quad (8)$$

$$\Delta A_{CD} = A_L - A_D = \frac{4\pi * \theta_{abs} [mdeg]}{180 * \ln(10)} \approx \frac{\theta_{abs} [mdeg]}{32982} \quad (9)$$

With I_L and I_D intensity of left- and right-handed polarized light after the sample, A_L and A_D the absorbance of the sample toward left- and right-handed light.⁵²

Another interesting point is the ability of the PEM to behave as a half-wave plate or neutral, making it also possible to measure linear dichroism (LD). Herein care was taken to check the LD of each sample since, if a sample present a strong LD signal ($\Delta A_{LD} = A_{//} - A_{\perp} \geq 10^{-3}$), this would induce a significant artefact on the detected CD signal. Finally, the absorption dissymmetry factor (g_{abs}) is defined as shown below⁵² and can take values in between -2 and 2 (in which case the sample act as an ideal circular polarizer).

$$g_{abs} = \frac{\Delta A_{CD}}{A} \approx \frac{\theta_{abs} [mdeg]}{32982 * A} \quad (10)$$

In the case of chiral molecules in solution, the absorption dissymmetry factor is independent of concentration and wavelength. But when the molecules can aggregate, they may show concentration dependency as the chiroptical properties of monomeric chromophore and aggregates may be different.³⁷

3-e.ii Circularly Polarized Luminescence (CPL)

Circularly polarized luminescence (CPL) of the materials suspended in water or organic solvents were characterized using a Jasco CPL-300 with a xenon lamp (UXL-150S) and a head-on photomultiplier tube (Hamamatsu R376) as detector. The sample chamber is thermostated using a

Peltier device (PTC-517) from 4 to 20°C. Samples were stirred at 1000rpm during measurement and every spectra is the accumulation of 50-200 scans.

A CPL spectrometer is used to measure the difference of left to right circularly polarized light emitted by a sample. Note that most of the emitted light is non-polarized, and does not enter in the measure of the ellipticity (θ_{lum}) represented in the Figure II-20.

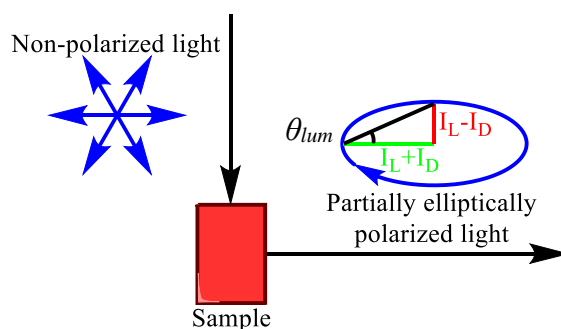


Figure II-20: Illustration of ellipticity in CPL

The measurement is similar to a CD spectrometer. However, the excitation light is depolarized, and the sequence of optics before the sample (linear polarizer then PEM) is reversed and placed after the sample, as shown in Figure II-21.

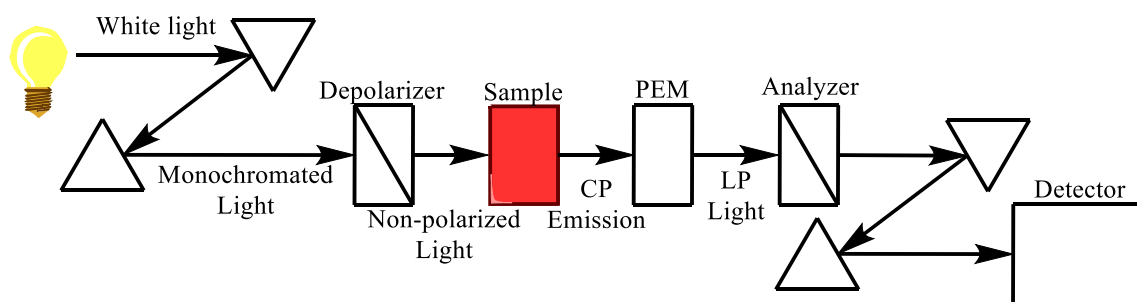


Figure II-21: Schematic representation of a CPL spectrometer

The luminescence from the samples will go through the PEM (acting as $\pm\lambda/4$ quarter-wave plate). The emitted CP signal are thus converted into LP light, which is analyzed by the linear polarizer after the PEM (called analyzer in this case). This allows the determination of both components of the circularly polarized light. Thanks to this two values, the ellipticity of the emitted light can be calculated using same equation than for CD (equation 8).

For each sample, LD and linearly polarized luminescence (LPL) were also measured as both of these properties would induce an artefact on the CPL measurement. This artefact is considered negligible if both LD and LPL are low ($\leq 10^{-3}$). Finally, the emission dissymmetry factor (g_{lum}) is defined as follows.⁵²

$$g_{lum} = \frac{\Delta I_{CPL}}{2I} \approx \frac{\theta_{lum}[\text{mdeg}]}{14324 * I[\text{V}]} \quad (11)$$

With I being the direct current detected as a result of the total luminescence of the sample.

CHAPTER III: INDUCTION OF CHIROPTICAL PROPERTIES TO NON-CHIRAL CHROMOPHORES

As discussed in Chapter I:3-a, several systems were reported in which achiral fluorophores show chiroptical properties due to a chiral environment. For this to occur, one approach is to add a chiral group to the fluorescent molecule which will induce a chiral supramolecular morphology upon aggregation. Casting a film of such molecules will induce the formation of aggregates from which high polarization of the emitted light is possible (dissymmetry factor up to 1.7×10^{-2}).⁵³

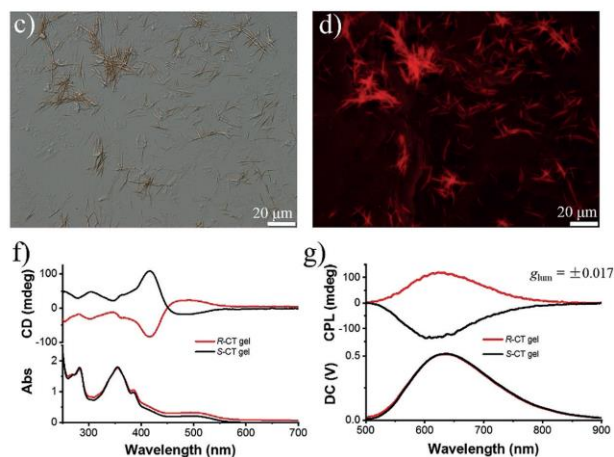


Figure III-1: Optical (top left) and fluorescence (top right) microscopy images and chiroptical spectroscopy (bottom) of casted film of chiral aggregates⁵³ (Reprinted with permission from Han, J. et al., *Angew. Chem. Int. Edit.* **2019**, 58, 7013-7019. Copyright (2019) Wiley-VCH)

It was also shown that chiral induction can be triggered by the use of a chiral template (chiral silica fibers) for nano-particles such as lanthanide oxides.⁵⁴ In this case chiral induction occurs from the environment during the synthesis of the particles. And a dissymmetry factor of the emitted light of 5×10^{-3} could be achieved.

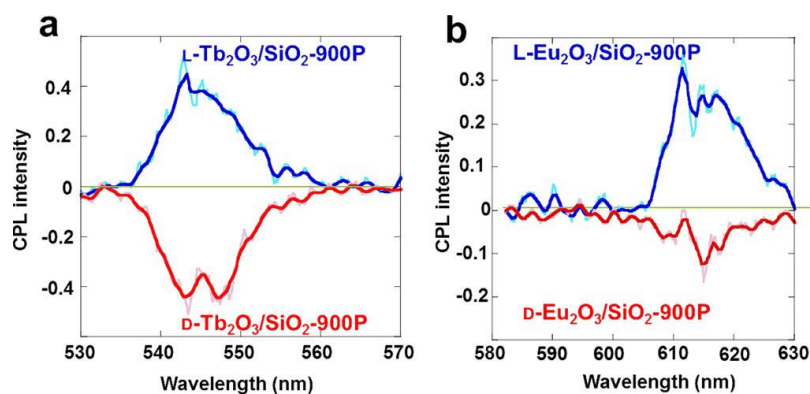


Figure III-2: Induction of CPL on lanthanide oxide nano-particles⁵⁴ (Reprinted with permission from Sugimoto, M. et al., *Chem. Eur. J.*, **2018**, 24, 6519-6524. Copyright (2019) Wiley-VCH)

1. Chirality induction from hybrid helices

In order to induce chiroptical properties to achiral fluorescent chromophores, we have chosen two approaches. The first approach is to incorporate the achiral dyes in the matrices based on hybrid organic/inorganic nano-helices.⁴¹ Previous examples developed in the CMA group with others types of molecules are described below.

1-a. Interaction between chromophores and hybrid helices (previous studies)

1-a.i Hybrid structure and interaction with external chromophores

After the polycondensation of tetraethylorthosilicate (TEOS) around the organic template of 16-2-16 tartrate (cf Chapter II:1-b, page 25), it is possible to retain the organic template inside the structure. By doing so, hybrid structures are formed, constituted of an organic helix with a silica shell around it (also having a helical shape), as shown in Figure III-3.

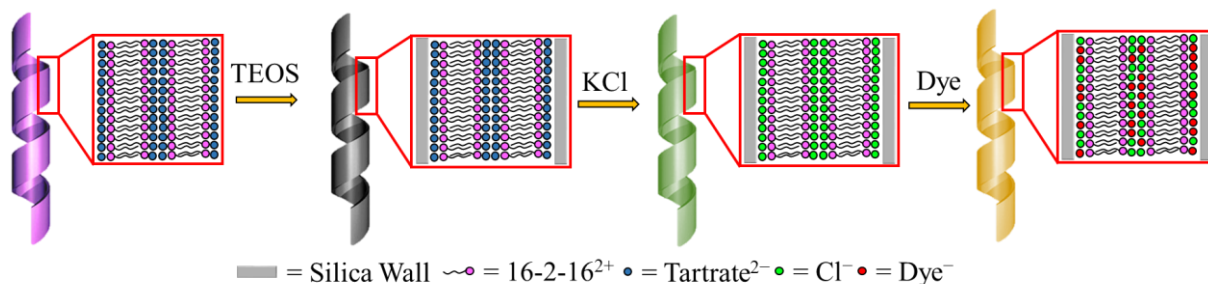


Figure III-3: Detailed structure of a hybrid helix

As previously reported,^{4,41} it is possible to keep the amphiphilic moieties of the organic template, the gemini 16-2-16, within this hybrid structures and only exchange the counter-ion without modification of the helical morphology. The scheme in Figure III-3 shows how tartrate counter-ions can be replaced by chloride to remove any molecule absorbing in the short wavelength range. As detailed in Chapter VI:2 (page 115), the previous study has shown that the organic template form a

double-bilayer structure.⁵⁵ It is not clear where the chromophore may insert itself, as several locations are possible.

1-a.ii Methyl-orange⁴¹

In the report by Dr. RYU et al., hybrid helices are shown to retain a chiral structure upon ion exchange from tartrate to bromide. Interestingly, the gemini moieties kept inside this hybrid structure also keep the chiral molecular conformation reminiscent of when the tartrate counter-ion was present. This conformational chirality creates a chiral environment which then affects the organization of anionic chromophore such as methyl-orange (**MO**) after a secondary ion exchange.

Upon the addition of hybrid helices containing bromide counter-ions into a solution of **MO** (40 μ M), the absorption peak of the chromophore at 505nm decreases while a new peak appears at 373nm, attributed to H-aggregates of **MO**. At the same time, the sample starts showing a CD signal with a split Cotton effect around the new absorption peak. This tendency continues until a ratio of 5:8 (**MO** to 16-2-16 Br⁻). Above this ratio, the absorption shifts slightly to the red and the CD signal drops by 85% (following the absorption shift) (Figure III-4).

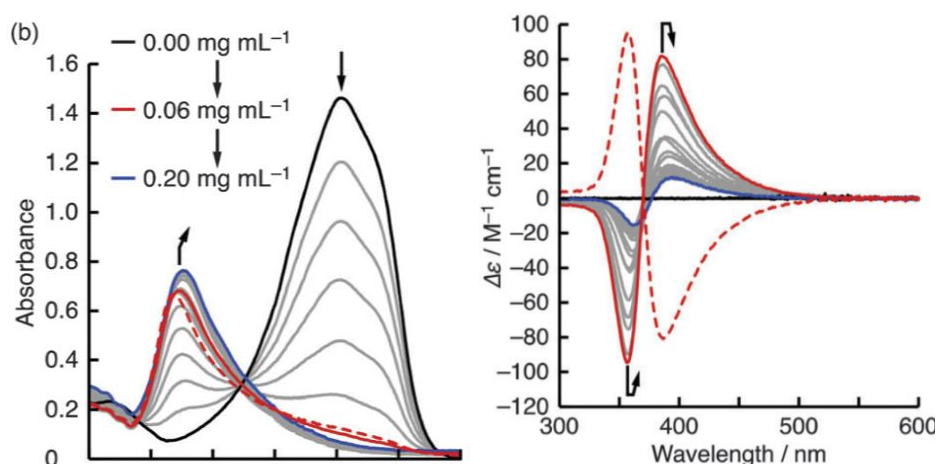


Figure III-4: Evolution of absorption and CD upon addition of hybrid helices bromide in **MO** solution (Reprinted with permission from Ryu, N. et al., *Chem. Comm.*, **2016**, 52, 5800-5803. Copyright (2019) Royal Society of Chemistry)

This behavior might be explained by the fact that until the optimum ratio of 5:8, two species are in the sample: free **MO** in solution and chiral H-aggregates in the organic part of the hybrid. At this

point, no free **MO** remains and the hybrid is saturated with **MO**. After the concentration of hybrid helices exceeds this ratio, a looser H-aggregate appears, with less chirality induction and a smaller shift to the blue.

This first result seems to be replicated using others ions, and this project began with the objective of developing a wide range of chiroptical materials.

1-a.iii Mono-atomic anions⁴

The chirality of mono-atomic species has been widely studied in the case of cations.^{3,54,56} However, anions are less studied as their absorption is at low wavelengths, overlapping with the absorption of the aromatic molecules generally used to prepare the chiral template. In the case of hybrid helices formed by gemini, the CD analysis of anions included in the system is possible, as no absorption is present above 190nm.

Following the previous procedure, several hybrid helices with halide counter-ion (chloride, bromide and iodide) were synthesized. For both hybrid helices bromide and iodide, a CD signal was detected, proving the chiral induction on the anion (Figure III-5).

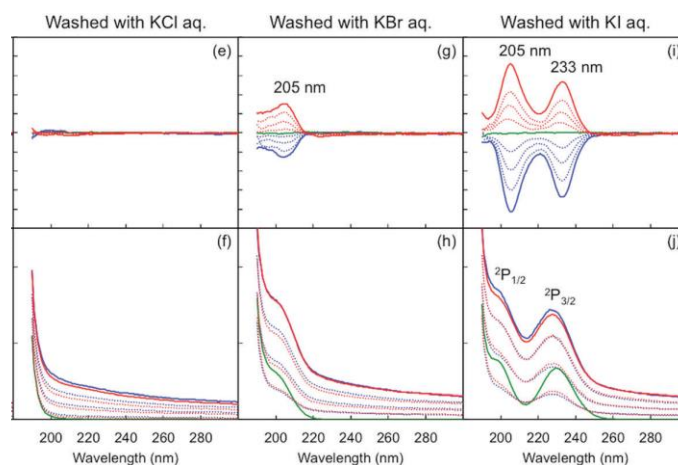


Figure III-5: Highlighting of chiral induction on mono-atomic anions⁴ (Reprinted with permission from Okazaki Y. et al., *Chem. Comm.*, **2018**, 54, 10244-10247. Copyright (2019) Royal Society of Chemistry)

To go further, the hybrid helices with halide counter-ions were used as a chiral reactor for the oxidation of the iodide and the formation of a cuprous iodide. Using hydrogen peroxide and copper sulfonate, the induction of chirality in the reaction product was obtained, despite the absence of any

strong interaction between the product and the hybrid system (Figure III-6). This proves the possibility to induce chirality to various types of molecules using this hybrid system. In order to obtain a wide range of CPL, the use of organic fluorescent molecules appears to be the best choice due to their commercial availability.

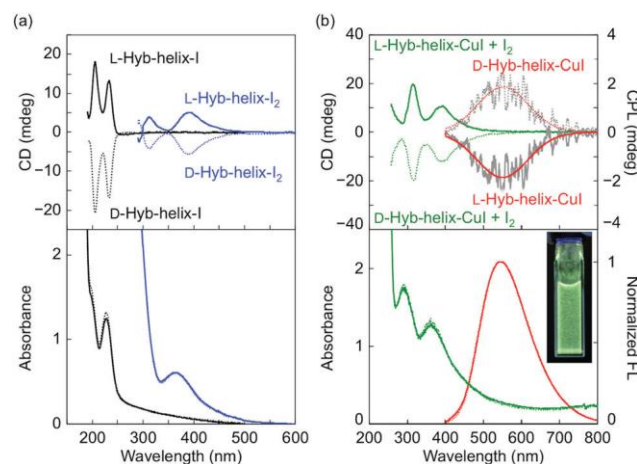
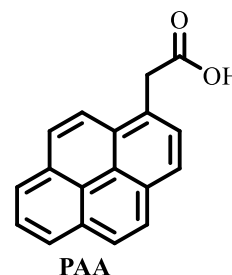


Figure III-6: Chiral induction on I_2 (left) and CuI (right)⁴ (Reprinted with permission from Okazaki Y. *et al.*, *Chem. Comm.*, 2018, 54, 10244-10247. Copyright (2019) Royal Society of Chemistry)

1-b. Interaction between organic fluorophore and hybrid helices (new study)

1-b.i Using pyreneacetic acid

1-Pyreneacetic acid (**PAA**) is soluble in ultrapure water at a concentration of 400 μ M due to the deprotonation of the acid in neutral pH. In this condition, it is possible to make use of ionic interaction between the chromophore and the cationic surfactant as explained in Chapter III:1-a.i. The addition of helical hybrid structures into a solution of **PAA** gives rise to a CD signal shown in Figure III-7.



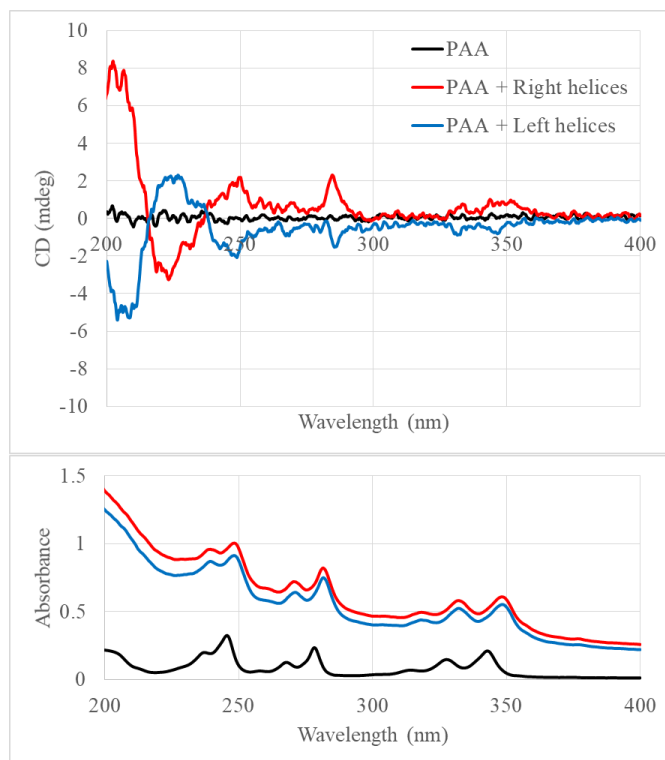


Figure III-7: CD (top) and absorption (bottom) spectra upon addition of hybrid helices (170 μ M) in a solution of PAA (50 μ M)

Two phenomena can be seen during this experiment. First, the appearance of CD signals corresponding to every absorption band of the pyrene derivative. Second, a bathochromic shift of the absorption bands. The absorption bands being due to $\pi\pi^*$ transition, such a shift in the absorption signal can be attributed either to the stacking of PAA molecules (in a J-aggregates-like geometry), or to an increase of the environmental polarity, which may be due to the proximity of cations from the gemini. This polarity increase might also be due to hydroxyl groups from residual tartrate counter ions, which might be the origin of the CD peaks at 205 and 225nm. Additionally, as mentioned above, CD signals can be detected from $S_0 \rightarrow S_2$, $S_0 \rightarrow S_3$ and $S_0 \rightarrow S_4$ transitions with the following dissymmetry factors after removing the part of the scattering contribution from the absorbance (Table 2).

Transition	PAA + Left helices	PAA + Right helices
$S_0 \rightarrow S_2$ ($\lambda = 353\text{nm}$)	-0.5×10^{-4}	1.0×10^{-4}
$S_0 \rightarrow S_3$ ($\lambda = 285\text{nm}$)	-1.4×10^{-4}	2.1×10^{-4}
$S_0 \rightarrow S_4$ ($\lambda = 247\text{nm}$)	-1.2×10^{-4}	1.1×10^{-4}

Table 2: Dissymmetry factors on the different transitions of PAA in hybrid helices

In theory, only the sign should differ between two enantiomeric systems. Here, a large difference in the values can be seen, this might be due to the kinetics of the system. The experiment were done considering the equilibrium would be achieved instantaneously. However, if the diffusion of molecules in the solution is very fast, the diffusion inside the hybrid nano-helices, due to the confinement of the molecules, may be slow. In order to verify this hypothesis, the time dependent dissymmetry factor was evaluated (at a wavelength for which only aggregated **PAA** absorb light), results are shown in the figure below, confirming an important time dependency of the chiroptical properties of the samples in the first hours after mixing.

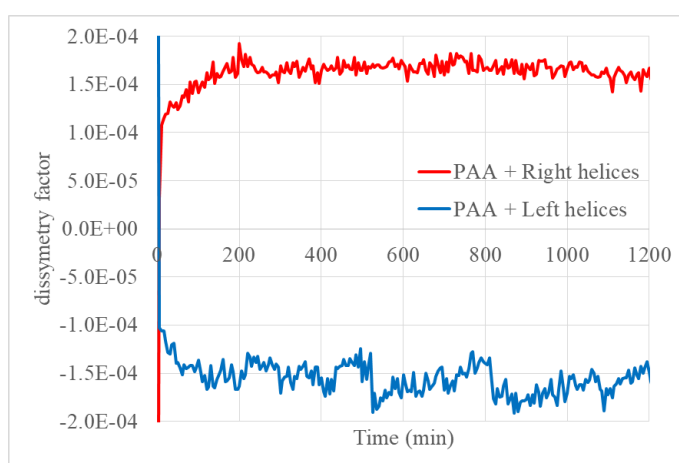


*Figure III-8: Time dependency of dissymmetry factor in a solution of hybrid helices (100 μ M) upon addition of **PAA** (100 μ M) after 5min (scan at 282nm)*

Figure III-8 shows two tendencies. First, a rapid increase can be observed immediately after the addition of **PAA**. This rapid increase come from a chirality induction from the gemini to individual **PAA** molecules. This process is followed by slow increase which is attributed to the chiroptical effect of aggregated **PAA**. It is important to note that these conclusion can only be done because the measure is done at a wavelength which shows almost no absorption of the monomer in solution, but does for the molecules in the hybrid (here at 282nm)

Previous experiments were performed with a ratio of 1 to 1 between the chromophores and the organic gemini inside, however in order to optimize the solution, the evolution of chiroptical properties with this ratio was measured (Figure III-9).

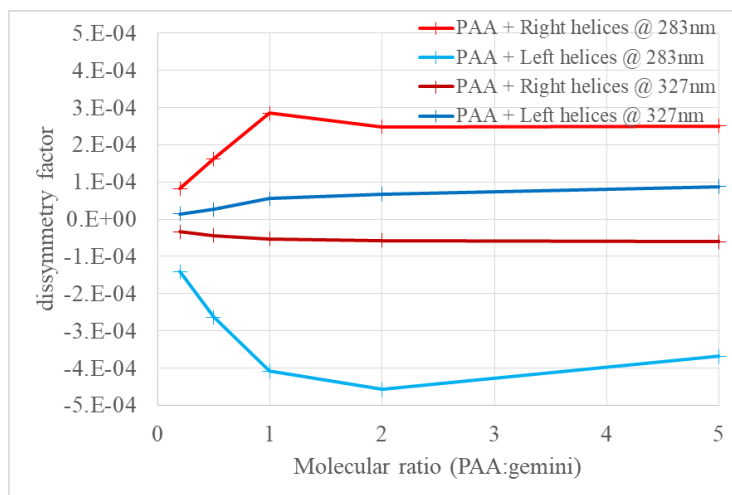


Figure III-9: Evolution of the dissymmetry factor at 2 different wavelength (283nm and 327nm) with the ratio **PAA** to **gemini** ($[gemini]=100\mu M$ except for ratio of 5:1 where $[gemini]=40\mu M$) 2 hours after mixing

The dissymmetry factor increases until a ratio of 1:1, then remains stable. This is due to the fact that below a 1:1 ratio, most of the molecules are alone in the hybrid, so their chiroptical properties will only come from an induction from the chiral **gemini** to the isolated chromophore. However, when the concentration increases, aggregates will be formed inside the hybrid. These aggregates may be more sensitive to chirality induction due to their supramolecular morphology. The **gemini** being dicationic and the **PAA** mono-anionic, the dissymmetry factor was expected to increase until a ratio of 2:1, but it remain stable above 1:1. The reason for this phenomena is still under investigation.

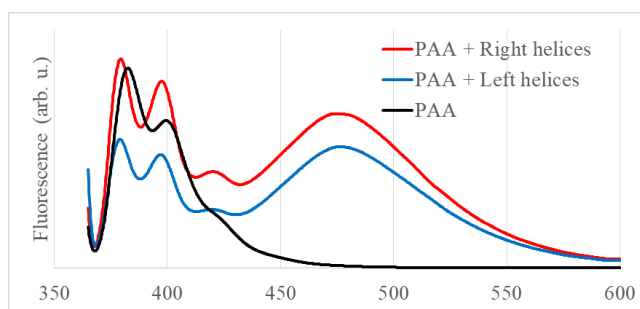


Figure III-10: Fluorescence spectra of $200\mu M$ **PAA** + $100\mu M$ hybrid helices under excitation at 340nm

Using fluorescence spectroscopy (Figure III-10), a new peak can be observed at 478nm is assigned to excimer emission, this confirming an interaction between the **PAA** molecules inside the hybrid structure. Note that the blue shift in this case is due to a calibration of the spectrometer between the measurements. The ratio of excimer to monomer seems higher in the case of left helices, this

difference might explain why the dissymmetry factor was also higher (see Figure III-9): due to more chiral aggregation of the **PAA** molecules in this case. CPL spectroscopy did not detect a significant signal, indicating that the chirality induction is lost in the excited state.

1-b.ii Using pyrenesulfonic acid sodium salt

Considering that **PAA** gave promising results, it may be interesting to use a molecule with different anionic group in order to compare how important the strength between the chromophore and the hybrid is. Many pyrene derivatives are commercially available and we choose to use 1-pyrenesulfonic (PSA) acid to compare with **PAA**. We choose **PSA** for its higher hydration free energy than **PAA**, which may allow it to replace chloride ion with higher efficiency.⁴ The addition of hybrid helices in a solution of **PSA** give the spectra shown in the Figure III-11, in order to avoid kinetic effects, samples were prepared 1h before analysis.

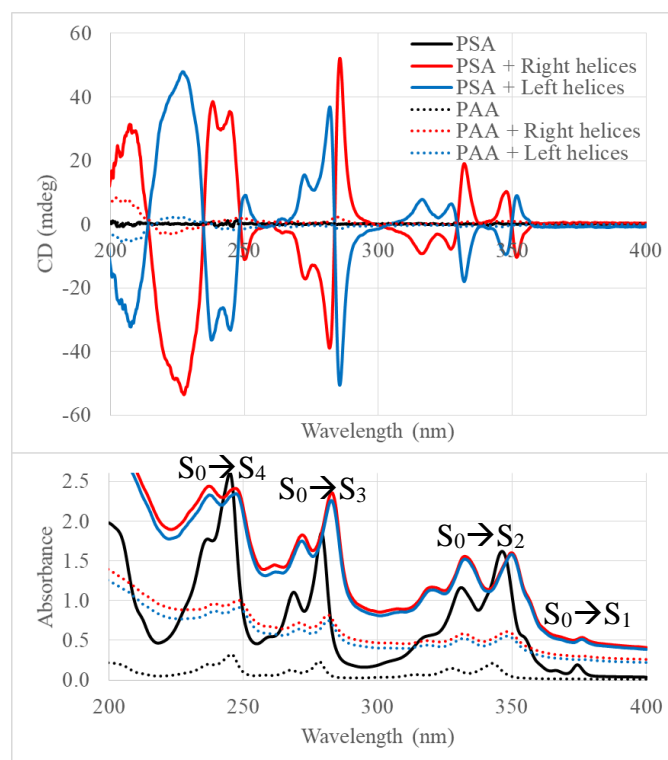
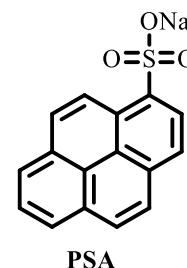


Figure III-11: CD (top) and absorption (bottom) spectra upon addition of hybrid helices (100 μ M) in a solution of **PSA** (50 μ M) in comparison with **PAA**

The interaction between **PSA** and hybrid helices have a similar shift on absorbance than for **PAA**, but with smaller value as shown in Table 3.

Transition	PAA	PSA
$S_0 \rightarrow S_1$	a	+1.5nm
$S_0 \rightarrow S_2$	+5nm	+2.5nm
$S_0 \rightarrow S_3$	+6nm	+3.5nm
$S_0 \rightarrow S_4$	+2.5nm	+0.5nm

Table 3: Peak shift upon integration of **PAA** and **PSA** into hybrid helices (a: peak not detected)

The smaller shift might be due to a lower sensitivity of **PSA** toward polarity difference than **PAA** as the negative charge will be more delocalized with sulfonate group than carboxylate. On the CD induction, we can see a much higher impact compare to **PAA**, confirming the importance of the hydration free energy of the chromophore for the replacement of chloride counter-ion and for the formation of chiral aggregates, as shown in the Table 4.

	PAA + Left helices	PAA + Right helices	PSA + Left helices	PSA + Right helices
$S_0 \rightarrow S_2$	-0.5×10^{-4}	1.0×10^{-4}	3.1×10^{-4}	-3.6×10^{-4}
$S_0 \rightarrow S_3$	-1.4×10^{-4}	2.1×10^{-4}	-18.9×10^{-4}	18.6×10^{-4}
$S_0 \rightarrow S_4$	-1.2×10^{-4}	1.1×10^{-4}	-10.6×10^{-4}	11.3×10^{-4}

Table 4: Comparison of dissymmetry factors between **PAA** and **PSA** into hybrid helices

Note that if $S_0 \rightarrow S_1$ transition is visible on absorption spectra, no obvious signal is seen of CD for this transition, which is due to the very low absorption of this band. In order to compare with **PAA**, the kinetic of the exchange from chloride to **PSA** was also checked, by scanning the same sample immediately after mixing, then after 1h and finally after 4 days. In order to minimize the dissolution of the organic template into the aqueous solution, the samples were kept at 2°C during this time.

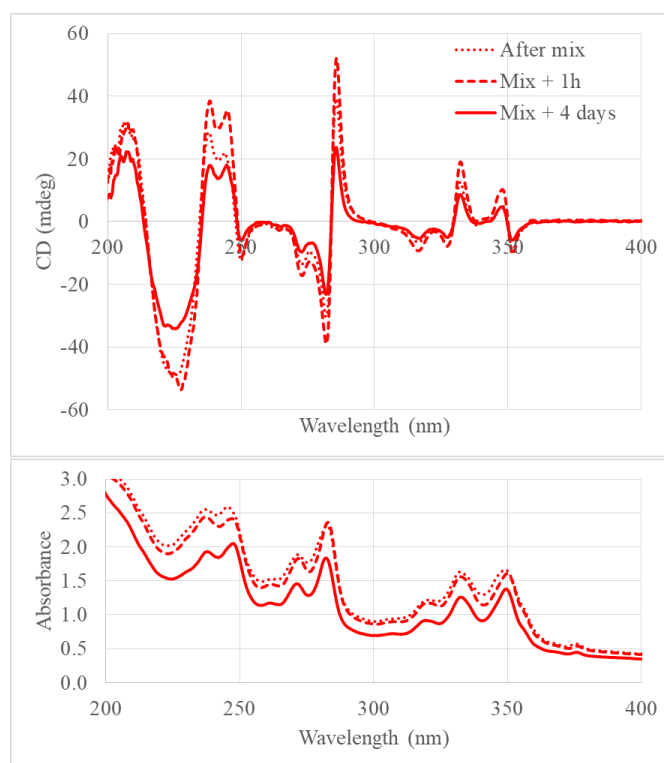


Figure III-12: Evolution CD (top) and absorption (bottom) of the mix **PSA** ($50\mu\text{M}$) with right hybrid helices ($100\mu\text{M}$) with time

During the first hour, we can see a small increase of the CD signal without noticeable change in the intensities of the absorption peaks, then, after 4 days, the CD signal decreases. However, when examining the dissymmetry factor, no evolution is noticed after 4 days. Based on the evolution of the absorption spectra, it is likely that part of the sample was lost during transfer, decreasing the concentration. We deduced that the exchange of the chloride counter-ion to **PSA** ($< 60\text{min}$) is faster than with **PAA** (around 200min).

As before, the chirality may come from two sources, either the chirality is induced at a molecular level from the gemini cation, or it comes from the chiral supramolecular organization of **PSA** inside the hybrid helical nano-structures. In order to know which is prevailing, the CD of a solution of hybrid helices was measured upon addition of **PSA**, the results are presented below. (Figure III-13)

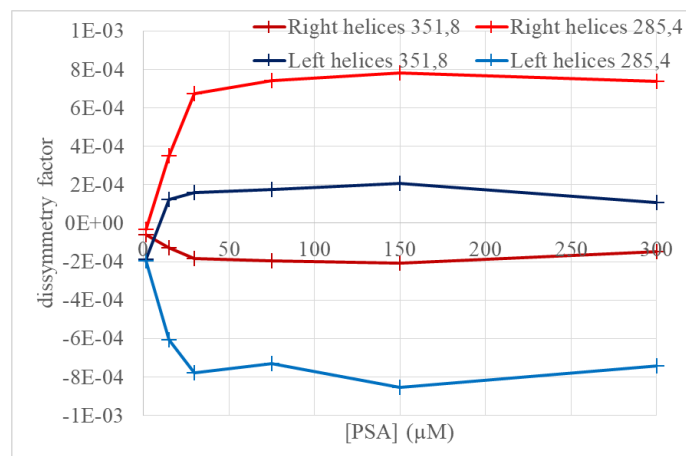


Figure III-13: Evolution of the dissymmetry factor of a solution of hybrid helices (150 μ M) upon addition of PSA at 351.8nm and 285.4nm

Two tendencies can be clearly identified in this spectra, upon first additions and until a 1:5 molecular ratio of **PSA** to gemini (i.e. $[\text{PSA}] < 30\mu\text{M}$), the dissymmetry factor increases strongly, showing the chirality is mainly induced to the chiral aggregate of chromophores, as if the chirality was mainly induced from the gemini molecules, the dissymmetry would stay constant upon addition. Once a 1:5 ratio is reached, a plateau is observed until reaching a 1:1 ratio (i.e. $30\mu\text{M} < [\text{PSA}] < 150\mu\text{M}$), this is due to the fact that every molecule forms pair and only the concentration of aggregate increase, so CD and absorbance increase together, without changing the dissymmetry factor. Above a 1:1 ratio (i.e. $[\text{PSA}] > 150\mu\text{M}$), a small decrease is observed which may indicate that at this ratio, the exchange sites are saturated. All excess of **PSA** remain in solution, increasing the absorbance without any further change in the CD, inducing a decrease of the dissymmetry factor.

A surprising fact is the ratio at which the second change of tendency appear, since **PSA** is a mono-anion and gemini is a bi-cation, a ratio of 2:1 was anticipated. The reason for this may be the inside structure of the organic template constituting the core of the hybrid system. As described in Chapter VI:2-c (page 116), the 16-2-16 tartrate forms a double bilayer, and if the tartrate in the interlayer can be replaced by chloride as demonstrated previously (see Chapter II:1-c.i, page 28), a bigger anion like **PSA** might not be able to exchange at this position. It is also possible that, also due to the size of **PSA**, every chloride ion cannot be replaced and only half of them do. In order to discriminate between these hypotheses, fluorescence spectra were performed with a 1:1 ratio of **PSA** to gemini (Figure III-14).

If the second hypothesis is true, then no excimeric emission should be observed as the molecules would not be able to stack together.

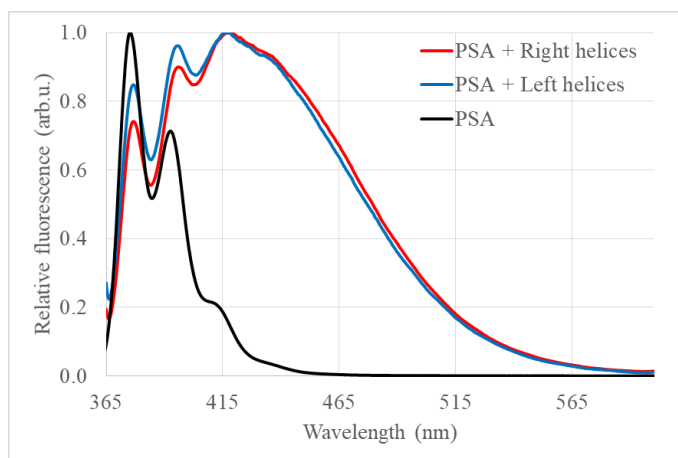


Figure III-14: Fluorescence spectroscopy of **PSA** ($150\mu\text{M}$) with and without hybrid helices ($150\mu\text{M}$) upon excitation at 340nm

As shown above, the addition of hybrid helices in a solution of **PSA** lead to the appearance of an excimer fluorescence peak around 440nm , proving that **PSA** molecules are able to stack together inside the hybrid, so that it is not possible to have a chloride anion between each **PSA** molecules. In order to confirm the hypothesis behind the change of tendency observed in CD, fluorescence dependency toward **PSA** concentration was performed (Figure III-15).

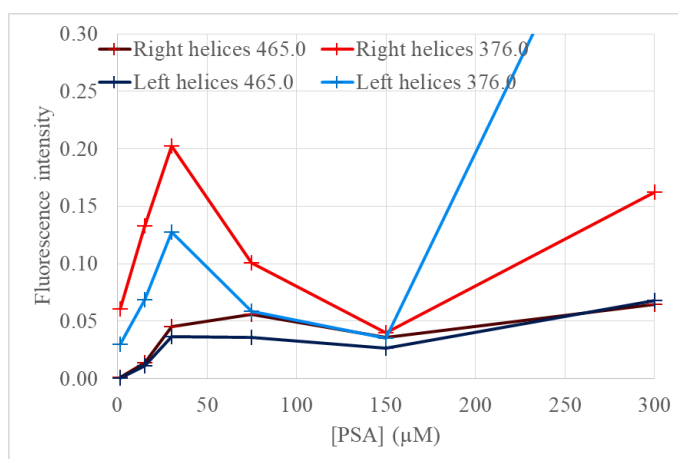


Figure III-15: Evolution of fluorescence intensity (at 465nm and 376nm) upon addition of **PSA** in a solution of hybrid helices ($150\mu\text{M}$) upon excitation at 340nm

In this spectra, the two lights curves show the fluorescence of the peak attributed to the monomer (emitting at 376nm) while darker curves show an excimeric fluorescence (emitting at 465nm) due to

PSA aggregates. Upon addition of **PSA** we can confirm the three tendencies we had before. At low concentration, the amount of both free monomer and aggregated chromophore increases, then the monomer disappears, as every added molecule will aggregate with another one already present in the hybrid. Then, beyond the 1:1 ratio, the monomeric emission increases again, but this new emission does not come from the hybrid helices anymore, but from chromophore in solution. The observation of a CD signal with dissymmetry factor above 10^{-3} and the appearance of emission from excimer is promising for circularly polarized emission.

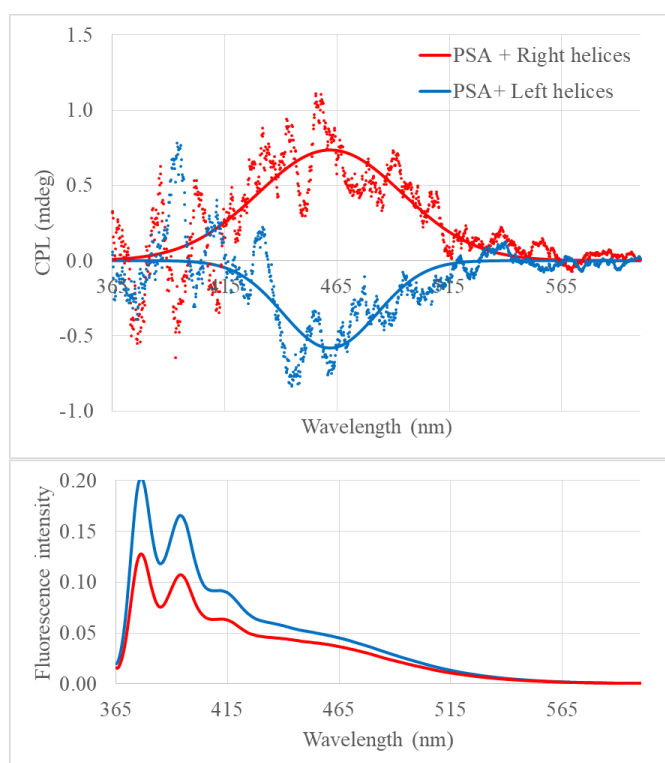


Figure III-16: CPL (top) and fluorescence (bottom) of a 30 μ M PSA solution in presence of 150 μ M hybrid helices upon excitation at 340nm

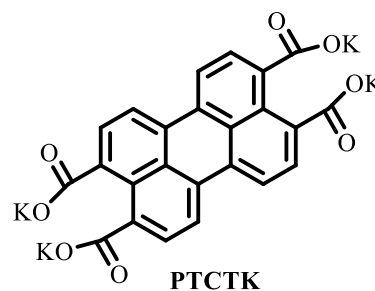
As shown on Figure III-16, the chiral induction is not confined to the ground states, but also affects the excited species. The raw CPL data (dotted line) was fitted using Voigt's function (solid line). In this case a dissymmetry factor in emission of 12×10^{-4} is measured in the sample containing **PSA** with right helices at 472nm (-10×10^{-4} with left helices). As expected, the CPL comes exclusively from the excimer emission, proving that the chiroptical properties in excited state come from chiral aggregation of chromophores.

However, the CPL signal was detected only at 1:10 and 1:5 ratios of **PSA** to hybrid helices, with similar values of dissymmetry factor. In case of the lower concentration of fluorophores, we can suppose that the chromophore aggregation was too low to allow a chiral induction. On the contrary, the reason why CPL disappears at higher concentration of **PSA** is unclear. However, based on the fluorescence decrease with concentration increase (Figure III-15) we can suppose that with the aggregation of chromophores a quenching effect occurs, decreasing the fluorescence and making it impossible to detect CPL.

Based on these results, we can conclude that the association between the chromophore and the assembly plays a major role to obtain efficient chiral induction. Additionally, we can see that higher absorption dissymmetry factors do not necessary mean that the CPL is going to be better, as side effects such as aggregation induced quenching may overcome it.

1-b.iii Using perylene-tetracarboxylic potassium salt

Perylene derivatives were used for covalent grafting (see in part 2- of this chapter), and we decided to also include a symmetrical derivative into the hybrid helices. To do so, perylene-3,4,9,10-tetracarboxylic acid tetra potassium salt (**PTCTK**) was chosen as it present 4 carboxylate functions able to complex with the gemini cation, also making it highly soluble in water.



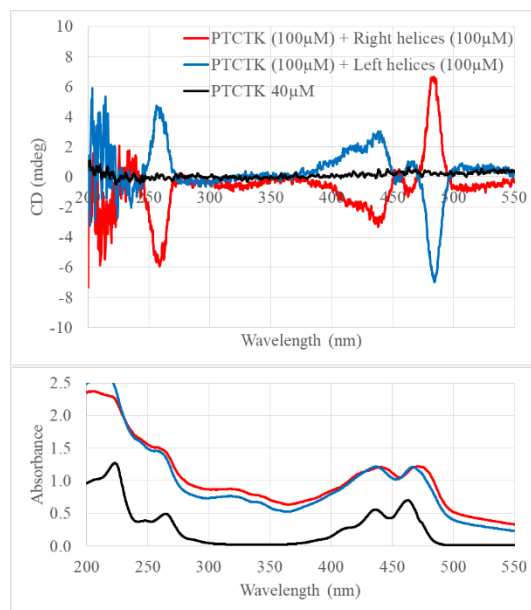


Figure III-17: CD (top) and absorbance (bottom) of PTCTK solution upon addition of hybrid helices

From the absorption spectra in Figure III-17, we can see a bathochromic shift of the $S_0 \rightarrow S_1$ transition, which is consistent with effects detected using **PAA** and **PSA**. Chiral induction is also detected on both $S_0 \rightarrow S_1$ and $S_0 \rightarrow S_2$ transitions, with a maximum for the dissymmetry factor of 2.0×10^{-4} on right-handed helices at 438nm (-2.7×10^{-4} for left-handed helices). In order to verify the optimal ratio of **PTCTK** to gemini, the measurement of the dissymmetry factor in function of this ratio was performed (Figure III-18).

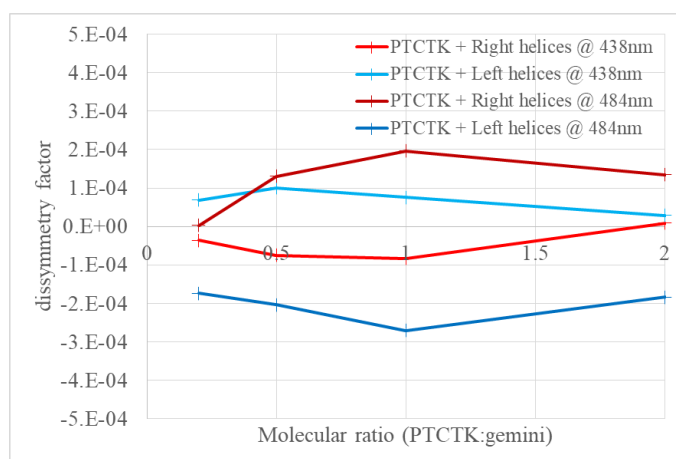


Figure III-18: Evolution of the dissymmetry factor at 2 different wavelengths (438nm and 484nm) with the ratio **PTCTK** to gemini (with $[gemini]=100\mu M$)

This analysis show the same tendency at the low ratio of **PTCTK** to gemini. However, between ratios of 1:1 to 2:1, the dissymmetry factor already begins to decrease without showing a plateau.

Based on this result, we verified if the same phenomena can be observed in fluorescence spectroscopy (Figure III-19).

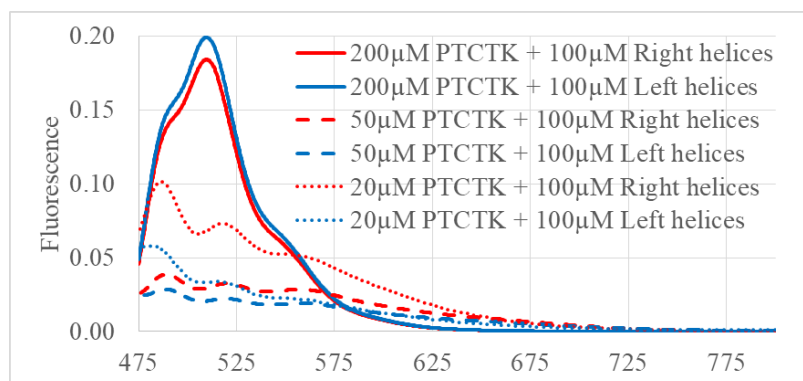


Figure III-19: Fluorescence spectra of **PTCTK** in hybrid helices with different ratios upon excitation at 430nm

From the spectra of Figure III-19, we can see first a decrease of the fluorescence, until both concentrations are equal at which point no emission was detected, followed by an increase upon addition of **PTCTK**. Another interesting remark is that upon increase of the fluorescence, a red shift can be observed along with a narrowing of the peaks, which is typical of J-aggregates. This results were very promising and CPL spectroscopy was performed on the sample with a ratio of 2:1 (Figure III-20).

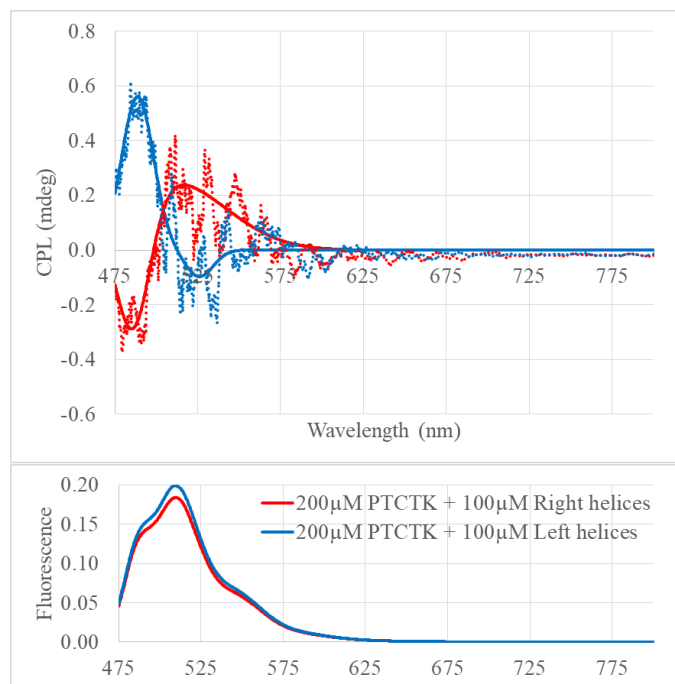


Figure III-20: CPL (top) and fluorescence (bottom) spectra of **PTCTK** in hybrid helices upon excitation at 430nm

As expected CPL was detected for this sample, showing that the chiral induction is also working in excited aggregates. Based on this spectra we can clearly see two peaks, one at 486nm and the other around 525nm. The first peak may be attributed to chirality induction from the gemini molecules to **PTCTK**, while the second would be the **PTCTK** J-aggregates for which the chirality is only induced from the chiral conformation due to the confinement in the helices. The dissymmetry factors of these two effects are shown in the Table 5.

Source of CPL	PTCTK + Left helices	PTCTK + Right helices
Monomeric PTCTK (486nm)	2.8×10^{-4}	-1.6×10^{-4}
J-aggregation (529nm)	-0.6×10^{-4}	1.4×10^{-4}

Table 5: Dissymmetry factor of **PTCTK** in hybrid helices with 2:1 ratio

Samples with different ratios were also analyzed by CPL spectroscopy, but no noticeable signals were detected. Based on these results, we can conclude that if the strength of the interaction between the gemini and the chromophore can be increased by changing the anion, the number of anions on the chromophore can also affect chiral induction. Additionally, we confirm the possibility to form J-aggregates using the confinement of fluorophores in hybrid helices and that chiroptical properties can also be induced on those aggregates.

2. Chirality induction using silica template

The previous section investigated the possibility to induce chiroptical properties to achiral fluorophores by using hybrid helices composed of a silica matrix containing an organic template. However, these chiral systems still present some inconvenience. For example, they are not very stable to many environments, as it is necessary to maintain them into conditions which do not disturb the supramolecular arrangement of the organic template. In order to improve the stability of the system toward the environment, we decided to use the silica shell alone after removing the organic template.

2-a. Covalent grafting on silica surfaces

The grafting of molecules on silica substrates is a widely studied topic, and could be achieved by several methods. The most common consists of the modification of the silica surface using 3-aminopropyltriethoxysilane (APTES) in order to have a terminal amine function on the surface.⁵⁷ This method leads to good coverage of the surface, even if the resulting surface is not generally covered by a mono-layer of APTES.⁵⁸ Using this method, several studies focused on the grafting of fluorophores on silica nano-particles,⁵⁹ often to force these molecules to be closely packed in order to have energy transfer⁶⁰ or excimer formation.⁶¹

*2-b. Chirality induction on polyoxometalates*⁶²

This is not the first study in the CMA group using inorganic helical structure to induce chiroptical properties to achiral molecule. A 2018 publication presents a method to electrostatically graft polyoxometalates (**POM**) on the surface of nano-helices.⁶² The surface of the helices was first modified using APTES in order to make it positively charged, then helices were mixed with **POM** (anionic in water). Chiroptical properties of **POM**-grafted silica nano-helices were checked and show that it is possible to induce a CD signal to the grafted species thanks to its chiral organization (Figure III-21).

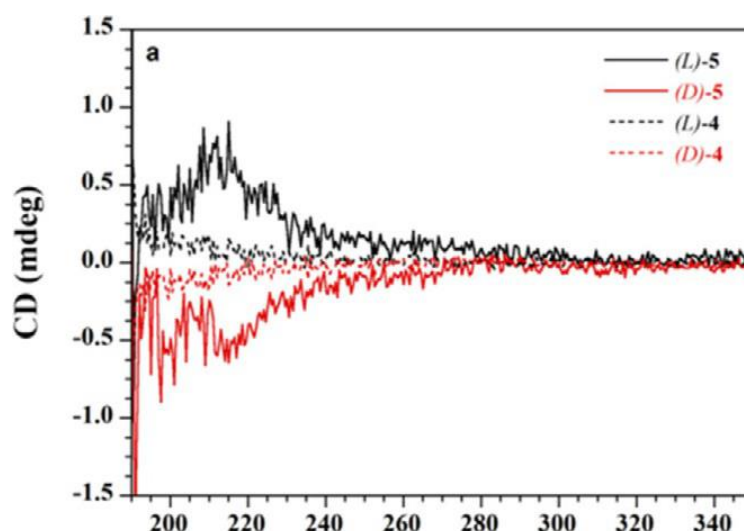
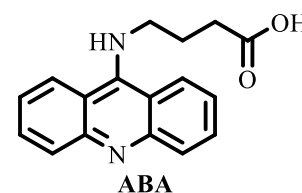


Figure III-21: CD spectra of silica nano-helices before (4) and after (5) **POM** grafting⁶² (Reprinted with permission from Attoui, M. et al., *Chem. Eur. J.* **2018**, *24*, 11344-11353. Copyright (2019) Wiley-VCH)

TEM analysis after several days also show a good stability of this system in ethanol. Based on those results, there was good chance to be able to get similar results using organics chromophores instead of **POM**.

2-c. Grafting by acridine derivatives

The first fluorophore we used for the covalent grafting on the surface of silica helices was 4-(acridin-9-ylamino)butanoic acid (**ABA**). However, no grafting was detected on the surface of amine functionalized helices after reaction of the corresponding activated anhydride. In order to understand



why the reaction did not proceed, the anhydride was reacted with absolute ethanol and the product was analyzed by HSQC NMR spectroscopy giving the following spectra.

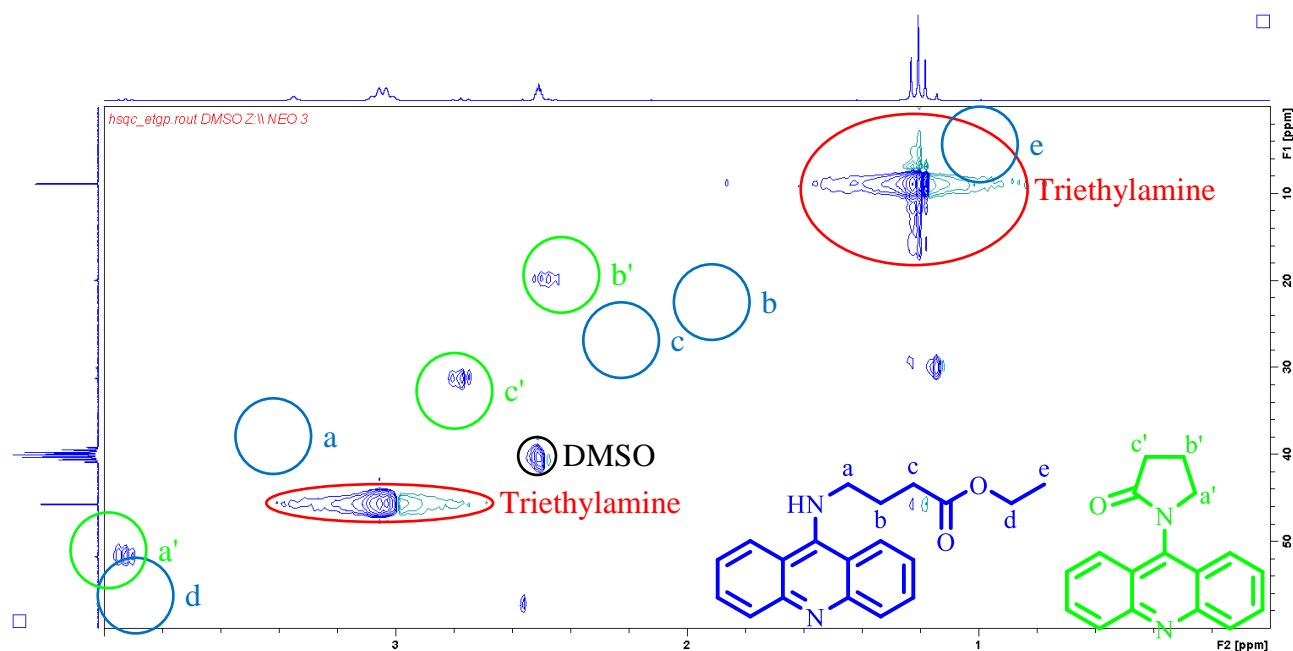


Figure III-22: Non-aromatic part of the HSQC NMR after making react activated ABA with ethanol

In Figure III-22, the circles represent the predicted positions of the expected peaks for the product of the reaction (in blue), as we can see, none of the actual peak match with those position. A possible side-reaction would be the cyclisation of the side chain after activation, the position of the peaks were predicted (in green) with a close match to the actual spectra. HSQC predictions were done on the website *nmrdb.org*.^{63,64} In order to prevent the cyclisation reaction, the reaction of 9-chloroacridine with shorter chains was pursued using glycine or β -alanine, however those reactions did not conduct of the desired product.

The direct grafting of 9-chloroacridine on the surface of APTES functionalized silica spherical nano-particle was also attempted, but the use of liquefied phenol, required for 9-chloroacridine reaction (cf. Chapter VI:1-d.ii), destroyed the silica as shown on TEM images (cf Figure III-23).

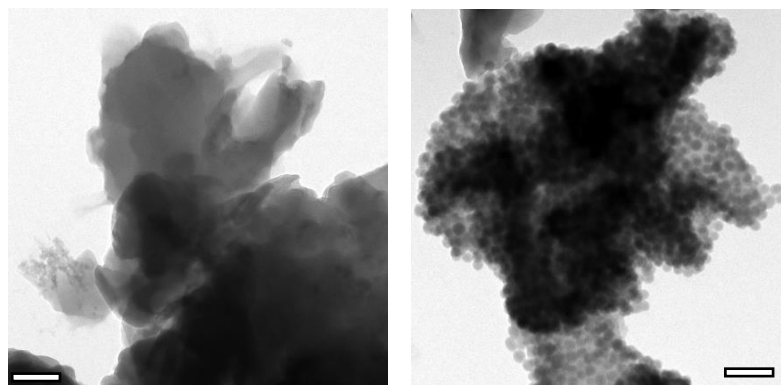


Figure III-23: TEM image of silica nano-particles after grafting of 9-chloroacridine (120kV / scale bars: 200nm)

Finally, we synthesized a derivative of **ABA** with a six carbon chain, which would lead to a less-favored seven-atoms cycle. The product, called 6-(acridin-9-ylamino)hexanoic acid (**AHA**) was successfully grafted on the surface of silica helices.

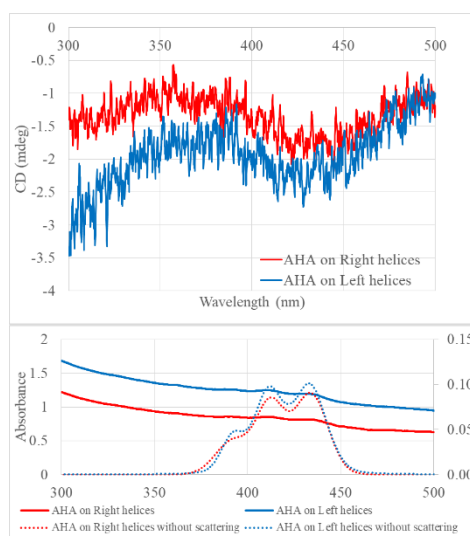


Figure III-24: CD (top) and absorption (bottom) spectra of silica nano-helices grafted by **AHA** in ethanol

Figure III-24 shows that, from the absorption spectra, **AHA** was successfully grafted on the surface of silica helices. However, it is not obvious due to scattering (raw spectra presented as solid line), and a mathematical treatment, based on Voigt's functions approximation, was applied to remove the scattering signal (result presented as dotted line). Unfortunately, no CD signal can be seen from those samples (the signal being not flat only due to the large scattering of the sample). The absence of CD might be due to the distance between the molecule and the structure due to the length of the spacer in

addition to that of the APTES molecule, which will prevent the aggregation to be forced in a chiral way. In order to try to compensate for this distance we decided to force the formation of dimer by adding a di-acid in the solution acting as a tweezer between two molecules (Figure III-25).

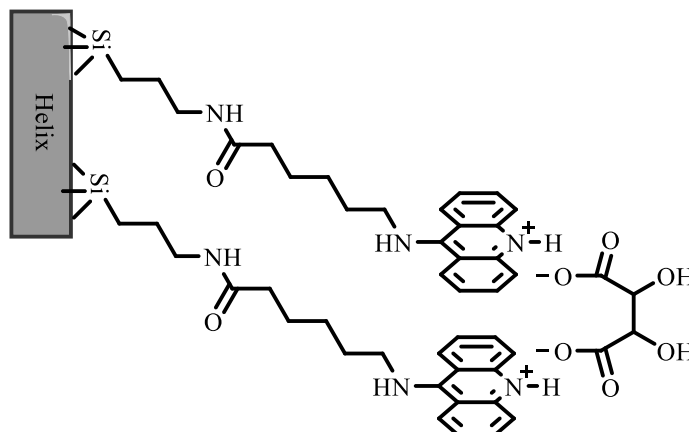


Figure III-25: Forced dimer of **AHA** by addition of tartaric acid

To do so, the sample was transferred into water to protonate the amine in position 10. Then, a racemic mixture of tartaric acid sodium salt was introduced ($10\mu\text{M}$) as a bi-anion to complex with the **AHA** and force its aggregation, giving the results shown in Figure III-26.

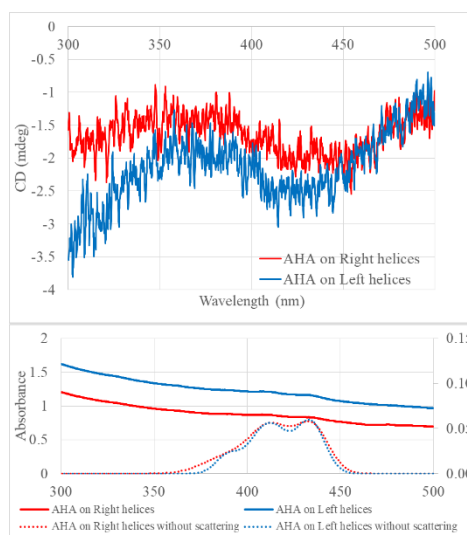


Figure III-26: CD (top) and absorption (bottom) spectra of silica nano-helices grafted by **AHA** in water with $10\mu\text{M}$ of tartaric acid sodium salt

A decrease of the **AHA** absorption can be observed, along with a slight broadening of the absorption peaks, which might be due to the protonation of the molecule. However, no obvious change appears in the CD spectra.

2-d. Grafting by pyreneacetic acid

In order to compare with the results of **PAA** complexed into the hybrid structures, we investigated its covalent grafting on the surface of inorganic nano-helices gave the following absorption spectra.

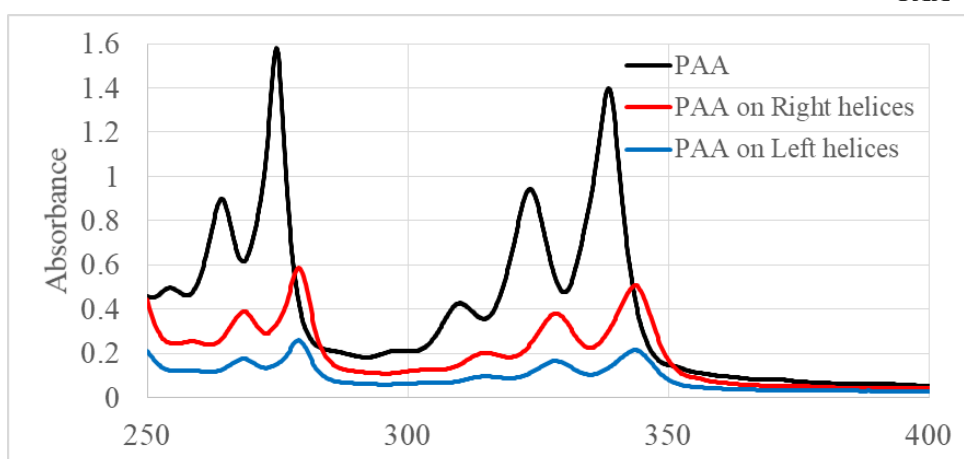
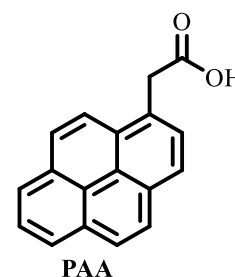


Figure III-27: Absorption of **PAA** alone ($50\mu\text{M}$) and after grafting on the surface of silica nano-helices

As in the hybrid system, we can observe a bathochromic shift due either to the interaction of the **PAA** molecules with each other or to an increase of the local polarity. However, in this situation, the possibilities for a change in polarity are limited as there are no ions in solution, whereas in the hybrid nano-structures, the interaction was electrostatic and led to close proximity between the chromophores and the ammonium group of the gemini. Despite the presence of inter-chromophore interactions, no CD signals were detected from these samples.

In order to increase the chirality of the silica helices, we proceed to calcinate the structures before grafting. The process of calcination was already reported by to increase the chirality as seen by vibrational circular dichroism.⁶⁵ Here, the calcination process was optimized in order to decrease the aggregation of the structures. After grafting of APTES, the helices were lyophilized, then calcined at 900°C for 2h. This is followed by surface reactivation using softly basic sodium hydroxide solution (pH between 8 and 9) before a new grafting of APTES. TEM pictures of resulting helices are presented in Figure III-28.

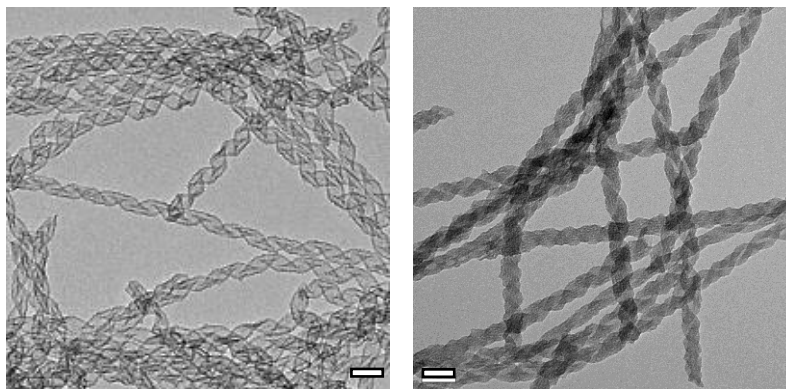


Figure III-28: TEM pictures of right silica nano-helices before and after calcination at 900°C (120kV / scale bars: 50nm)

Following the calcination and second functionalization, grafting of **PAA** gave the following results.

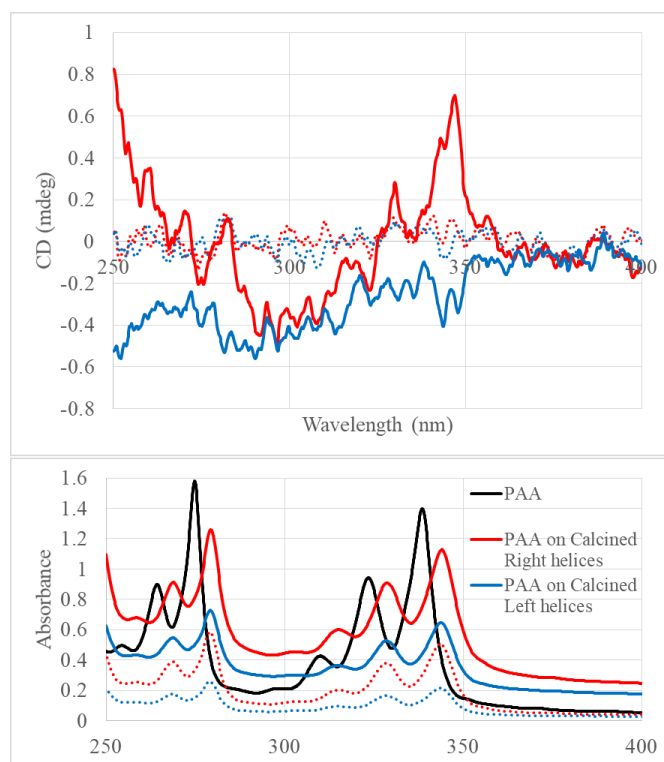


Figure III-29: CD (top) and absorption (bottom) spectra of PAA grafted nano-helices.

In Figure III-29, we can observe the appearance of a CD peak from the grafted calcined helices which was not present without calcination. This peak is much smaller for the left-handed helices than for the right-handed ones. However, this might be due to the concentration difference, as suggested from the absorption spectra. The grafting difference between calcinated and non-calcinated helices is also significant, which might be due to the more compact structure after calcination. However, the

APTES present after calcination was not quantified. In order to increase further the quantity of **PAA** on the surface, the grafting was repeated again with a 5mM solution of activated **PAA** instead of 1mM.

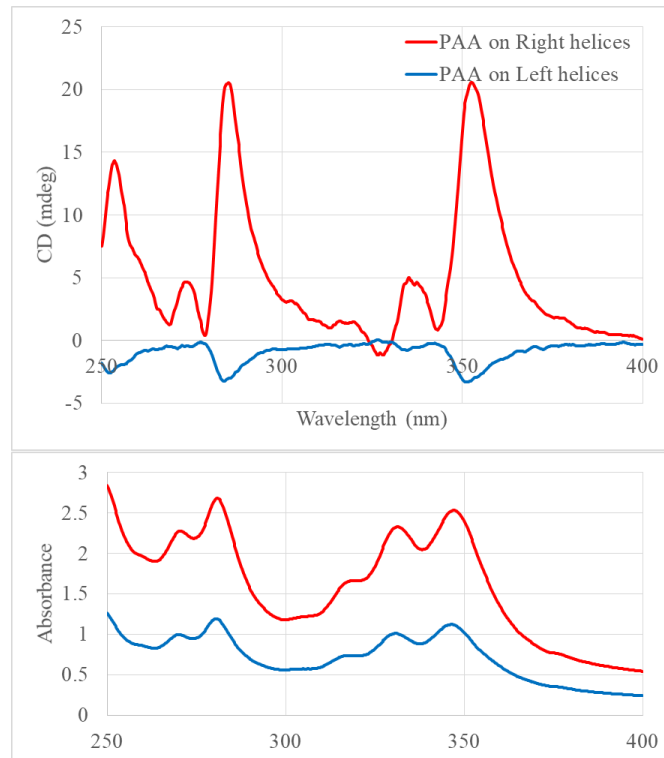


Figure III-30: CD (top) and absorption (bottom) spectra of PAA grafted on nano-helices (5mM solution)

From the absorption spectra presented in Figure III-30, we can see a high increase of the **PAA** absorption, showing more important grafting on the surface. However, a non-negligible increase of the scattering is also seen. This increase is due to a higher aggregation of the helices during the calcination process, as freeze-drying was performed on concentrated solutions. The dissymmetry factor are calculated to be 4.9×10^{-4} for the right handed helices and -1.6×10^{-4} for the left handed ones at 358nm (after removing the scattering from the absorption spectra by approximation using Voigt's functions). This difference could be explained by a higher grafting onto the right-handed helices compared to the left-handed ones. We decided to quantify the **PAA** on the surface of these samples based on the absorption spectra, the surface being quantified as previously described (see Chapter II:3-d.i page 37). The quantity of **PAA** was calculated around 0.28 PAA/nm^2 on right handed helices and 0.19 PAA/nm^2 on left handed ones, which is consistent with the difference we observe in dissymmetry factor.

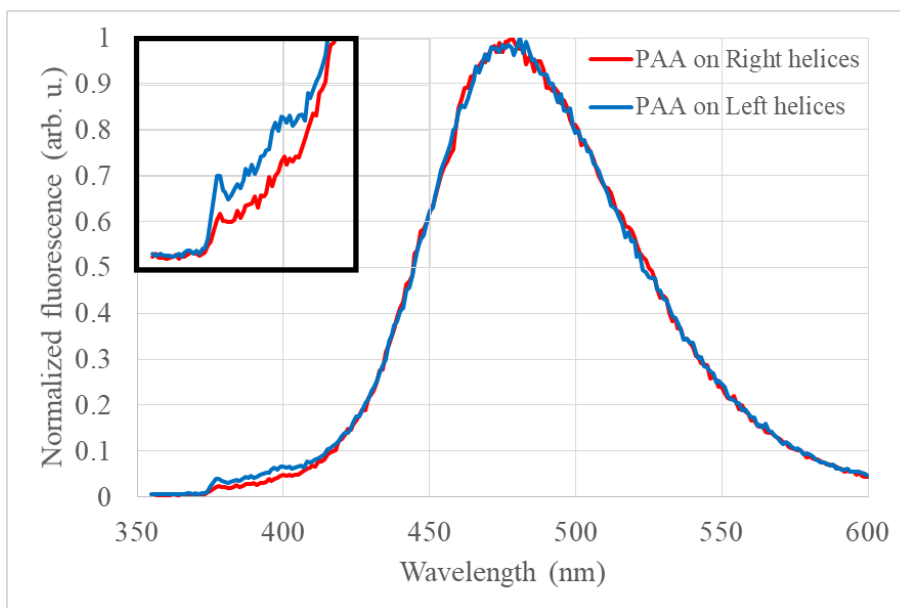


Figure III-31: Fluorescence spectra of **PAA** grafted on nano-helices upon excitation at 340nm

From the emission spectra, we can see a strong excimer contribution to the emission of the pyrene, proving a strong interaction between **PAA** molecules. Considering the density of **PAA** on the surface, the average space between molecules should be 4-5Å, which is a bit high compared to the ratio of excimer to monomer intensity we observe. This may be consistent with the grafting not being homogeneous at the surface of helices. Despite these promising results, no CPL signal were detected from these samples.

2-e. Grafting by perylene derivatives

Perylene derivatives are widely used to prepare aggregated nano-materials having various characteristics due to their high stability and their ability to form H or J-aggregates, and especially their ability to stack strongly together.^{66,67}

2-e.i Dissymmetric perylenes derivatives

To investigate the grafting of perylene derivatives onto the surface of the silica structures, we collaborated with Prof. SASTRE-SANTOS (University Miguel Hernández de Elche, Bioengineering Institute), who kindly provided two dissymmetric perylene derivatives suitable for these studies. The first (**DPBI-OPh**) is presented on the right.

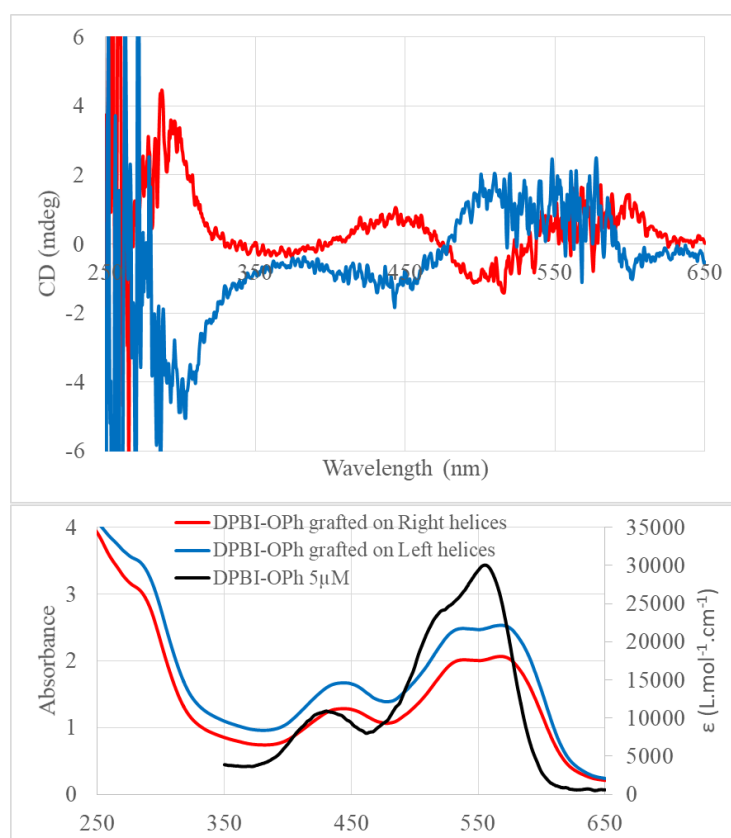
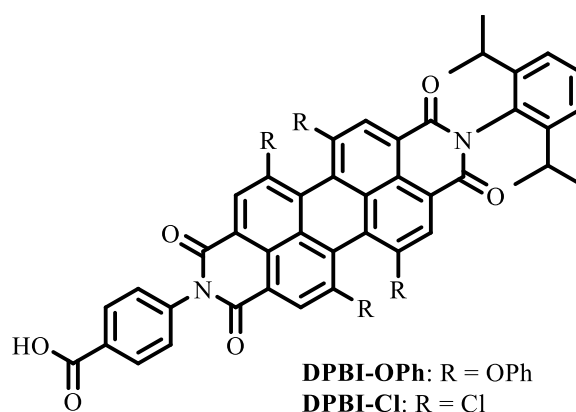


Figure III-32: CD (top) and absorption (bottom) spectra of **DPBI-OPh** grafted on silica nano-helices

We can observe that grafting of **DPBI-OPh** on the structures is successful judging by the absorption spectra, and that some J-aggregation is present as shown by a small red shift. We can also see a chiral induction in the CD spectra. Due to the phenol groups in the 1,6,7 and 12 positions, the molecule of **DPBI-OPh** is distorted, inducing a molecular chirality (Figure III-33).

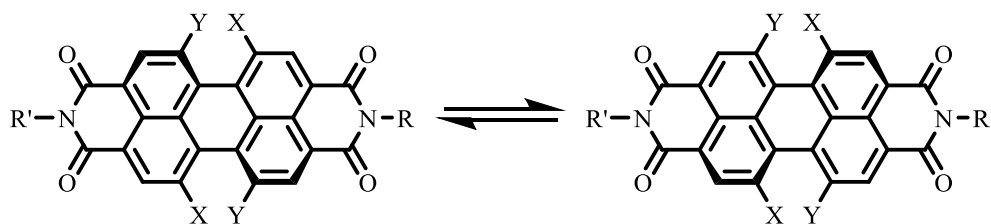


Figure III-33: The two enantiomers of general asymmetric perylene

However, these perylene derivative possess racemization half-lifetime of several hours at room temperature,^{49,68} whereas the grafting process on the surface on silica helices takes several days, making it likely that full equilibrium is reached during this study. Nonetheless, it is possible that grafting on the chiral surface of the helices may favor the formation of one of the enantiomers, and that this phenomena would increase the chiral induction to the chromophore aggregate. However, the induction is weak as shown by the dissymmetry factor obtained (Table 6).

Wavelength	DPBI-OPh + Left helices	DPBI-OPh + Right helices
500nm	3.6×10^{-5}	-2.4×10^{-5}
455nm	-2.4×10^{-5}	1.4×10^{-5}
328nm	-3.8×10^{-5}	0.9×10^{-5}

Table 6: Dissymmetry factors of DPBI-OPh at different wavelength

The difference between the left and right handed dissymmetry factor could be explained by a difference in the density of chromophore on the surface of the structures between the samples. However, the calculation show a higher coverage of right handed helices compare to left handed ones (0.38 molecule/nm² for left handed and 0.41 molecule/nm² for right handed). TEM images show a good preservation of the morphology of the structures (Figure III-34). Some destroyed helices can be found in both samples, but no major difference could be seen.

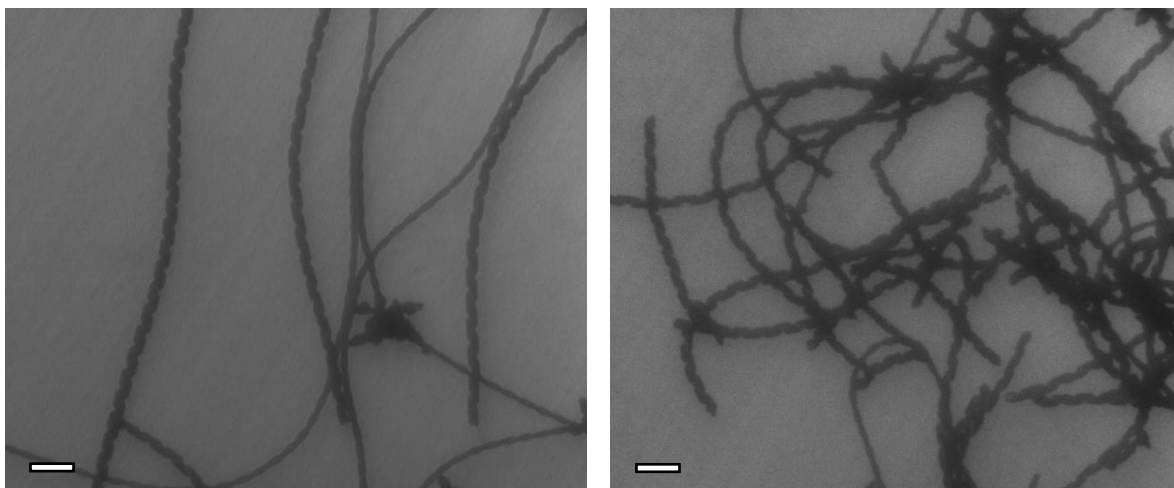


Figure III-34: TEM pictures of left and right handed helices after grafting of **DPBI-OPh** (5kV / scale bars: 100nm)

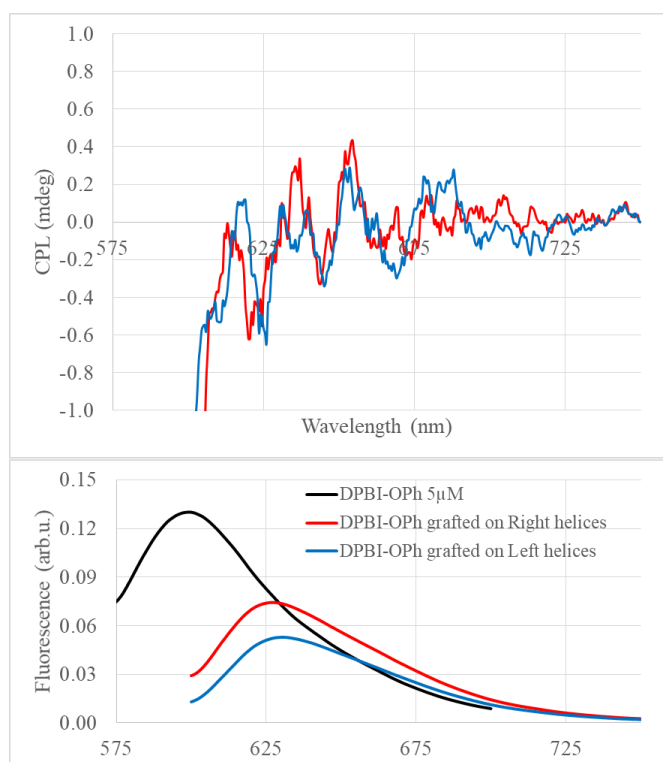


Figure III-35: CPL (top) and fluorescence (bottom) spectroscopy of **DPBI-OPh** grafted on nano-helices under excitation at 550nm

In Figure III-35, we can see an important red shift of the fluorescence which is consistent with the hypothesis of J-aggregation on the surface of the objects. However, J-aggregation is also expected to show a narrowing of the peak. Here, the fluorescence peak became broader. The broadening could be an instrumental artefact, as these spectra were recorded on the CPL spectrometer, which use slits with

higher opening than a usual fluorimeter. No CPL signal was recorded, which could be anticipated as the dissymmetry factor on CD was on the order of 10^{-5} , which cannot be detected by the CPL spectrometer.

Another perylene in which the phenol groups were replaced by chlorides was also investigated (**DPBI-Cl**). In this case, as with **DPBI-OPh**, the molecule is distorted due to the 1,6,7,12 substitution. However, chloride is smaller than phenol, which might lead to higher grafting density.

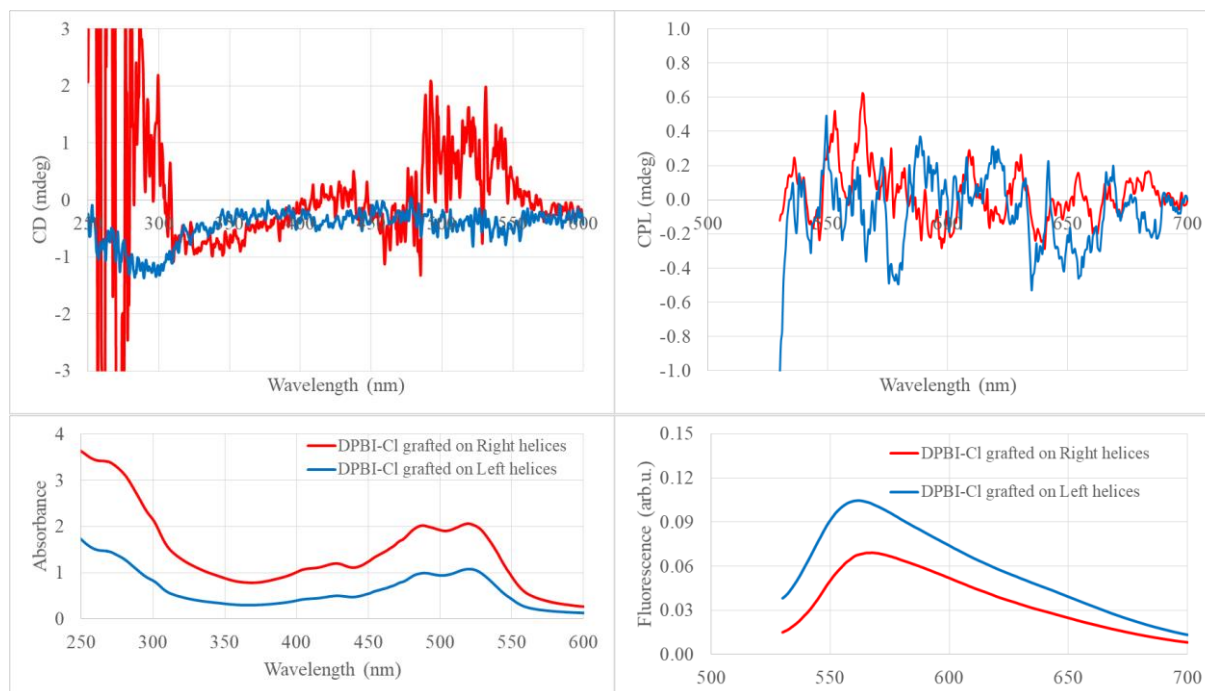


Figure III-36: CD (top left), CPL (top right), absorption (bottom left) and fluorescence (bottom right) spectra of **DPBI-Cl** grafted on silica nano-helices

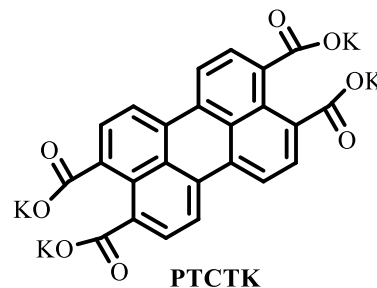
From Figure III-36, similar phenomena as for **DPBI-OPh** can be observed. The signal from right-handed helices is noisier due to a higher aggregation of the structures in the sample. However, the CD signal can easily be seen despite the noise. Signal intensity and calculated dissymmetry factors are comparable to those of **DPBI-OPh** (between 1×10^{-5} and 2×10^{-5}). Fluorescence also shows similar behavior as **DPBI-OPh**, with an important red shift and a broadening of the peaks.

Based on these result, we can conclude that it is possible to induce chirality to asymmetric perylene derivatives using the silica nano-helices. However, this induction is not strong enough to allow the detection of CPL signal using the current spectrometers. Also, the use of a pro-chiral molecule did

not improve the chirality induction, as **PAA** grafted samples shows higher dissymmetry factor than **DPBI-OPh** or **DPBI-Cl**. However, this might also be due to a decrease of the chromophore interaction due to the bulky groups.

2-e.ii Perylene-tetracarboxylic potassium salt

In order to know if the presence of groups on 1,6,7 and 12 prevents an aggregation of the molecule, but also to confirm the absence of effect from the pro-chirality of the chromophore, we decided to try a symmetrical derivative of perylene, which was already used for the



hybrid system, **PTCTK**. However, in this case, no activation using ethyl chloroformate was possible due to the precipitation of the chromophore in any solvent except neutral or basic water. For the grafting, we simply mixed the **PTCTK** with amine functionalized helices and let adsorption occur overnight. This provides red-colored samples, attesting the adsorption of the perylene onto the inorganic structures.

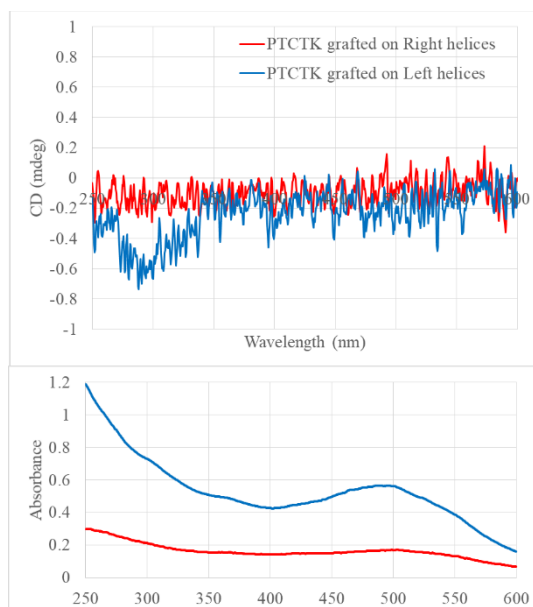
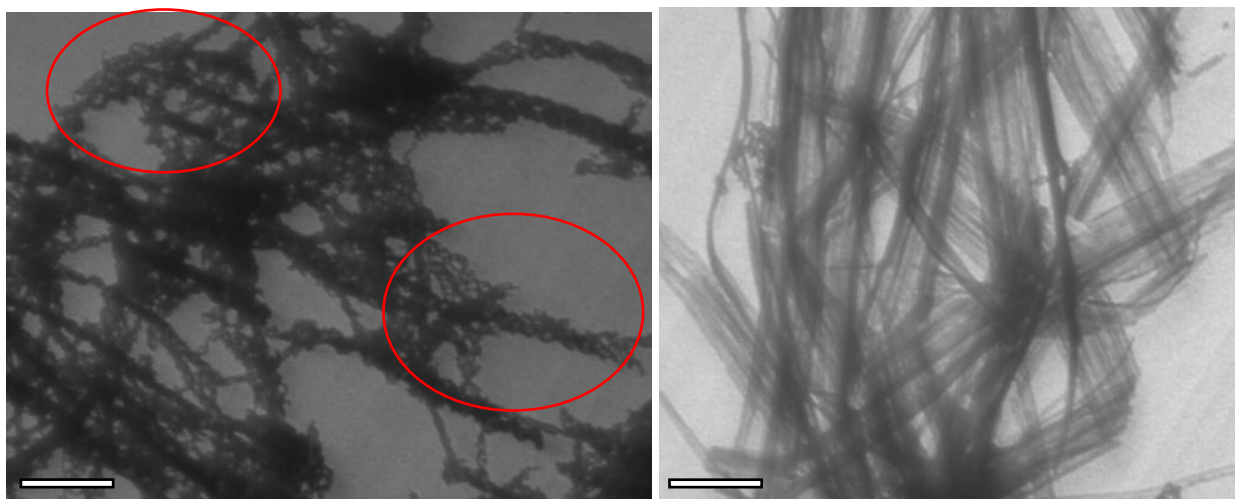


Figure III-37: CD (top) and absorbance (bottom) spectra of **PTCTK** grafted silica nano-helices

The analysis of absorption and CD spectra (presented in Figure III-37) shows that although the adsorption of **PTCTK** was successful, no induction of chiroptical properties could be observed in any handedness. To understand the reason behind the absence of CD, TEM was performed. Checking

the morphology of the helices show that helices are partially destroyed (red circles on left picture of Figure III-38) and some long and straight aggregates are formed into the sample (right picture of Figure III-38). This might be due to the basicity of **PTCTK**, which would increase the local pH around the structure, destroying it. In this case the new structures could be the aggregated molecules which were around the silica and remain together thanks to weak interaction (π -stacking and H bonding).



*Figure III-38: TEM pictures of left handed helices after **PTCTK** grafting (5kV / scale bars: 200nm)*

A solution has yet to be found on a way to graft **PTCTK** on the structures to be able to conclude on the impact of the pro-chirality of the grafted fluorophore.

3. Conclusion

When it comes to chiroptical properties, the most common way today to obtain high efficiency for the generation of circularly polarized luminescence (i.e. high dissymmetry factor) is to use inherently chiral chromophores such as helicenes⁶⁹ or chirally perturbed ketones.⁷⁰ When we look at chiral induction, is it even possible to have higher dissymmetry factors when using lanthanides such as Europium.^{71,72} However, few studies have focused on chiral induction using chiral nano-structures, and those with high dissymmetry factors are mostly using nano-particles such as quantum-dots.⁷³ In the case of nano-particles grafted on chiral templates, it has even been noticed that the bigger the grafted particles are, the more efficient the induction is.⁴² Concerning organic molecules in a chiral template, several studies have been pursued, however the template used is generally an assembly of chiral molecules.^{44,74}

In this study, we confirmed the possibility to induce chirality to organic chromophores from hybrid nano-structures (cf part 1, page 44). In this case, the chiral source was double, first from the supramolecular shape of the template, but also at the molecular scale with the organic pro-chiral molecules forced into one conformation. By doing so, we were able to observe circular dichroism for several types of achiral chromophores, as well as circularly polarized luminescence for two of them.

Additionally, we also demonstrated that it is possible to induce chiroptical properties even without any chiral or pro-chiral molecules in the system by grafting organic fluorophores onto the surface of inorganic helical nano-structures (cf part 1-b.iii, page 58). However, in this case, the chiral induction was much weaker than from hybrid helices. This weakening might be due to several factors, like the absence of chirality induction to the molecules which are too far from each other to interact through electron transfer, or the distance to the chiral source because of the APTES chain. Due to this weak chiroptical signals, we were not able to detect CPL despite promising results in CD and fluorescence.

This brings us to new questions: as we have a pro-chiral structure, if chiral chromophores become aggregated, would it be possible to tune the chiroptical properties? And what if we disturb a chiral aggregate showing chiroptical properties to force it into another type of aggregation? Finally, there is

more and more examples of chirality induction to quantum dots, but would it be possible to form carbon-based quantum dots with intrinsic chiroptical properties?

CHAPTER IV: TOWARD MORE COMPLEX SYSTEMS

1. Chiral chromophores

Probing the possibility of inducing chiroptical properties to achiral chromophores naturally raises the question of how to tune the chiroptical properties of chiral chromophores. In order to explore this idea, two types of chromophores were chosen: first, 10-camphorsulfonic (**CSA**) which is optically active in solution. Second, perylenebisphenylalanine (**PBPA**), which was described in Chapter II:2-b.i (page 31) and that show no chiroptical property in solution but only upon aggregation as described in literature.⁵⁰

1-a. Optically active chiral center

CSA is such a well-known molecule in the field of chiroptical materials because it is used for the calibration of CD and CPL spectrometers.^{70,75} A solution of **CSA** alone in water give the following spectra (Figure IV-1).

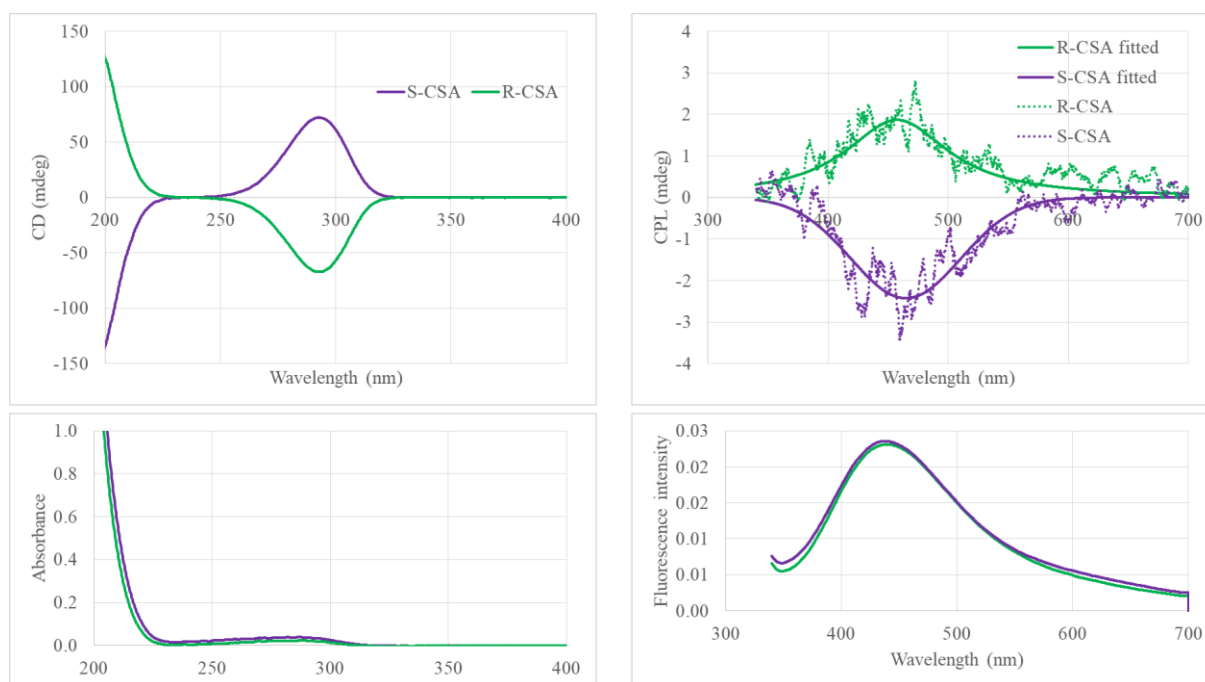
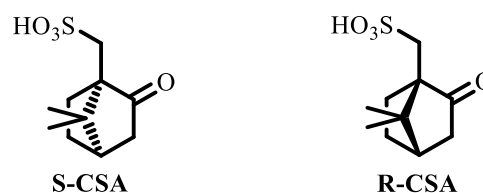


Figure IV-1: CD (top left), CPL (top right), absorbance (bottom left) and fluorescence (bottom right) spectra of a 1mM CSA solution (excitation wavelength for CPL and fluorescence is 291nm)

Figure IV-1 shows a remarkably high CD signal spectra whereas the molecule shows very weak absorbance due to a $n\pi^*$ transition. The dissymmetry factor in absorption of **CSA** has been calculated to be between 0.05 and 0.06.⁷⁵ The same conclusion can be made from the CPL spectra, with a dissymmetry factor in emission of 7×10^{-3} . Based on these results, mixtures of **CSA** with hybrid helices suspensions containing increasing quantity of hybrid structures were prepared.

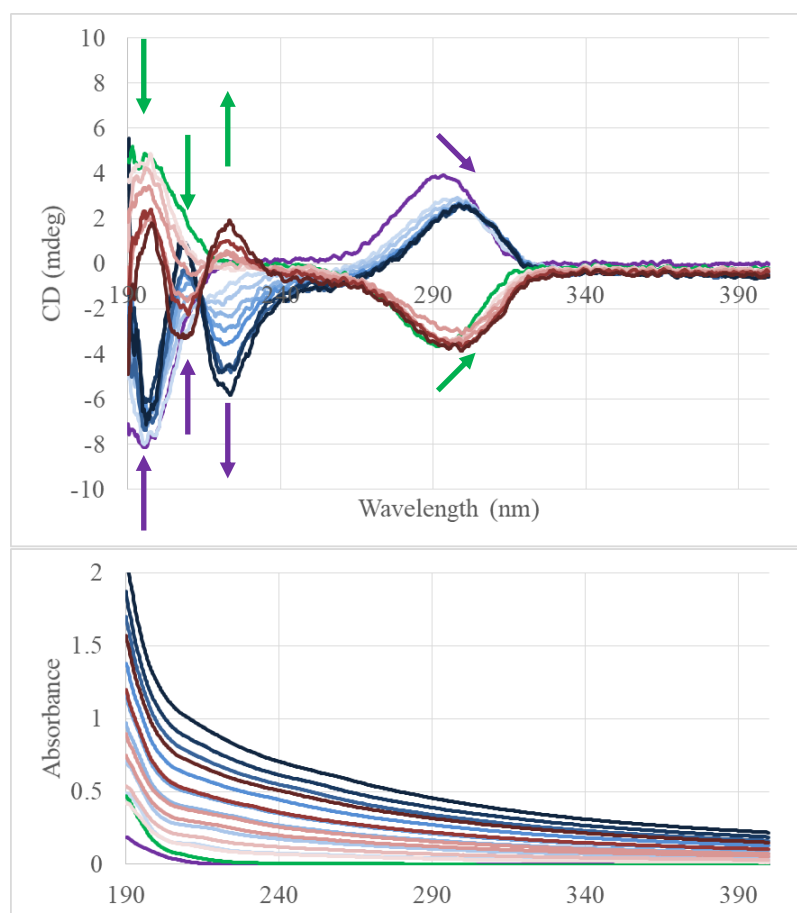


Figure IV-2: CD (top) and absorbance (bottom) spectra of **CSA** ($50\mu\text{M}$) upon addition of hybrid helices (from clear to dark, $21\mu\text{M}$ addition, $[\text{Hybrid}]_{\text{final}} = 168\mu\text{M}$)

First of all, we have to note that on Figure IV-2, the baseline of the CD signal is shifting to negatives values of CD at low wavelength upon addition of hybrid helices due to scattering. In this experiment, we only mix **S-CSA** with right handed hybrid nano-helices and **R-CSA** with left handed ones.

In Figure IV-2, a bathochromic shift of the CD peak of **CSA** (at 295nm) can be observed, which cannot be seen in the absorption spectra. However, CD is based on differential absorption, so the peak

positions in both spectra are related. Contrary to molecules used in Chapter III:1, this shift cannot be attributed to an increase of the polarity around the molecule, as such an increase would be expected to shift the transition to higher energy (the transition being $n\pi^*$ and not $\pi\pi^*$). So, this shift can be attributed either to a polarity decrease around the molecule, or to J-aggregation of **CSA** molecules. J-aggregation is very unlikely to happen for **CSA** and has never been reported to the best of our knowledge. However, a polarity decrease around the molecule would not be consistent with what we saw in the previous chapter. Additionally, Figure IV-2 shows the appearance of two new peaks in the CD signal at 210 and 225nm. These two peaks might come from the immobilization of **CSA** in the hybrid.

In summary, fluorescence and CPL analysis of **CSA**/hybrid sample was only possible at higher concentration of hybrid helices, and only after centrifugation of these samples to increase their concentration 10 fold due to the very weak emission of **CSA**. Because of this, the accurate concentration of **CSA** in the samples is unknown but, due to the large excess of hybrid compare to **CSA** and based on the fast exchange previously observed using **PSA** (see Chapter III:1-b.i), it has been considered that all the **CSA** present is contained inside the hybrid structures. Using CD spectroscopy to validate this hypothesis was unsuccessful due to the high scattering we obtain for such solutions (which appear white and opaque).

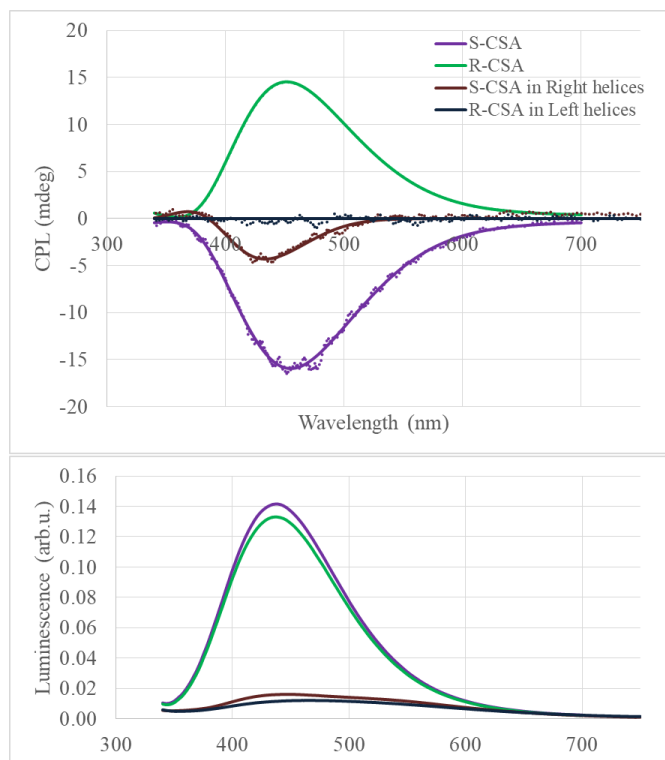


Figure IV-3: CPL (top) and emission (bottom) spectra of **CSA** (estimated at 500µM) in hybrid helices (1680µM) upon excitation at 291nm

Figure IV-3 shows an important decrease of the emission of **CSA** which might be due to the scattering of the sample, thus decreasing the detected light from **CSA** emission in the sample. In the CPL spectra, only the **S-CSA** in right helices sample gave a signal. The absolute value of the CPL signal is lower than before the interaction with helices. However, this decrease is much smaller than the one observed in the fluorescence emission. If we compare the dissymmetry factor, it increases from 7×10^{-3} (at 438nm) to 18×10^{-3} (at 388nm) which can be explained by the assembly of **CSA** in the structure, and the chirality induction from the organic molecules inside the hybrid nano-structures to **CSA**. In order to get more reliable data, another experiment was performed using higher concentration of **CSA** (1mM). However, it was impossible to increase the concentration of hybrid helices proportionally, so it was kept at 210µM. In this situation, the previous experiment shows a smaller, but visible effect (based on CD spectra). Also note that hybrid tartrate were used instead of hybrid chloride, causing a signal from the tartrate counter-ions which was taken into account.

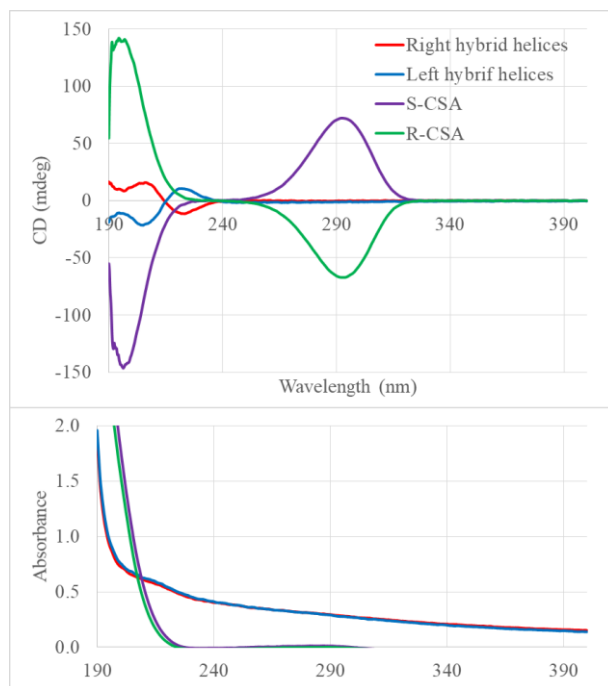


Figure IV-4: CD (top) and absorption (bottom) spectra of solutions containing either CSA (1mM) or hybrid helices (210 μ M)

Based on Figure IV-4, the signals of the mixture of these solutions were predicted by addition of the signals of each components. These predictions would be true if and only if there are no synergistic (or antagonistic) effects between the CSA and the hybrid helices.

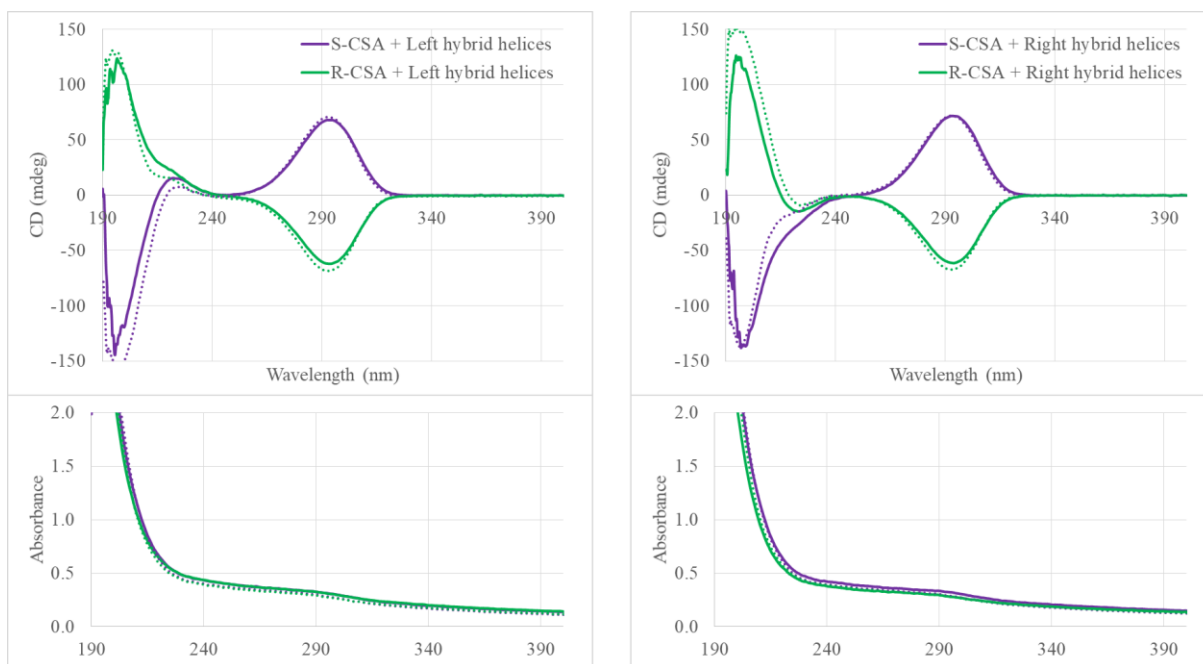


Figure IV-5: Effect of the addition of hybrid helices (210 μ M) in CSA solution (1mM), dotted line are the sum of the signals before mixing while solid line are measured spectra

Results shown in Figure IV-5 reveal a small cooperative effect on the peak at 225nm (peak from the tartrate counter-ion) for every combination of enantiomer. However, when examining the peak of **CSA** at 200nm, whereas the combination of **S-CSA** with left handed helices and **R-CSA** with right handed ones shows no effect, the opposite combination shows a partially destructive effect since the absolute value of the CD is lower than expected. Compared to previous experiments, we can also notice the absence of red-shift on the peak at 295nm. This may be explained by the ratio of **CSA** to hybrid which is much larger in this case than in the previous one. Based on the conclusion that **S-CSA** shows synergy with left handed helices (and **R-CSA** with right handed ones), we measured the CPL spectra of these samples (shown in Figure IV-6).

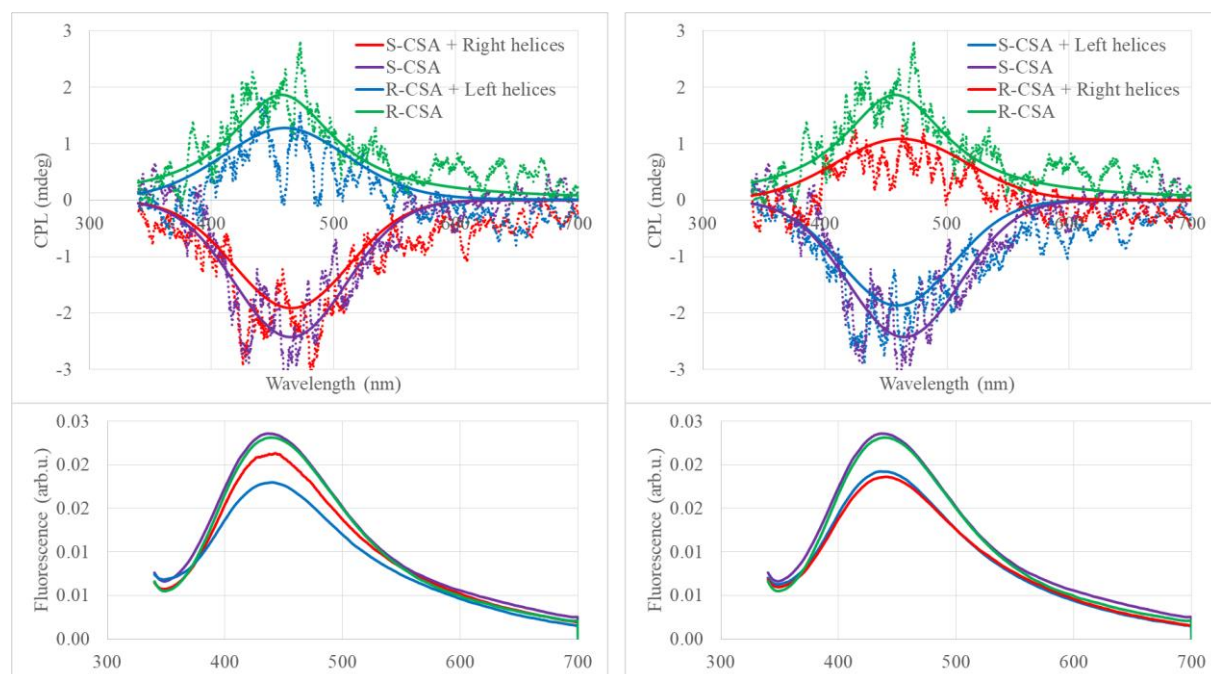


Figure IV-6: CPL (top) and fluorescence (bottom) spectra of **CSA** in hybrid helices with synergetic (left) and antagonist (right) enantiomers with raw data in dotted and fit in solid line upon excitation at 291nm

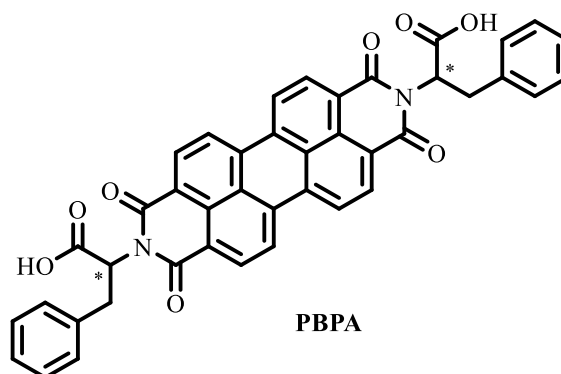
In every case, we can see a decrease of both the CPL and fluorescence signals. This decrease can be explained by the scattering which will decrease the quantity of light emitted by **CSA** reaching to the detector. The calculation of the dissymmetry factor does not show any significant effect of the addition of the hybrid helices, which may be due to the ratio which is reversed compare to the previous experiment. This could have been expected by the CD spectra, as no noticeable change occurs on the

peak at 295nm (corresponding to the $S_0 \rightarrow S_1$ transition), since the fluorescence will come from this transition.

Unfortunately, it is not possible to increase the quantity of helices to attain the previous ratio with this quantity of **CSA**, and decreasing the quantity of **CSA** would lead to CPL signals that are too low to quantify (Figure IV-3). Based on this we conclude that it is complicated to tune the chiroptical properties of this chiral chromophore. However, if the chiroptical properties were coming from an assembly, modified upon interaction inside hybrid helices, it may be possible to adjust these properties.

1-b. Chiral aggregates

The choice of chromophore for this part lead us to perylenebisphenylalanine acid (**PBPA**) as it shows no chiroptical properties in solution, and can be synthesized from **PTCTK** in a single step. If the synthesis of **PBPA** has been described several



times^{76,77} its self-aggregation in water and resulting chiroptical properties has only been described recently.⁵⁰ For this work, the reaction of the **PTCTK** with D-phenylalanine was incomplete, leading to non-opposite CD signals. For this reason, only the behavior of **L-PBPA** will be presented here.

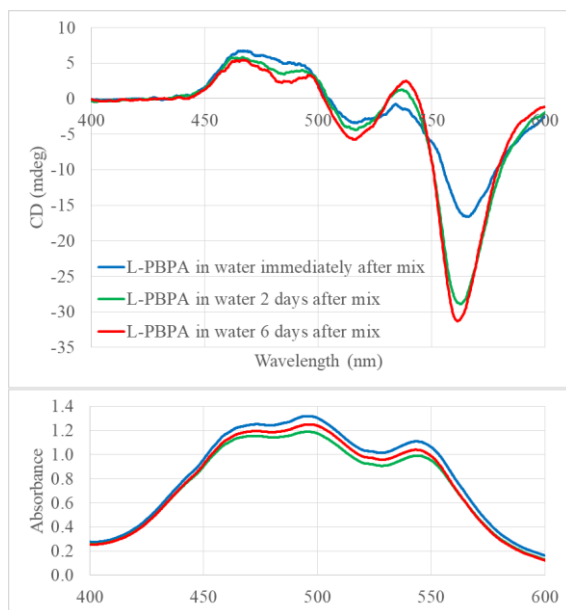


Figure IV-7: CD (top) and absorption (bottom) spectra of **L-PBPA** in water after 0, 2 and 6 days

Because **PBPA** forms chiral aggregates, the dynamics of this system were studied by CD spectroscopy. Figure IV-7 show an important evolution of the chiroptical properties over the first two days, with an increase of the dissymmetry factor at 565nm from -7.4×10^{-4} immediately after mixing and reach in an equilibrium value of -14.1×10^{-4} after two days. The small increase between 2 and 6 days is attributed to evaporation of the solvent (dissymmetry factor at 6 days: -14.8×10^{-4}). From these results, the behavior of **PBPA** in hybrid helices will be studied after resting for 2 days.

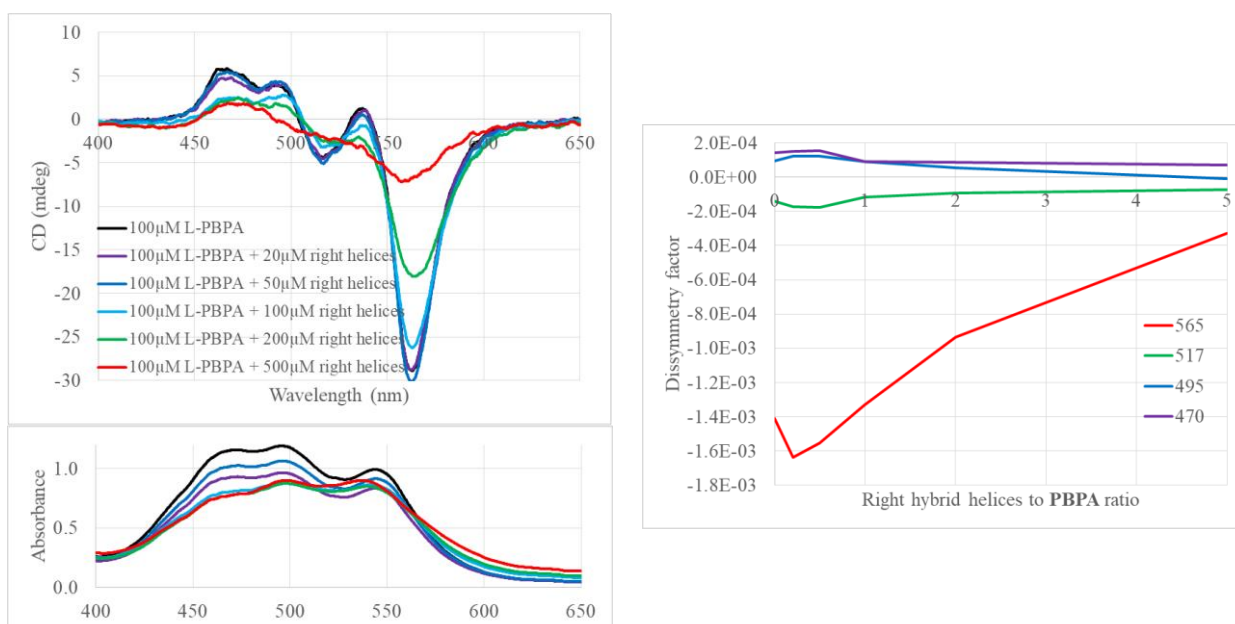


Figure IV-8: Left: Evolution of the CD signal (top) and absorbance (bottom) upon addition of right-handed hybrid helices in a 100 μM solution of **L-PBPA** (2 days after mix) / Right: Evolution of the dissymmetry factor depending of the ratio of right-handed helices to **L-PBPA** at several wavelength

Based on Figure IV-8, showing the evolution of the CD signal, absorbance and dissymmetry factor upon addition of hybrid helices in **PBPA** solution, we can deduce that an interaction exists between **PBPA** and the hybrid helices. At low concentration of hybrid helices (with a ratio to **PBPA** of 1:5 or 1:2), this interaction affects the aggregates of **PBPA** causing its chiroptical properties to increase. However, upon further addition of hybrid helices in the solution, a strong decrease of the dissymmetry factor is observed. Additionally, we can see a change in the relative intensities and a hypsochromic shift of the absorption peaks. This might be due either to a decrease of the local polarity, or to a change in the aggregation. As **PBPA** in water is already aggregated, this evolution was attributed to a change in the aggregation type. More specifically, since previous literature evidences a red-shift of the absorption band upon addition of water into a **PBPA** solution in DMSO,⁵⁰ the blue-shift we observe upon addition of hybrid helices might be due to looser aggregates which would be closer to a solution state, also explaining the decrease of the CD signal.

From these two phenomena, we can observe that when the packing of **PBPA** in hybrid helices is high, the chiroptical properties are enhanced thanks to the hybrid helices. However, increasing the quantity of hybrid helices leads to a decrease of the packing density, which leads to a decrease of the

chiral induction. In a second step, we investigated the effect of the helix handedness on the aggregation of **L-PBPA**.

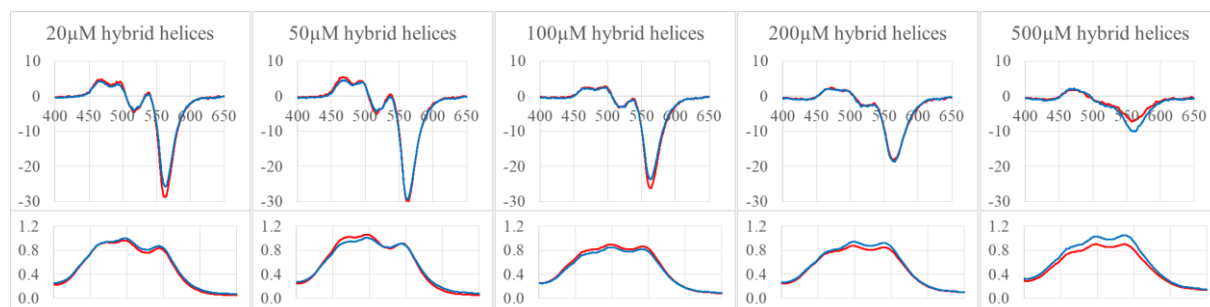


Figure IV-9: Comparison of CD (top) and absorption (bottom) spectra upon addition of left-handed (blue) or right-handed (red) hybrid helices in a $100\mu\text{M}$ solution of **L-PBPA** (2 days after mixing)

As shown in Figure IV-9, the addition of left-handed helices also leads a cooperative effect at a low concentration of hybrid helices, followed by a destructive effect when the ratio is higher than 1:1. The intensities of left and right-handed helices are very similar without significant difference between the two handedness. The effect of hybrid helices was also investigated using CPL spectroscopy.

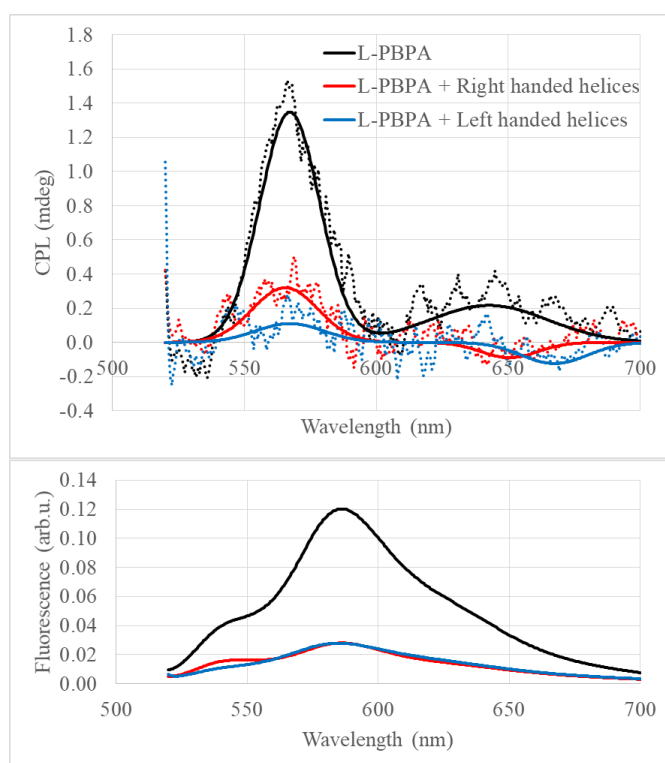


Figure IV-10: CPL (top) and fluorescence (bottom) spectra of **L-PBPA** with and without hybrid helices ($[\text{PBPA}]=100\mu\text{M}$ and $[\text{gemini}]=50\mu\text{M}$) upon excitation at 470nm

As shown in Figure IV-10, an important decrease of the fluorescence can be observed in the presence of hybrid helices. This might be due to an aggregation mode that reduce the emission. Upon further addition of hybrid helices, the fluorescence disappears. Because of this, we might assume that the fluorescence we see on Figure IV-10 corresponds to **PBPA** aggregates which are not inside the hybrid helices. However, when calculating the dissymmetry factor at 565nm, although no significant difference can be seen with and without right-handed helices (12×10^{-4} versus 13×10^{-4} for **L-PBPA** with helices and alone, respectively), left-handed helices show a non-negligible decrease of the dissymmetry factor (4×10^{-4}). This attests to a better affinity of right-handed helices with **L-PBPA** whereas left-handed helices have a destructive effect on the chiroptical properties of **L-PBPA**.

This also shows that the fluorophores inside the helices are also emissive (otherwise the dissymmetry factor would be the same for both handedness). However, the reason why the fluorescence disappears with further addition of hybrid helices was not determined.

This work shows that it is possible to change the chiroptical properties of a chromophore forming self-assemblies by affecting them negatively. In the case of high loading ratio (from 5:1 to 2:1 ratio of **PBPA** to gemini) of hybrid helices to chromophores, a small enhancement of the chiroptical properties was achieved, as observed of CD spectra. Upon further addition of hybrid helices, the chiroptical properties decrease strongly, this destructive effect might be due to the low matching of the shape of helices compare to self-aggregation of **PBPA**. If this is true, the use of a different shape of template, closer to the original organization of **PBPA** might allow a stronger enhancement of the chiroptical properties. Such a shape can be achieved using 16-2-16 tartrate with shorter aging time before silica polycondensation (as explained in Chapter II:1-b.i).

2. Formation of carbon dots from the organic template

The formation of carbon-based quantum dots (also named carbon dots or CDots) is now widely described in the literature starting from a great variety of materials,⁷⁸ from simple molecules⁷⁹ or natural amino acids⁸⁰ to complex mixtures like milk.⁸¹ These structures are nano-particles ranging from 1-100nm^{78,79,82} composed of graphene sheets formed by the oxidation of organic molecules. This oxidation can be done by many ways, but we will here focus on the carbon dots prepared through pyrolysis.

Carbon dots do not usually show any absorption peak, but an absorption band that tail out toward to the visible wavelengths. This is due to the multiplicity of the aromatic structures which are formed during pyrolysis. The fluorescence of carbon dots is dependent on the excitation wavelength due to the excitation of different aromatic compounds depending on the irradiating light.^{79,83} Short excitation wavelength induce an emission from the smaller structures at shorter wavelength, whereas long excitation wavelength excites larger graphitic structures, with longer emission wavelength.⁸⁴

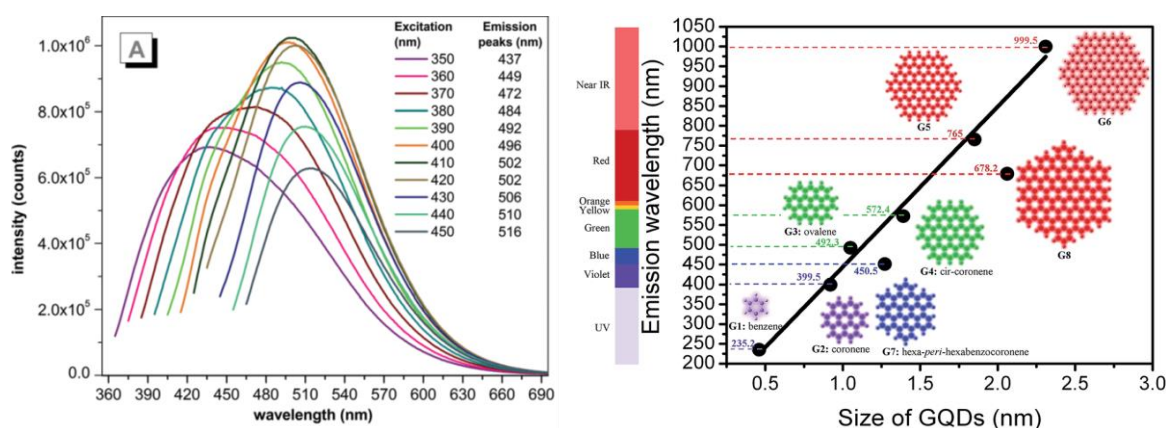


Figure IV-11: Fluorescence spectra of *N*-hydrosuccinimide based carbon dots in water at various excitation wavelength⁷⁹ and emission wavelength dependency in function of the size of graphitic sheet⁸⁴ (Reprinted with permission from Stan C. S. et al., *J. Matt. Chem. C*, **2015**, 3, 789-795 and Sk M. A. et al., *J. Matt. Chem. C*, **2014**, 2, 6954-6960. Copyright (2019) Royal Society of Chemistry)

Although some recent studies have shown the emergence of chiral carbon dots showing CD signals,⁸⁵⁻⁸⁷ only few are able to show weak CPL signals.⁸⁸ Although if the formation of chiral carbon

dots was previously reported,⁸⁷ to the best of our knowledge no CPL signal were recorded without addition of external source of chirality in the system.

We envisaged that the pyrolysis of the organic component of hybrid helices may lead to the formation of graphitic carbon dots confined within the chiral silica matrices, thus leading to the emergence of chiroptical properties. To synthesize carbon dots, we proceed to pyrolyse hybrid helices at different temperatures in an oven under a nitrogen flux.

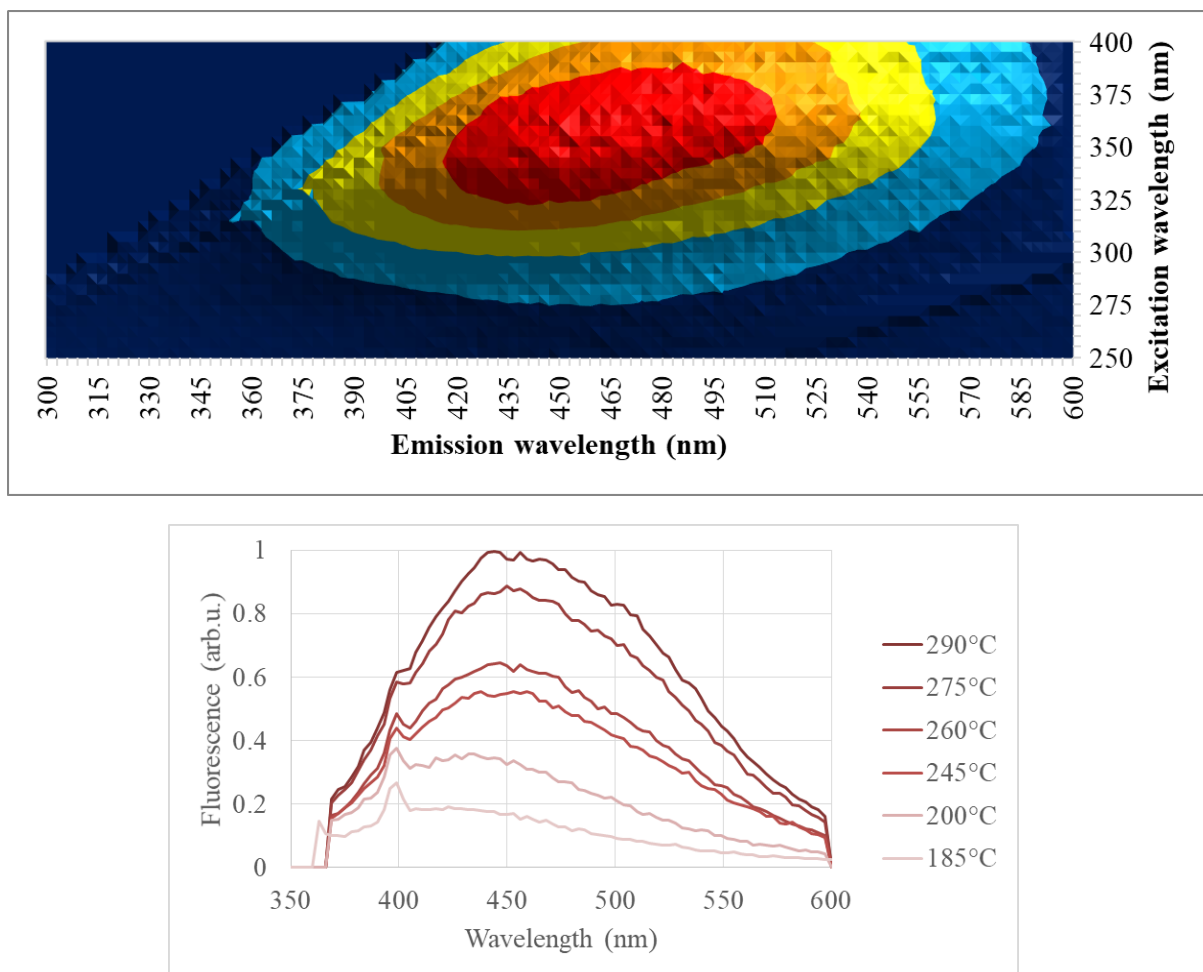


Figure IV-12: 2D fluorescence spectra of carbon dots formed at 290°C (top) and fluorescence of carbon dots form at various temperatures upon excitation at 350nm (bottom)

The 2D fluorescence spectra in Figure IV-12 shows the typical fluorescence resulting from the formation of carbon based quantum dots in the hybrids nano-helices. Based on the dependency of the fluorescence with pyrolysis temperature (Figure IV-12), we can see that higher temperatures lead to the formation of more emissive carbon dots.

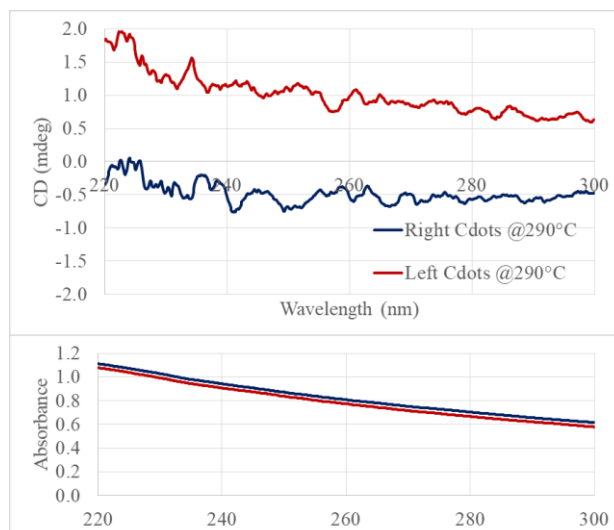


Figure IV-13: CD (top) and absorption (bottom) spectra of carbon dots form from left (blue) and right (red) handed helices at 290°C

The CD spectra of the samples were measured for the dots formed at 290°C, but no obvious signals could be observed (Figure IV-13) other than what can be attributed to scattering.

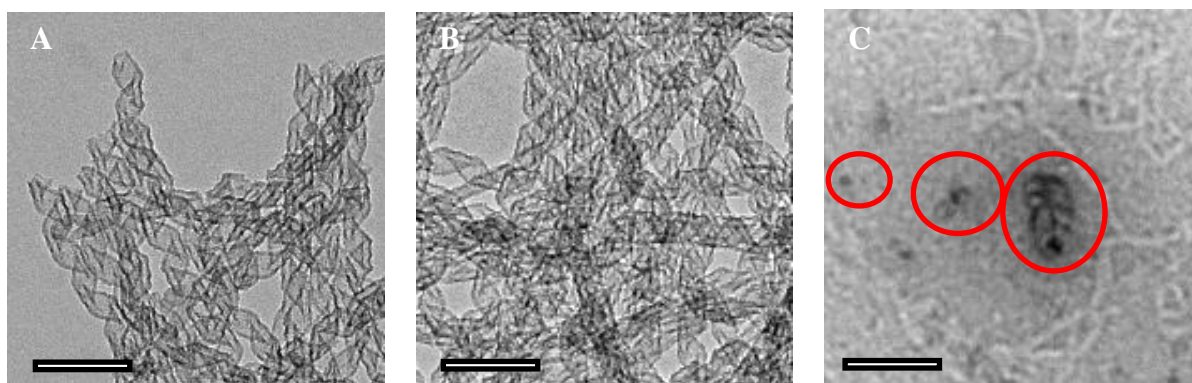


Figure IV-14: TEM image of left (A) and right (B) handed helices after formation of carbo dots at 290°C and of the dots after destruction of the silica membrane using NaOH solution (C) (120kV / scale bars : 100nm)

As shown in Figure IV-14 A and B, no difference can be seen by TEM after pyrolysis of the hybrid nano-helices except for a strong aggregation of the structures. Once the helices are destroyed, some black dots can be found, attributed to be carbon dots aggregates (framed in red on Figure IV-14 C). To favor the formation of helical graphene sheets that may display better chiroptical properties, pyrolysis was performed at higher temperature (600°C) and under inert atmosphere. In order to do so, the hybrid nano-helices were lyophilized into an NMR quartz tube that was then sealed under vacuum

(10^{-7} mbar). Then, the sample was heated in an oven at 600°C . This led to the formation of a black powder which was dispersed into ultrapure water.

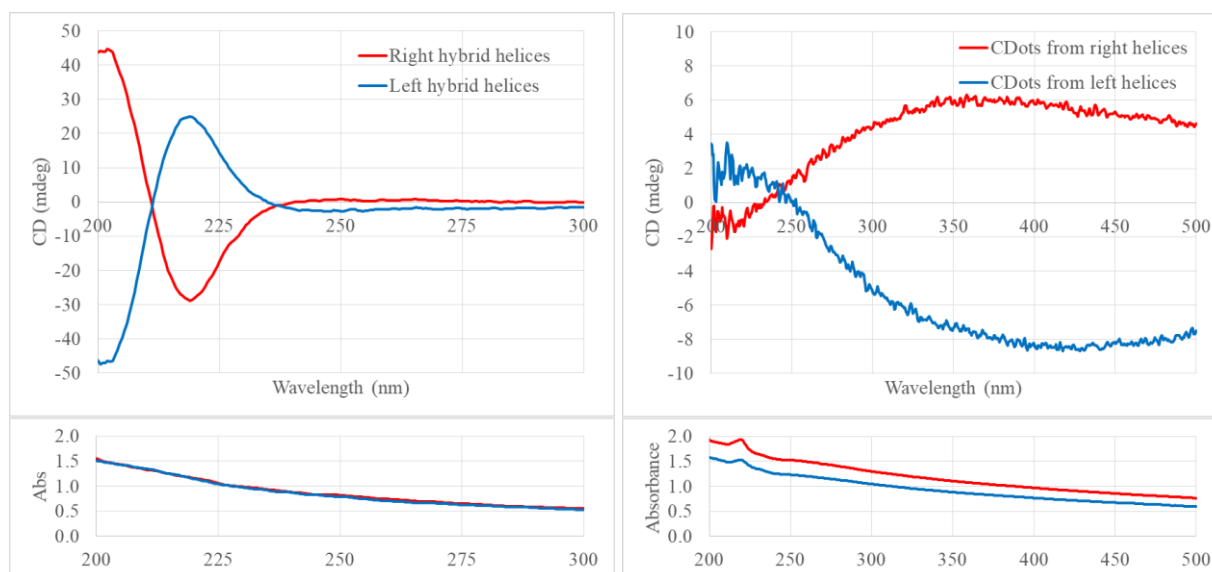


Figure IV-15: CD (top) and absorbance (bottom) spectra of hybrid helices before (left) and after (right) graphitization

From the absorption spectra shown in Figure IV-15, we can see the appearance of a peak at 219 nm and a shoulder around 250 nm attesting the formation of new structures after the pyrolysis. From the CD spectra at low wavelength (below 250 nm) we can confirm the total transformation of the tartrate ions. A new CD signal also appears above 250 nm, with an increasing intensity until 375 nm then a slow decrease. The dissymmetry factor was determined to be 2.3×10^{-4} for carbon dots from right-handed helices (-2.6×10^{-4} for left-handed helices). Based on these promising results, we decided to measure the CPL spectra of these samples.

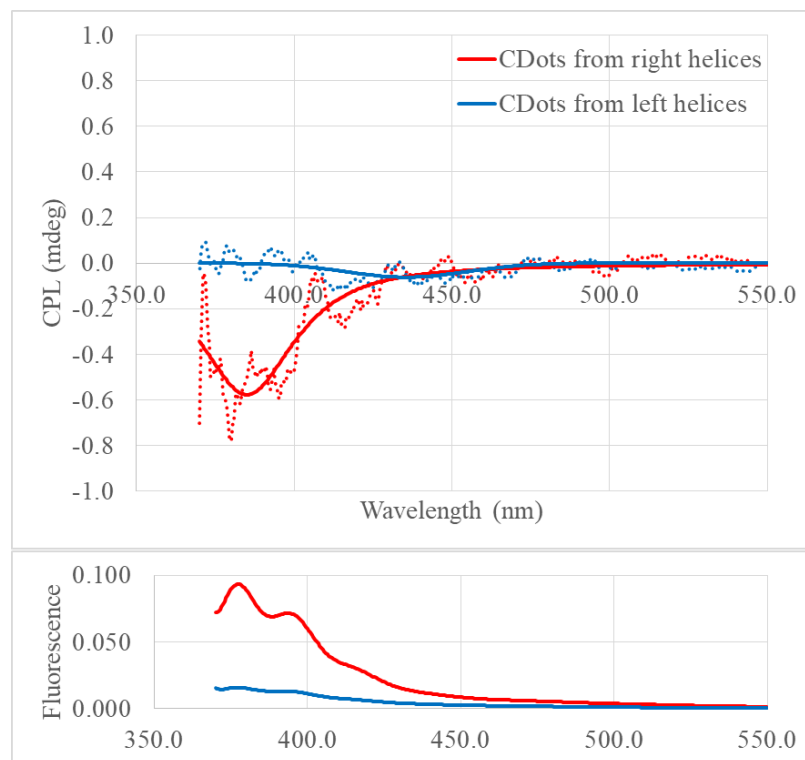


Figure IV-16: CPL (top) and fluorescence (bottom) spectra of carbon dots after graphitization of hybrid helices upon excitation at 330nm

Although an obvious chirality induction on one of the enantiomers of carbon dots is clearly visible in the CPL spectra in Figure IV-16 showing a dissymmetry factor in emission of -5.7×10^{-4} , the left handed helices sample is barely fluorescent. The absence of CPL signal from the sample based on left-handed helices might be explained by small differences during sample preparation. The experiment was performed again after keeping the sample under vacuum (10^{-7} mbar) for 10min before sealing, leading to the following results.

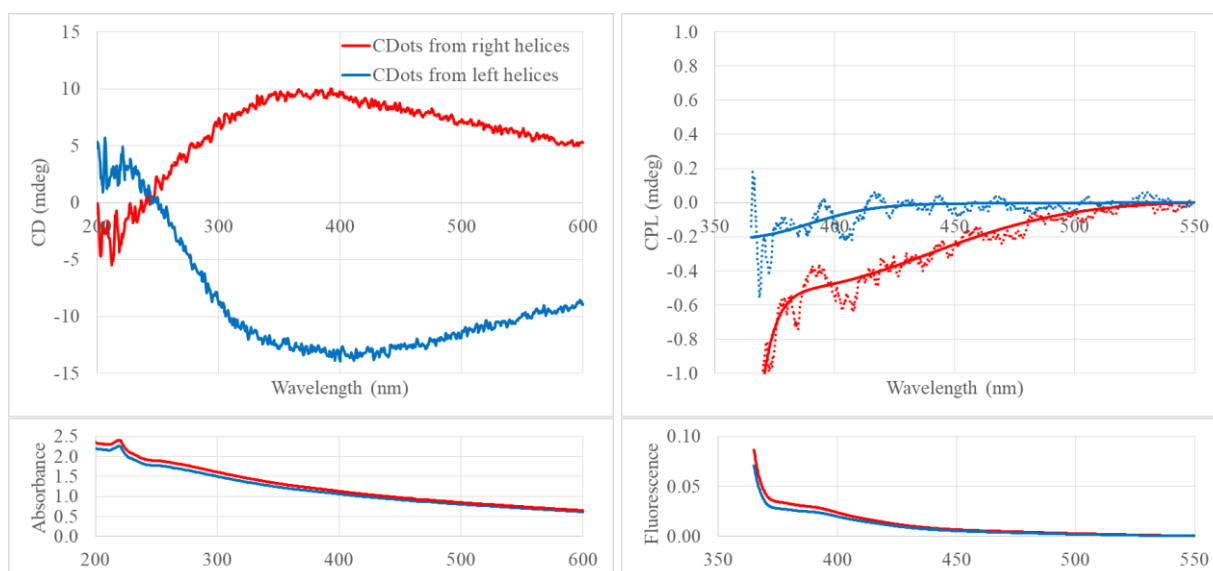


Figure IV-17: CD (top left), absorbance (bottom left), CPL (top right) and florescence (bottom right) spectra of carbon dots from hybrid helices after 10min desorption upon excitation at 320nm

We can see in Figure IV-17 that the CD properties are higher than those obtained using the previous method. Additionally, the CD signal is higher for carbon dots from left-handed helices. However, the fluorescence we obtain is very low, and is similar to the carbon dots from left-handed helices in the previous method. Once again, only right-handed helices seems to show a CPL signal, which seems to be higher than the previous method, but due to the very low fluorescence of this sample, the accuracy of the measure is low. The dissymmetry factors calculated after removing the contribution of the excitation light to CPL signal for these samples are listed in the Table 7.

	Left-handed	Right-handed
CD (at 375nm)	-3.2×10^{-4}	2.4×10^{-4}
CPL (at 390nm)	-4×10^{-4}	-12×10^{-4}

Table 7: Dissymmetry factor in absorption (CD) and emission (CPL) of carbon dots made from left or right-handed helices

Keeping the helices under vacuum before pyrolysis seems to lead to an increase of the chiroptical properties in absorbance. However, if some CPL may be detected on right-handed helices, this might also be an artifact due to the extremely low fluorescence of the sample, close to the one detected from left-handed helices in the previous experiment (Figure IV-16).

Based on these results, we conclude that it is possible to obtain carbon dots with chiroptical properties in absorbance, and that the emission of circularly polarized light using carbon dots without any external molecules inducing the chirality is also possible. However, the pyrolysis process needs to be precisely controlled and the morphology of the hybrid and the size of the formed carbon dots might also need to be further optimized.

3. Conclusion

This chapter presented further possible developments of hybrid helices in tuning the chiroptical properties from systems described in the previous chapter. Although the supramolecular organization has a little direct effect on the chiroptical properties of chiral chromophores that are co-assembled with hybrid helices, the change in molecular aggregation can strongly affect the CD and CPL signals. By making the aggregates looser and forcing a change of their shape by adding hybrid helices, it is possible to decrease the induction of chiroptical properties. However, fine tuning of the quantity of template to molecule ratio can lead to small enhancement of the CD signal. Another difficulty is that when altering aggregation, other properties are also affected. In the case of **PBPA**, a strong decrease of the fluorescence forbid a precise measure of the CPL spectra upon addition of helices. Nonetheless, CPL measurement also highlight the importance of the supramolecular shape of the template as both handedness of the helices show very different signals.

Additionally, a new way for the synthesis of carbon dots were developed using silica helices as reactors. At low temperature (below 300°C), we obtained highly fluorescent carbon dots without chiroptical properties. At higher temperature (600°C) and under vacuum, lower fluorescence of the carbon dots but very interesting CD signals in all the visible spectrum were produced. Additionally, we proved that it is possible to obtain CPL signal with such system. However, the synthesis of this species is very sensitive to external parameters, and further studies are needed to understand which of these parameters allow the emission of CPL by the carbon dots.

CHAPTER V: CONCLUSION AND PERSPECTIVES

1. General conclusion

In this work, we explored new approaches to obtain materials showing chiroptical properties having a simpler synthesis and purification pathway than typical chiral molecules. To achieve this goal, we opted to use chiral nano-helices formed by the polycondensation of silica around an organic template of achiral gemini cationic surfactant with a commercially-available chiral counter-anion. Afterwards, the organic template can be kept inside, resulting in hybrid structures, or removed by washing with an organic solvent to provide inorganic helices.

To be able to use silica helices, an amine functionalization of the surface was performed, followed by the grafting of chromophores of interest. We showed that this process is sufficient to induce chirality in the aggregates which impact the electronic properties, resulting in the appearance of a differential absorption of circularly polarized light (circular dichroism). Additionally, we showed that the higher the density of chromophore is on the surface, and the more the molecules interact together, the stronger the induction is. However, and despite using a wide range of chromophores, no circular polarization was detected from the emission of light by the samples.

In the case of hybrid structures, they can be used directly in order to co-assemble chromophores. However, tartrate ions were first exchanged for chloride in order to remove residual optical properties in near UV range. Chromophores subsequently replaced the chloride ions upon mixing. With this approach, chiral induction was shown to be stronger than in the case of inorganic helices, as the chirality did not come only from the aggregation, but was also induced from the gemini template (in a chiral conformation). By using this system, we were able to generate CD signals, but several samples were also able to maintain their chirality in the excited state, showing circularly polarized luminescence (CPL). The comparison of the dissymmetry factors of the different samples allow us to begin understanding some of the key parameters of chiral induction, which are the hydration free energy, the number of ionic sites and the ability for the fluorophores to stack into emissive aggregates.

These observations on the induction of chiroptical properties from achiral molecules lead us to wonder what the effect of chiral template would be on the chiroptical properties of chiral molecules, if they would be constructive or destructive. We therefore investigated the interaction of chiral

chromophores with hybrid helices and analyzed the CD and CPL properties upon varying the ratio of gemini to chromophore. Chromophores having a low capacity to interact with surrounding molecules did not show important effects in the presence of the chiral template.

To go further in this study, we introduced a chiral molecule which is known to form chiral aggregates. In this case, as the gemini to chromophore ratio increases up to 1:1, we could observe a small enhancement of the chiroptical properties, attributed to tighter packing between chromophores. Higher ratio of gemini to chromophore (above 1:1) leads to a strong decrease of the chiroptical properties. The handedness of the helices used did not show any noticeable impact on the CD signal, proving that if the presence of the template allows us to change the interaction between chromophores, it does not allow a total change in the organization from one molecule to the other. However, the handedness of the hybrid helices affected the CPL signal, proving a better affinity of **L-PBPA** with left-handed helices. It was also observed that the fluorescence of the chromophore decreased strongly upon addition of hybrid helices, in agreement with the formation of non-emissive aggregates.

The production of twisted carbon based quantum-dots by using the hybrid helices as nano-reactors for the pyrolysis of the organic template was also explored. By this means, it was possible to create graphene-based species showing chiroptical properties in light absorption. We also detected CPL signals for some samples, but the parameters were not totally controlled and the reproducibility of the carbon dots synthesis was not optimal.

To conclude, this study shows the high interest presented by the possibility to organize achiral molecules using a chiral template. Not unexpectedly, these structures possess advantages and weakness. On one hand, inorganic systems are very robust toward environmental change but show limited ability to induce chirality, whereas induction of chiral signal from hybrid helices to achiral chromophores is stronger but these structures are very sensitive to their environment. At the same time, we showed the possibility to enhance or diminish the chiroptical properties of chiral self-assemblies by forcing them into a new shape. Finally, we proved the possibility for carbon based quantum-dots to show chiroptical signals without needing to have an external source of chirality.

2. Perspectives for futures studies

In the case of hybrid structures, although the organization of the gemini molecules inside the structures was precisely determined, the evolution of the CD signal upon addition of the hybrid helices shows an optimal ratio of 1:1 between the chromophore (**PSA**) and the gemini surfactant. However, the gemini is bi-cationic, and a ratio of 2:1 could be expected for complete ion exchange from chloride to the fluorophore. This discrepancy may be due to the inaccessibility of chromophores to all the cationic sites in the hybrid. An extended study of the exact conformation of the hybrid containing chromophore might explain this difference.

On the tuning of chiroptical properties of chiral chromophores, a planar aromatic molecule could be used as **CSA** does not have the ability to aggregate. A chiral chromophore able to interact with neighboring molecules when forced into hybrid helices may be able to show larger chiral effects upon inclusion. Also, for molecules forming twisted ribbon self-assemblies such as **PBPA**, it may be interesting to use hybrid twisted ribbons instead of helical ribbons, in order to adopt a structure which is similar to that naturally adopted by the fluorophore upon self-aggregation.

In the case of carbon based quantum-dots, preliminary experiments done during this study are very promising, and this may lead to new source of circularly polarized light. In this case too, the use of twisted ribbon instead of helices may be interesting and should to be investigated. Optimization of the calcination conditions is key to obtain chiroptical properties.

CHAPTER VI: ADDITIONAL INFORMATION

1. Experimental section

1-a. Synthesis of 16-2-16 tartrate

The synthesis of 16-2-16 tartrate is divided into 3 steps: the synthesis of the amphiphilic moieties, 1,2-ethane bis(dimethylhexadecylammonium) (16-2-16 gemini) with bromide counter ions (16-2-16 bromide), then ion exchange from bromide to acetate and finally another ion exchange from acetate to tartrate.

1-a.i Synthesis of 16-2-16 bromide

N,N,N',N'-Tetramethylethylenediamine (Sigma / CAS: 110-18-9) is allowed to react with 2.5 equivalents of 1-bromohexadecane (Aldrich / CAS: 112-82-3) in acetonitrile under reflux (at 85°C) for 3 days, following the reaction pathway presented in Figure VI-1.

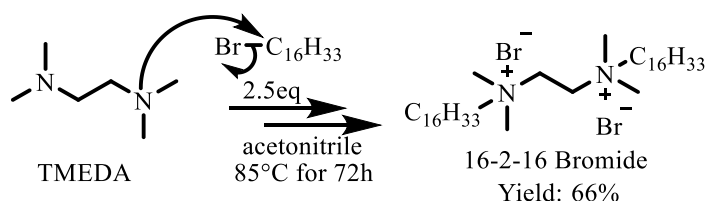


Figure VI-1: 16-2-16 bromide reaction scheme

In order to purify the product, the solution is centrifuged (5min / 3893g / 20°C) and the solid collected. Then, the powder is dispersed in acetone, sonicated in a sonication bath and then centrifuged again. In the following, this step of centrifugation and dispersion of powder or nano-objects in a solvent will be called washing. The washing is repeated 5 times. Then, the product is dried under vacuum, and characterized using NMR to verify the absence of starting reactants and of monoalkylated product.

Typical NMR spectra of 16-2-16 Br ^1H NMR (300MHz, d-MeOD, 25°C, δ ppm): 4.02 (4H, s), 3.49 (4H, m), 3.26 (12H, s), 1.84 (4H, s), 1.29 (52H, m), 0.90 (6H, t, $^3J=6.42\text{Hz}$)

1-a.ii Ion exchange to acetate

Starting from 16-2-16 bromide dissolved in methanol at 50°C, 3 equivalents of silver acetate (Acros / CAS: 563-63-3) are added into the solution and allowed to react during 24h, as shown on Figure VI-2.

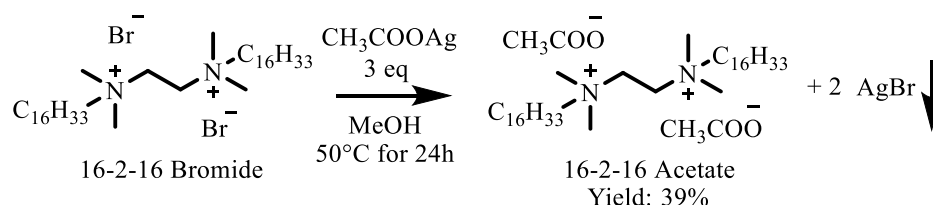


Figure VI-2: Ion exchange to 16-2-16 acetate

Purification of the product is done by filtration on celite, then the methanol is almost totally removed on a rotary evaporator, followed by addition of acetone until precipitation. The solid is collected by centrifugation (12min / 3983g / 4°C) and the powder is washed 4 times using acetone. Finally, the product is dried under vacuum overnight and verified by NMR to ensure the total exchange of bromide by acetate.

Typical NMR spectra of 16-2-16 Ac $^1\text{H NMR}$ (300MHz, d-MeOD, 25°C, δ ppm): 3.90 (4H, s), 3.41 (4H, m), 3.21 (12H, s), 1.90 (6H, s), 1.83 (4H, s), 1.29 (52H, m), 0.90 (6H, t, $^3\text{J}=6.38\text{Hz}$)

1-a.iii Ion exchange to tartrate

The 16-2-16 acetate is dissolved in a mixture of methanol and acetone (1:9). A solution containing 2 equivalents of enantiopure tartaric acid (Sigma / CAS: 87-69-4 for L and 147-71-7 for D) in the same solvent mixture is prepared. Typical quantities are 1g of 16-2-16 acetate for 220mg of tartaric acid. After that, slow addition the 16-2-16 acetate solution into the tartaric acid solution is followed by 2h of stirring (room temperature). This reaction is shown on Figure VI-3.

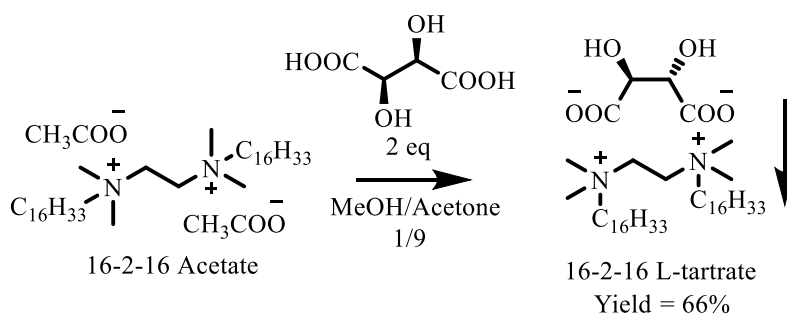


Figure VI-3: Ion exchange to 16-2-16 L-tartrate

Purification of the final product is done through centrifugation (12min / 3893g / 20°C). To the powder we add the methanol/acetone (1:9) solvent mixture, and disperse the powder by sonication, then centrifuge again. This washing step is repeated twice with methanol/acetone solvent then several times (5-8) with cold water (4°C) until the pH of the supernatant is around 5, then 2 more washing using acetone alone are performed. Finally, the powder is dried under vacuum overnight and analyzed by NMR.

Typical NMR spectra of 16-2-16 Tart ^1H NMR (300MHz, d-MeOD, 25°C, δ ppm): 4.30 (2H, s), 3.92 (4H, s), 3.41 (4H, m), 3.21 (12H, s), 1.82 (4H, s), 1.29 (52H, m), 0.90 (6H, t, $^3J=6.50\text{Hz}$)

1-b. Formation of silica coated chiral nano-structures

1-b.i Preparation of nano-helices organic gels

Solid 16-2-16 tartrate is suspended in ultrapure water and heated to 70°C (above the Kraft temperature: ~43°C for a 10mM solution). Typically, 20.0mg are dissolved into 28.0g of water (concentration 1mM). Once the solid is fully dissolved, the solution is separated into 5mL aliquots and maintained at 20°C on a roller-mixer for 15min, then allowed to rest horizontally for 4 days.

Note that the morphology of these organic nano-structures is time dependent, as shown on Figure VI-4. After 2h, twisted nano-ribbons are obtained, after 3-4 days the pitch decreases and change the shape into nano-helices, which then transforms into nano-tubes after several days (7-10 days in total). Each of these structures can be transcribed into hybrid or inorganic samples by starting the silica transcription at the desired time.

The formation of the organic template can be checked by transmission electron microscopy (TEM) using a contrast agent (uranyl acetate solution) as shown on Figure VI-4.

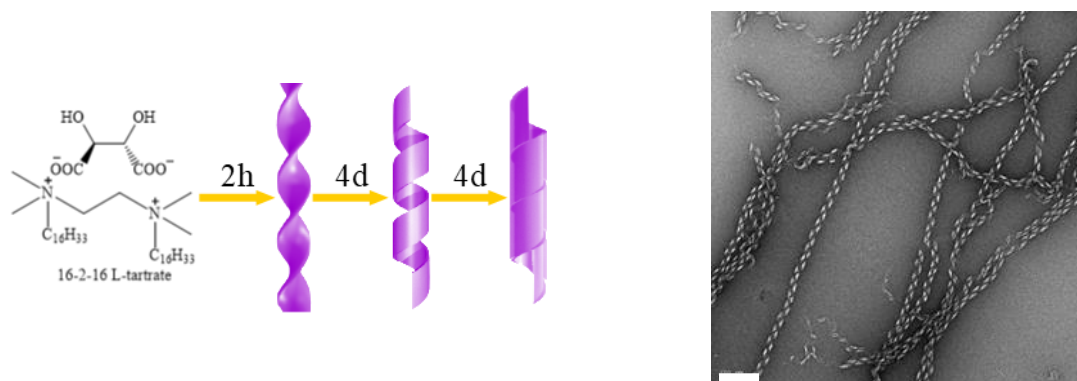


Figure VI-4: Left: Scheme of the aging effect on the formation of nano-structures / Right: TEM picture of nano-helices formed after self-assembling of 16-2-16 D-tartrate using uranyl acetate as contrasting agent (120kV / scale bar: 200nm)

1-b.ii Polycondensation of the silica shell

The silica shell is formed through polycondensation of tetraethylorthosilicate (TEOS). TEOS first needs to be hydrolyzed in an acidic medium. To avoid the multiplication of ions, which may destabilize the organic self-assembly, tartaric acid is used during this process. For this, 1.5mL of TEOS (Sigma / CAS: 78-10-4) is typically put in 30mL of a 10mM solution of L or D tartaric acid ($C_{\text{TEOS}} = 225\text{mM}$). This solution is energetically shaken by hand then kept on roller-mixer at 20°C for 6-7h.

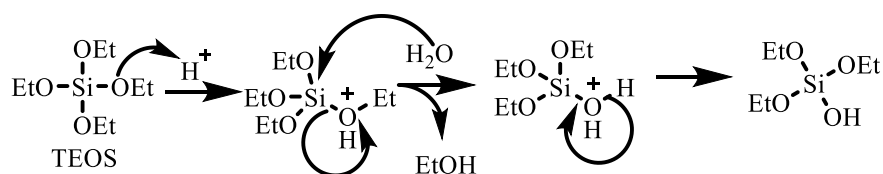


Figure VI-5: TEOS pre-hydrolysis reaction

During this time, the reaction of TEOS hydrolysis (shown on Figure VI-5) can occur. However, a total transformation is not necessary to pursue to the step of silica condensation. After the prehydrolysis, 5mL of TEOS solution were added in a tube containing 5mL of organic template (matching the enantiomers of tartaric acid of both solutions). Silica deposition occurs via

polycondensation of pre-hydrolyzed TEOS catalyzed by the surface of the organic helical template (Figure VI-6). This reaction is performed overnight on roller-mixer at 20°C.

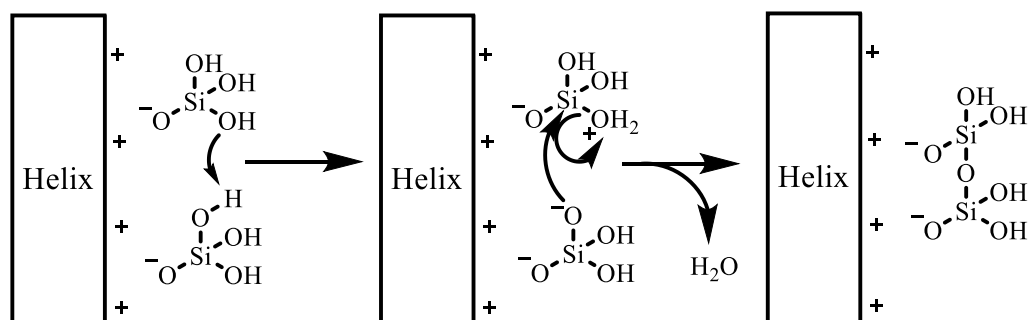


Figure VI-6: Polycondensation reaction, negatively charged part of the molecule interact with gemini part of 16-2-16 tartrate

1-c. Purification and final steps

The dispersion of helices is achieved by tip-sonication (20 pulses of 1s at 130W) without changing the solvent. Washing process and later steps depend on the desired composition: organic part inside (hybrid helices) or not (inorganic helices), and are described below.

1-c.i *Case of hybrid structures*

Hybrid helices are isolated by centrifugation (12min / 3893g / 4°C). The supernatant is removed add cold ultrapure water (4°C) added, followed by short sonication in a sonication bath (maximum 10 sec). This washing is repeated at least 5 times (until pH > 5). *NB: Afterwards, hybrid samples are stored at 2°C until used.* This is followed by the washing using potassium chloride and quantification as described in Chapter II:1-c.i (page 28).

1-c.ii *Case of inorganic structures*

In the case of inorganic helices, the purification process is similar except centrifugations are done at room temperature, methanol is used instead of water, and the sample is heated to 70°C for 5 min before each centrifugation step.

In order to make the silica surface reactive toward grafting, functionalization of the surface is performed using (3-aminopropyl)triethoxysilane (APTES / Aldrich / CAS: 919-30-2). This reaction is achieved in methanol at 80°C overnight (APTES concentration: 40mM). The mechanism of this reaction is the same as for the TEOS polycondensation.

Once this reaction is complete, the samples are washed 3 times by methanol using centrifugation (30min / 10000g / 20°C) with 5 min sonication in a sonication bath in between. Then, the grafting is repeated a second time (using the same protocol). After this reaction, the number of APTES on the surface of helices was quantified using NMR spectroscopy. The method for this quantification is described on page 36.

1-d. Synthesis of perylene and acridine derivatives

1-d.i Perylene

PTCTK was prepared in one step starting from perylene-3,4,9,10-tetracarboxylic dianhydride (Aldrich / CAS: 128-69-8). Typically, 5g of perylene-3,4,9,10-tetracarboxylic dianhydride were poured into 150mL of water containing 6g of potassium hydroxide. This mixture is heated to reflux and kept at this temperature for 14h, leading to the reaction presented on Figure VI-7.

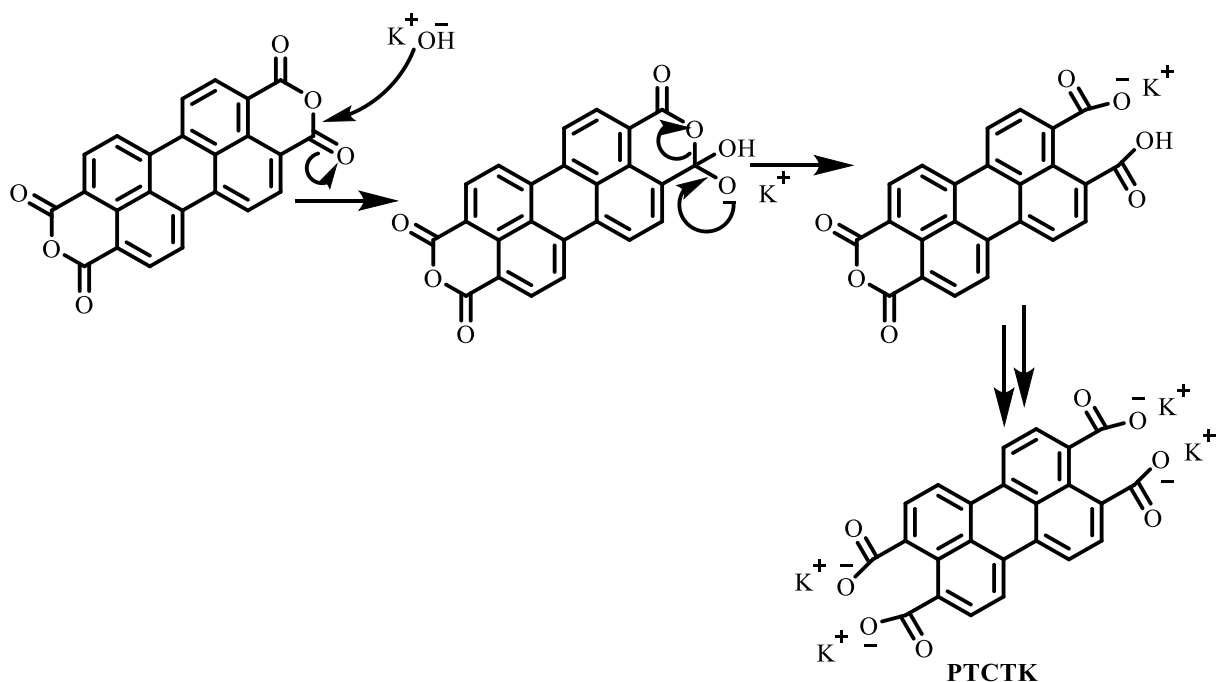


Figure VI-7: Synthetic pathway to **PTCTK**

After the reaction is complete, the product is precipitated in a mixture of isopropanol and acetone (1:1), collected by filtration and dried under vacuum. Residual water is removed by drying in an oven under low vacuum (100°C / 10mbar).

Typical NMR spectra of PTCTK ^1H NMR (300MHz, D_2O , 25°C, δ ppm): 8.35 (4H, d, $^3\text{J}=7.93\text{Hz}$), 7.74 (4H, d, $^3\text{J}=7.85\text{Hz}$)

The synthesis of **PBPA** was accomplished from 200mg of **PTCTK** in a mixture of water and ethanol (1:1). Then, 130mg of enantiopure phenylalanine are added (L: Sigma / CAS: 63-91-2) (D: Alfa Aesar / CAS: 673-06-3). The mixture is heated to reflux (95°C) and allowed to react during 2 days. The reaction scheme is presented in Figure VI-8.

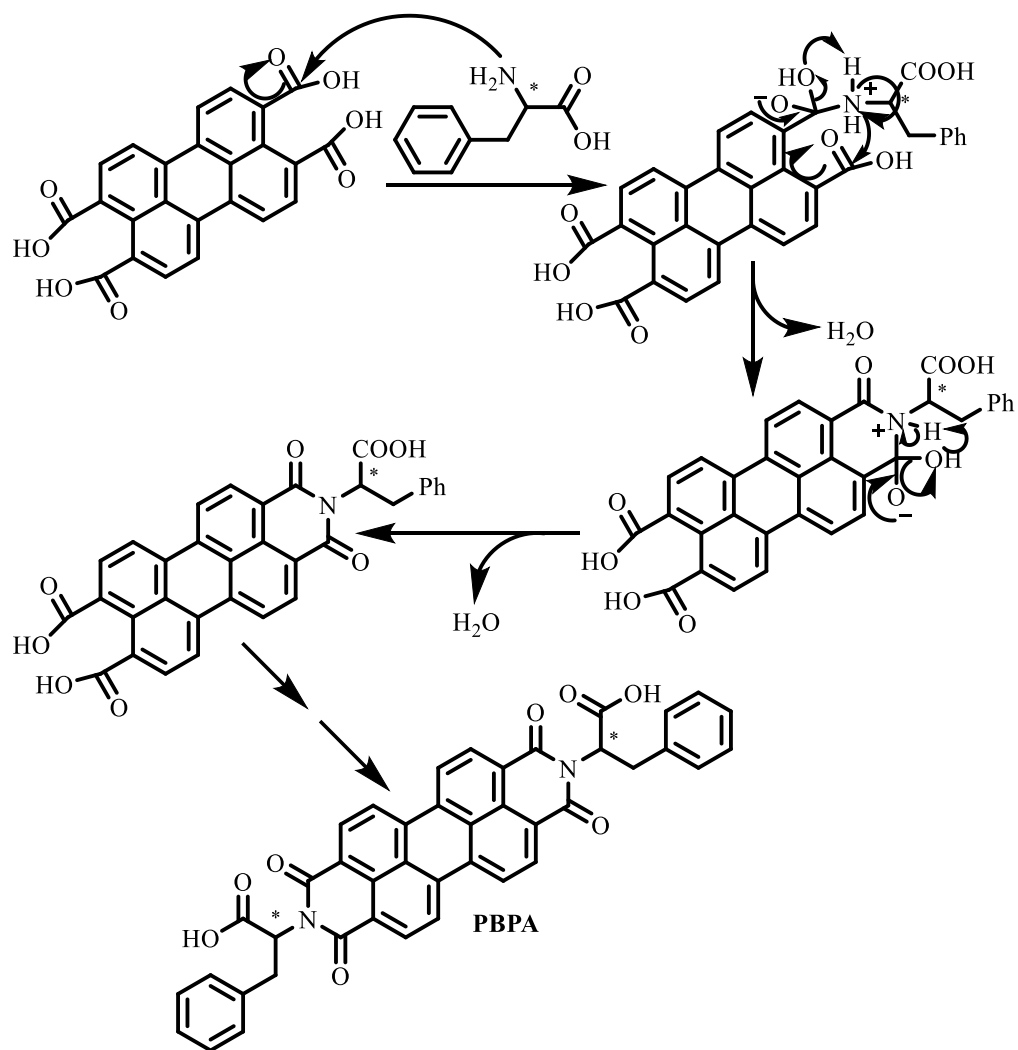


Figure VI-8: Synthetic pathway leading to **PBPA**

Purification is done by acidification of the solution (using hydrochloric acid) leading to the precipitation of **PBPA**. After that, the sample is centrifuged (3893g / 3min / 20°C) then washed using water. Remaining water is removed by freeze-drying.

Typical NMR spectra of PBPA ^1H NMR (300MHz, 6d-DMSO, 25°C, δ ppm): 12.9 (2H, sl), 8.30 (8H, m), 7.14 (10H, m), 5.92 (2H, m), 3.61 (4H, m) **Mass Spectroscopy** m/z , Da (FD+): 686.17 (100), 687.17 (50), 688.18 (15), 689.18 (5)

PBPA aggregates were formed by dissolving 6.96mg of **PBPA** in 1.015mL of anhydrous DMSO (10mM) then adding 30 μL of this solution to 2970 μL of ultrapure water in one portion while stirring (around 1000rpm).

1-d.ii Acridine

For the synthesis of ABA: starting from 1.98g of 9(10H)-acridanone (Sigma-Aldrich / CAS: 578-95-0), 30mL of distilled phosphorus oxychloride (Sigma-Aldrich / CAS: 10025-87-3) are added and the reaction is allowed to proceed (presented on Figure VI-9) for 2h under reflux (140°C). After that, the excess phosphorus oxychloride is removed by distillation and the yellow solid obtained is used in the next step without further purification.

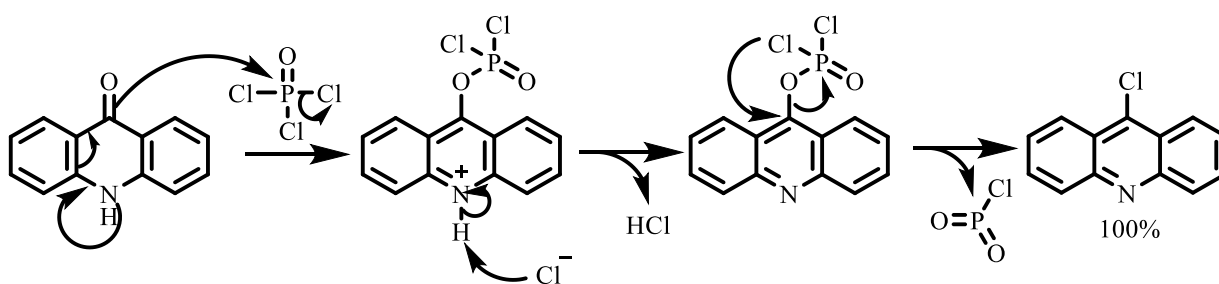


Figure VI-9: Activation of acridanone by $POCl_3$

5.9g of phenol are added along with 1.35g (1.2 equivalents) of γ -aminobutyric acid (Aldrich / CAS: 56-12-2). The reaction proceeds at 120°C overnight (as described on Figure VI-10) under argon after that the residue was dissolved in ethanol then added to diethyl ether. The precipitate was collected and recrystallized from methanol with an overall yield of 39%.

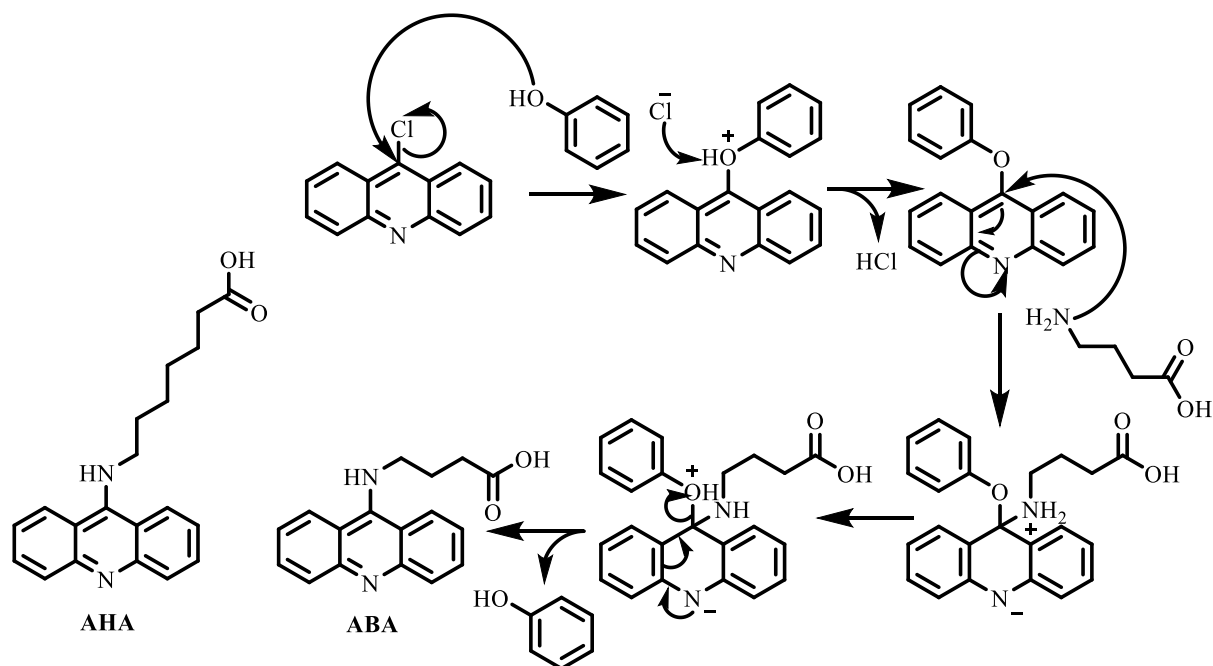


Figure VI-10: Nucleophilic substitution leading to ABA

Typical NMR spectra of ABA ^1H NMR (300MHz, 6d-DMSO, 25°C, δ ppm): 8.32 (2H, d, $^3\text{J}=8.67\text{Hz}$), 7.64 (4H, m), 7.26 (2H, m), 3.88 (2H, t, $^3\text{J}=6.57\text{Hz}$), 2.36 (2H, t, $^3\text{J}=6.72$), 1.95 (2H, q, $^3\text{J}=6.60\text{Hz}$) **Mass Spectroscopy** m/z , Da (Turbo Spray): 281.1 (100), 303.1 (94), 583.3 (3), 605.3 (10)

For synthesis of AHA: starting from 996mg of 9(10H)-acridanone (Sigma-Aldrich / CAS: 578-95-0), 30mL of distilled phosphorus oxychloride are added (Sigma-Aldrich / CAS: 10025-87-3) and the reaction is allowed to proceed for 2h under reflux (140°C). After that, the excess phosphorus oxychloride is removed by distillation and the yellow solid obtained is used in the next step without further purification. Then 2.0g of phenol are added along with 1.34g (2.0 equivalents) of 6-aminocaproic acid (Aldrich / CAS: 60-32-2). The reaction proceeds at 120°C overnight under argon after that the residue was dissolved in ethanol then added it in diethyl ether. The gum-like precipitate is dried under vacuum then recrystallized in acetone at -20°C then dried under vacuum. The reaction overall yield is 30.6%.

Typical NMR spectra of AHA ^1H NMR (300MHz, 6d-DMSO, 25°C, δ ppm): 8.20 (2H, d, $^3\text{J}=8.72\text{Hz}$), 8.05 (2H, d, $^3\text{J}=8.48\text{Hz}$), 7.49 (2H, m), 7.24 (2H, m), 4.21 (2H, t, $^3\text{J}=7.19\text{Hz}$), 2.45 (2H, t, $^3\text{J}=7.18$), 2.14 (2H, m), 1.85 (2H, m), 1.30 (2H, m) **Mass Spectroscopy** m/z , Da: 309.2

1-e. Carboxylic acid activation and surface reaction

The activation of the acid for covalent grafting on the surface of amine functionalized helices is done through the reaction with 2 equivalents of ethyl chloroformate (Sigma-Aldrich / CAS: 541-41-3) in dried acetone containing 2.5 equivalents of trimethylamine (Sigma-Aldrich / CAS: 121-44-8) under nitrogen at ambient temperature for 2h, the reaction pathway is represented in Figure VI-11.

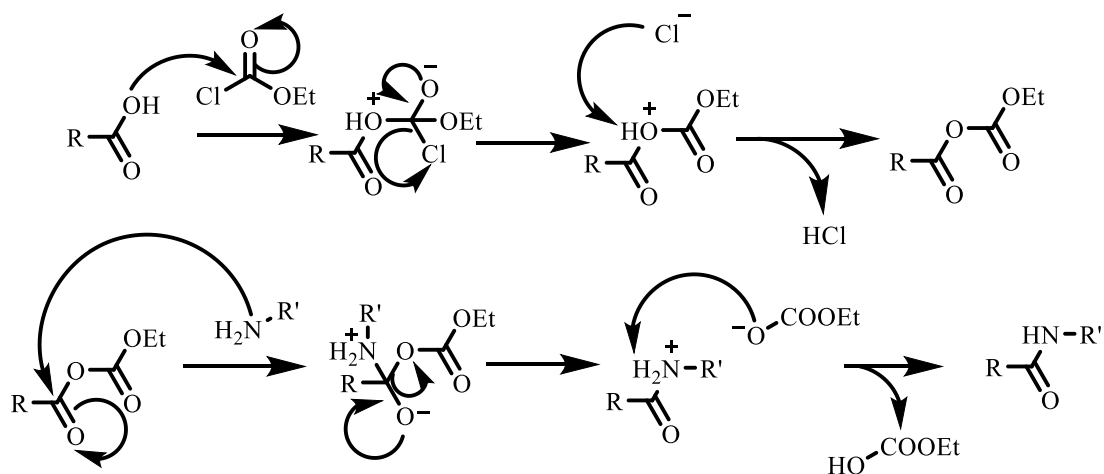


Figure VI-11: Activation using ethyl chloroformate and reaction with amine group (*R* is the chromophore and *R'* is attached to the helix)

In preparation for coupling, the APTES-Helices are washed 5 times using dried acetone. Once the reaction is finished, and without further purification, the solution of activated chromophore is introduced in the nano-helices (1 μ mol of chromophore / mg of helices). This reaction is conducted overnight, and the sample is washed 3 times using dried acetone using centrifugation (9800g / 10min / room temperature). After what, the grafting process is repeated again.

2. Details on the self-assembly of 16-2-16 tartrate^{55,89}

2-a. Molecular conformation

The cationic moiety of 16-2-16 tartrate may show 2 different conformations presented in Figure VI-12, and will stay in trans-like conformation (both chain going in opposite directions) when free in solution or complexed with a classic anion such as a bromide or acetate.

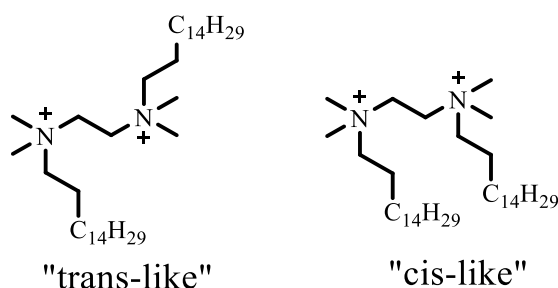


Figure VI-12: Two possible conformations of gemini moiety of 16-2-16

However, due to the interaction with tartrate, the gemini moiety will take a cis-like conformation (both chain going in the same direction) once bilayers are formed. Additionally, the tartrate ion will force the two carbon chain of the gemini into one conformation: one enantiomer of tartrate will induce a “backward Z” conformation while the other enantiomer will induce a “Z” conformation as shown on Figure VI-13. Note that if we represented here L-tartrate with “backward Z” gemini and D-tartrate with “Z” gemini, the reality may be reversed.

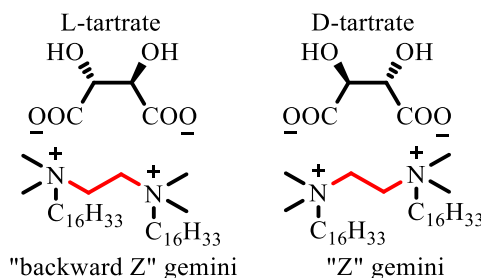


Figure VI-13: Molecular structure of L (on left) and D (on right) 16-2-16 gemini tartrate with the gemini part in the corresponding conformation. The “backward-Z” and “Z” part are shown in bold red

At the same time, due to the interactions of the aliphatic chains inside the bilayer, gemini from one side will be forced to have the opposite conformations from the ones on the opposite side of the

bilayer: if the gemini on one side is “Z”, the one on the other side will be “backward Z”. In the case of racemic solution, this will force the bilayer to have one tartrate enantiomer on one side and the other enantiomer on the other side of the bilayer.

2-b. Multiple bilayers structure

Due to the presence of tartrate on the outside of the bilayer, these supramolecular structures will be able to stack together into multiple bilayers by hydrogen bonding. These hydrogen bonding may only happen homochirally. So, in a racemic mixture, we will have an alternation of bilayers as shown in left of Figure VI-14, which can continue endlessly.

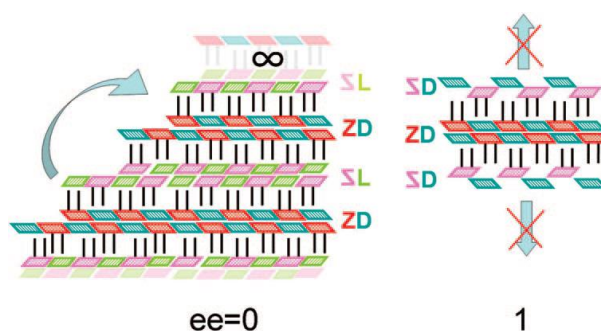


Figure VI-14: Schematic representation of multiple bilayer formation in the cases of racemic mixture and enantiopure solution of 16-2-16 tartrate⁵⁵

However, in the case of enantiopure solutions, if the contact between 2 bilayers can be homochiral, the outer layer of gemini will not match the tartrate in the solution. This mismatch will prevent the tartrate ion to interact perfectly with the double-bilayer and will prevent a further growth in the number of bilayers (Figure VI-14 on right).

2-c. Supramolecular morphology

In the case of racemic mixtures, once the bilayers combine, large flat ribbons can be observed in solution. However, in case of enantiopure solutions, twisted nano-ribbons are observed after short time, and these structures evolve into helical nano-ribbons (called nano-helices) for which the width increases until complete closure, forming tubules (Figure VI-15).

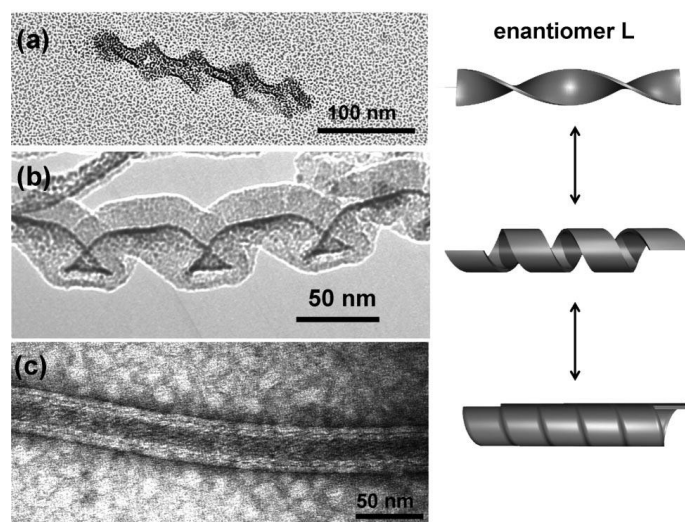
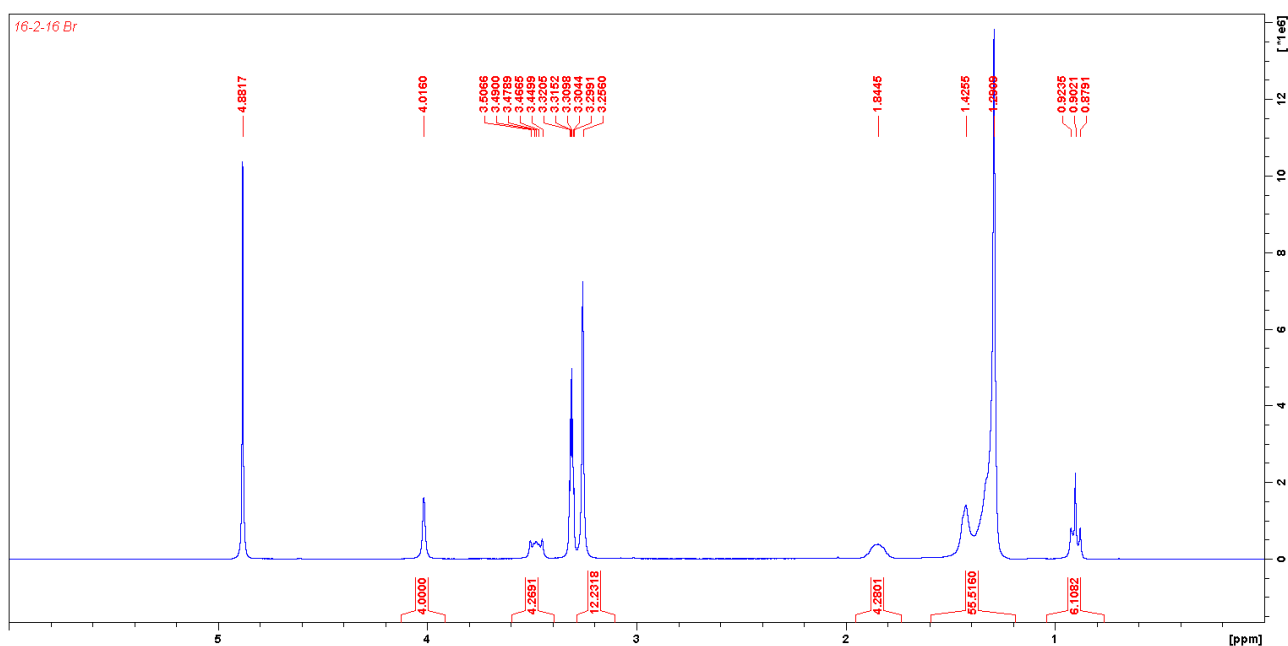


Figure VI-15: Evolution of the supramolecular morphology of 16-2-16 L-tartrate solution⁸⁹

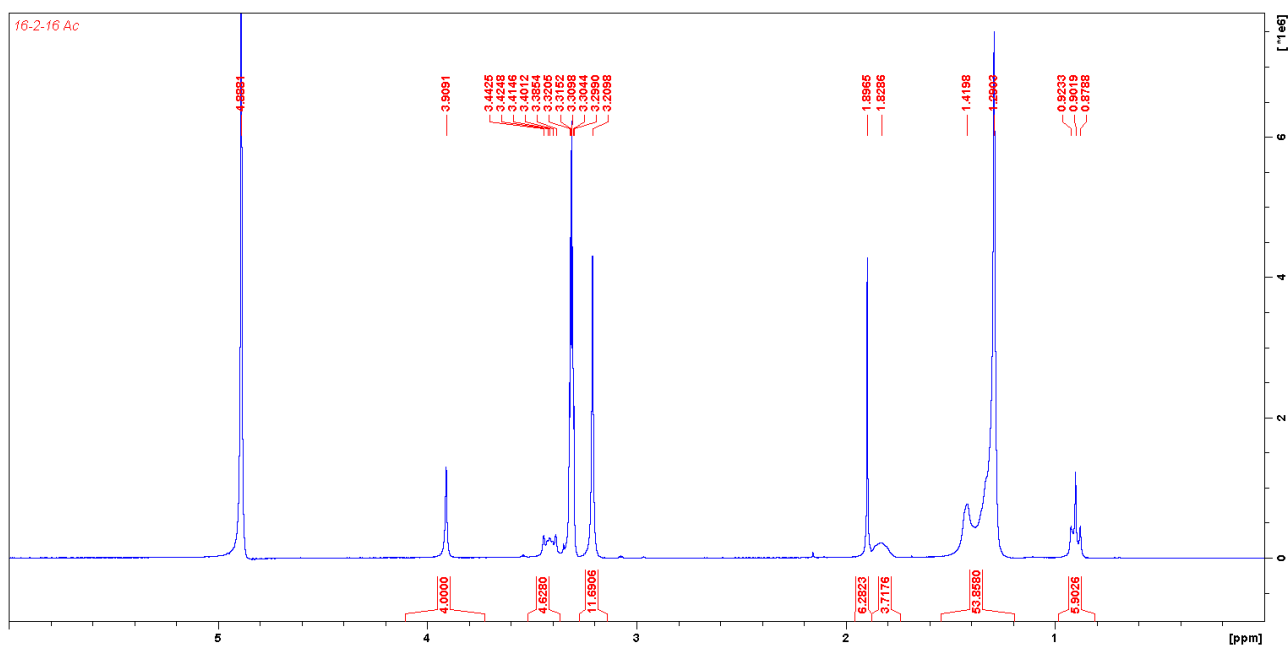
3. NMR spectra

3-a. Gemini molecules

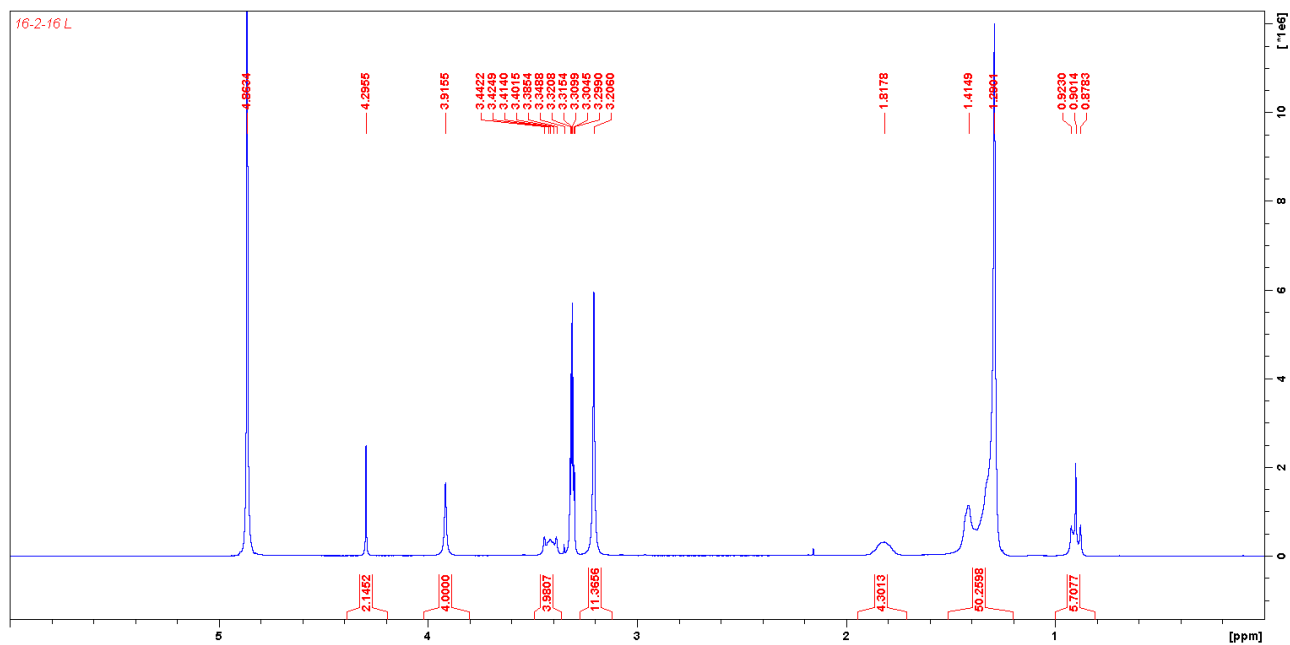
3-a.i 16-2-16 Bromide (300MHz, d-MeOD, 25°C, δ ppm)



3-a.ii 16-2-16 Acetate (300MHz, d-MeOD, 25°C, δ ppm)

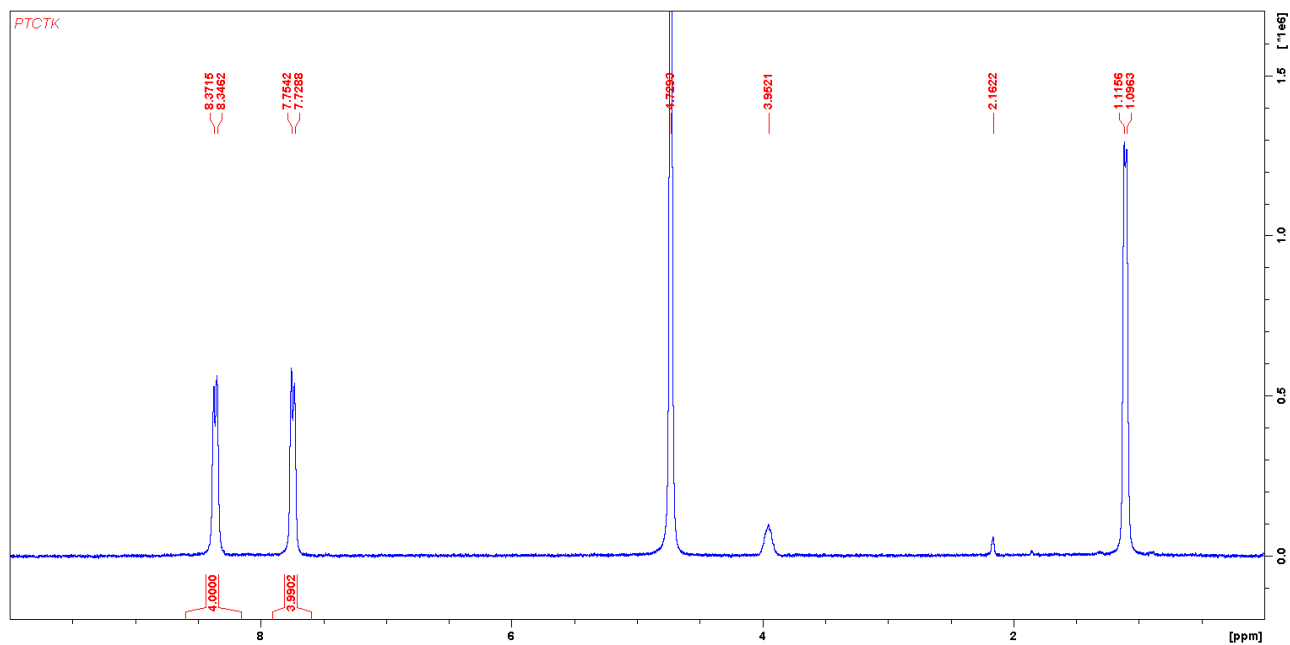


3-a.iii 16-2-16 Tartrate (300MHz, d-MeOD, 25°C, δ ppm)

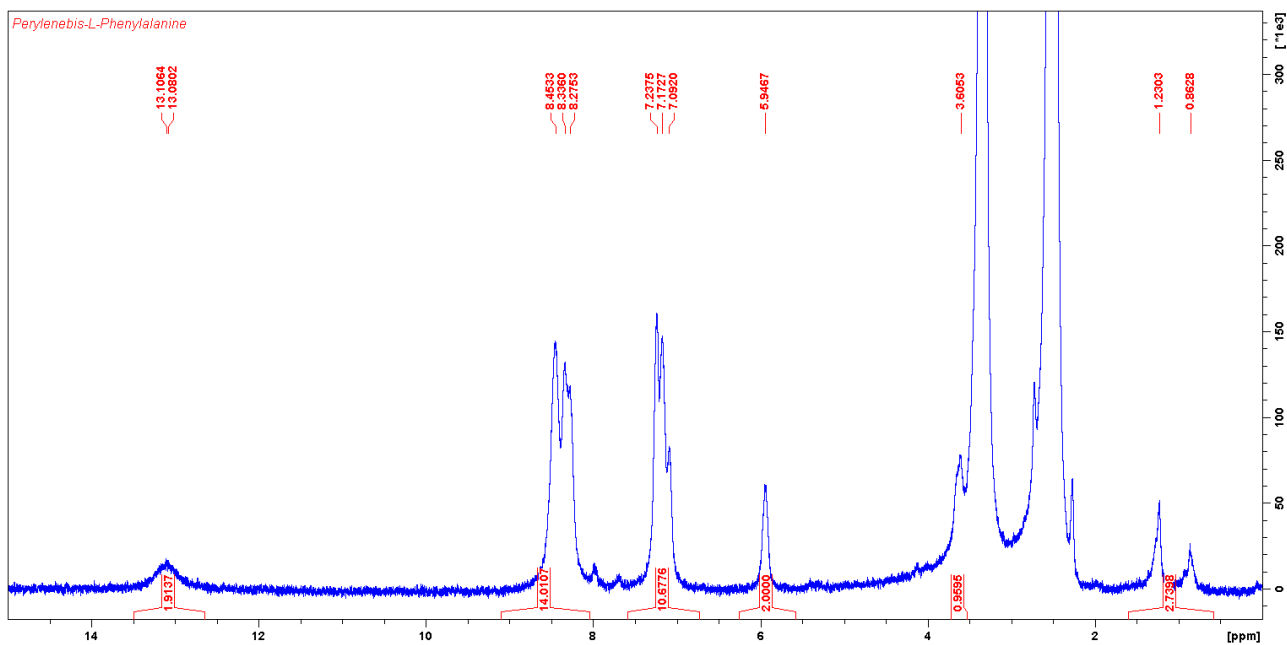


3-b. Organic chromophores

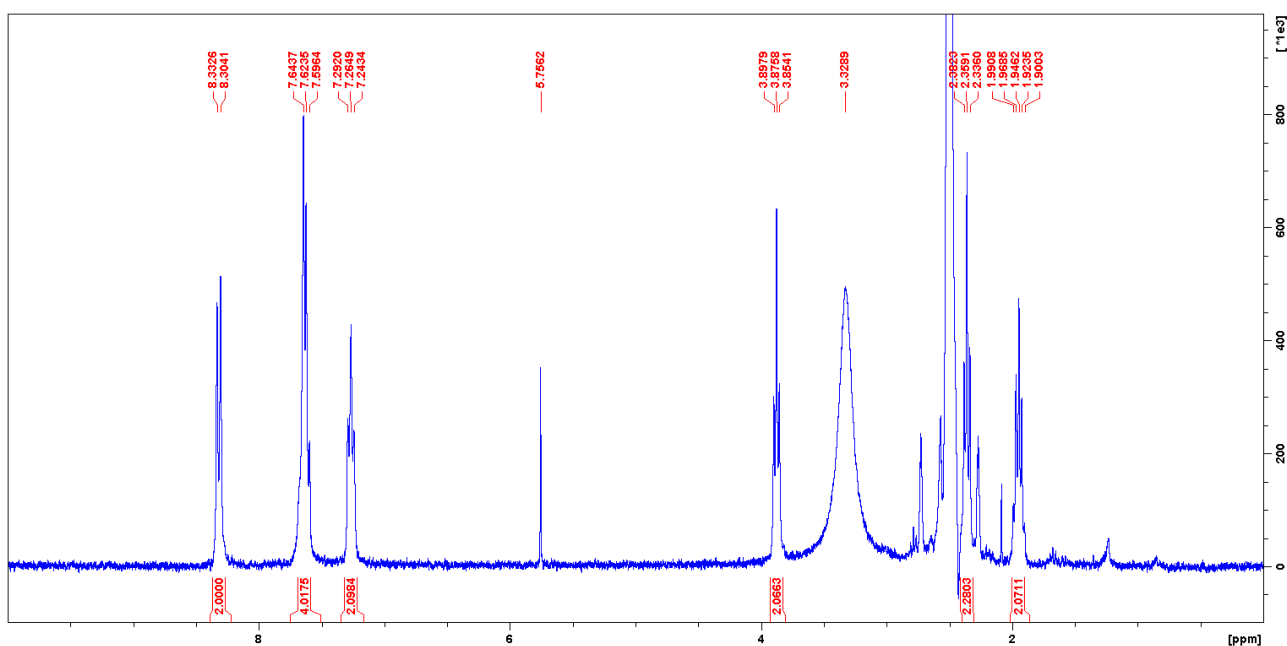
3-b.i PTCTK (300MHz, D₂O, 25°C, δ ppm)



3-b.ii PBPA (300MHz, 6d-DMSO, 25°C, δ ppm)



3-b.iii ABA (300MHz, 6d-DMSO, 25°C, δ ppm)



3-b.iv AHA (300MHz, 6d-DMSO, 25°C, δ ppm)

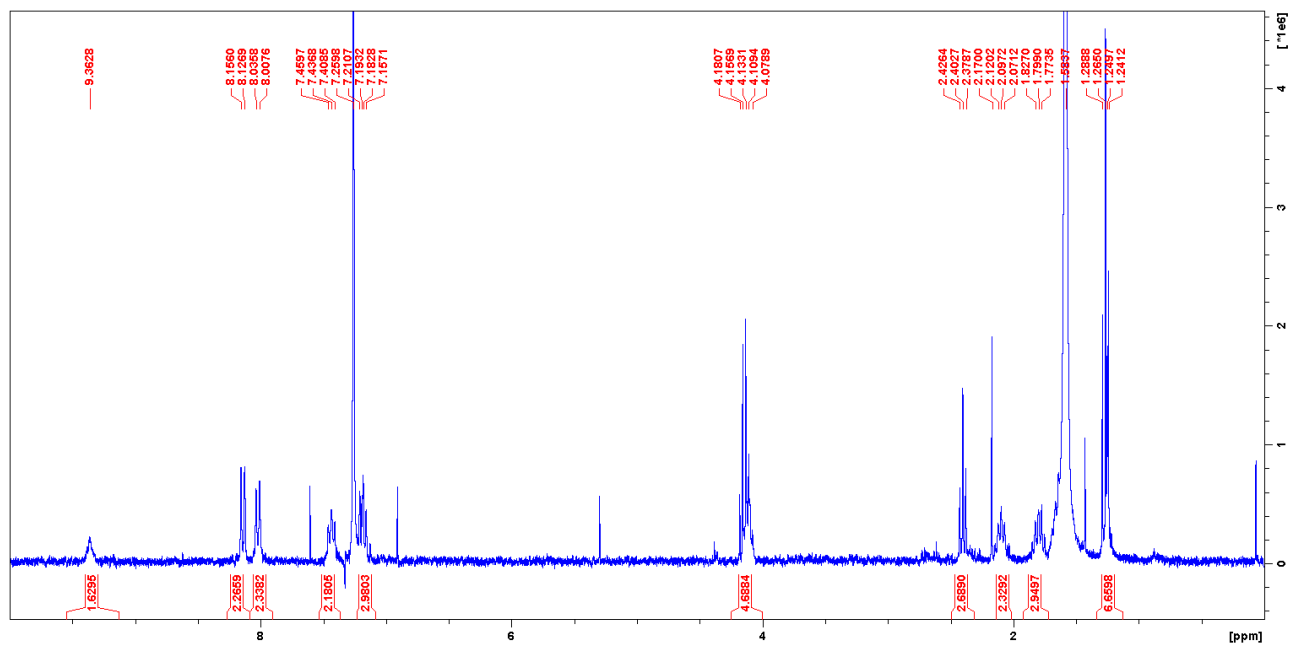


TABLE OF FIGURES

Figure I-1: Examples of chirality at every scale (scale in meter) -----	2
Figure I-2: Scheme of linearly and circularly polarized waves -----	3
Figure I-3: R- and S-methamphetamine -----	4
Figure I-4: Example of R and S molecules -----	4
Figure I-5: Induction of optical activity from fructose to calix[4]arene (Reprinted with permission from Kikuchi Y. et al., J. Am. Chem. Soc., 1992 , 114, 1351-1358. Copyright (1992) American Chemical Society) -----	5
Figure I-6: Structures of used compounds and resulting optical activity (Reprinted with permission from Mizutani T. et al., Tetrahedron Lett., 1997 , 38, 1991-1994. Copyright (1997) Elsevier Science Ltd) -----	5
Figure I-7: Different types of self-assembled structures (micelle, bilayer and vesicle) hydrophilic part represented as pink dot and hydrophobic tail by black curve and considering water as solvent	6
Figure I-8: Structure of DNA with its four components and the backbone molecule-----	7
Figure I-9: Representation of the domains of a protein with α -helices in blue and β -sheets in red	8
Figure I-10: Structure of a lipid forming twisted nano-ribbons and TEM image of the assembly (Scale bar : 100nm) ¹⁹ (Reprinted with permission from Ihara, H. et al., Langmuir 1992 , 8, 1548–1553. Copyright (2019) American Chemical Society)-----	8
Figure I-11: Stereospecific isomerization of citrate by aconitase ²¹ -----	9
Figure I-12: Electromagnetic spectrum range (picture source: DefenderShield website) with approximative wavelength in visible spectrum-----	10
Figure I-13: Schematics representation of $\sigma\sigma^*$ and $\pi\pi^*$ transitions -----	11
Figure I-14: JABONSKI-PERRIN diagram with name and speed range of represented processes ²⁵ (Reprinted with permission from Klan P. and Wirz J., John Wiley & Sons, Ltd, 2009 . Copyright 2019 P. Klan and J. Wirz)-----	12

Figure I-15: Left: Potential energy surfaces for excimer formation and relaxation ²⁵ / Right: Orbital diagram for the encounter of two molecule (Reprinted with permission from Klan P. and Wirz J., John Wiley & Sons, Ltd, 2009 . Copyright 2019 P. Klan and J. Wirz)-----	14
Figure I-16: Illustration of the two extremes aggregation type-----	15
Figure I-17: Schematic representation of absorption difference depending of aggregation type-	15
Figure I-18: Chiral aggregation of tetraphenylethylene derivative and associated CPL signal ³⁷ (Reprinted with permission from Li H. et al., J. Matt. Chem. C, 2015 , 3, 2399-2404. Copyright (2019) Royal Society of Chemistry) -----	18
Figure I-19: Evolution of absorbance and CD of methyl orange upon addition of hybrid helices ⁴¹ (Reprinted with permission from Ryu, N. et al., Chem. Comm., 2016 , 52, 5800-5803. Copyright (2019) Royal Society of Chemistry) -----	19
Figure II-1: Simplified scheme of the synthetic pathway toward helical nano-structures used in this study -----	22
Figure II-2: Schematic model of gemini n-s-m X (in this project n=m=16 and s=2) -----	22
Figure II-3: Synthetic pathway leading to 16-2-16 bromide-----	23
Figure II-4: Synthetic pathway to form 16-2-16 acetate-----	24
Figure II-5: Synthetic pathway to form 16-2-16 L-tartrate -----	24
Figure II-6: Left: Scheme of the aging effect on the formation of nano-structures / Right: TEM picture of nano-helices formed after self-assembling of 16-2-16 D-tartrate using uranyl acetate as contrasting agent (120kV / scale bar: 200nm)-----	26
Figure II-7: Polycondensation reaction, negatively charged part of the molecule interact with gemini part of 16-2-16 tartrate -----	27
Figure II-8: TEM pictures of left and right handed silica nano-helices without staining (120kV) -----	27
Figure II-9: CD (top) and absorption (bottom) spectra of hybrid nano-helices before and after ion-exchange to chloride ($C_{16-2-16X}=100\mu\text{M}$) -----	28
Figure II-10: Commercially available chromophores used during the project -----	30
Figure II-11: Perylene derivatives synthetized in DYSMOL group -----	31

Figure II-12: Synthetic pathway leading to PTCTK -----	32
Figure II-13: Synthetic pathway leading to PBPA -----	32
Figure II-14: Chiroptical properties of PBPA in various mixtures of DMSO/water ⁵⁰ (Reprinted with permission from Chen W. et al., PCCP, 2018 , 20, 4144-4148. Copyright (2019) Royal Society of Chemistry)-----	33
Figure II-15: Synthetic pathway leading to ABA -----	33
Figure II-16: Activation using ethyl chloroformate and reaction with amine group (R is the chromophore and R' is attached to the helix)-----	34
Figure II-17: Typical NMR spectra of APTES-Helices + TMSP 1H NMR (300MHz, D2O)----	38
Figure II-18: Schematic representation of a CD spectrometer -----	39
Figure II-19: Illustration of ellipticity due to CD-----	40
Figure II-20: Illustration of ellipticity in CPL -----	41
Figure II-21: Schematic representation of a CPL spectrometer -----	41
Figure III-1: Optical (top left) and fluorescence (top right) microscopy images and chiroptical spectroscopy (bottom) of casted film of chiral aggregates ⁵³ (Reprinted with permission from Han, J. et al., Angew. Chem. Int. Edit. 2019 , 58, 7013-7019. Copyright (2019) Wiley-VCH) -----	44
Figure III-2: Induction of CPL on lanthanide oxide nano-particles ⁵⁴ (Reprinted with permission from Sugimoto, M. et al., Chem. Eur. J., 2018 , 24, 6519-6524. Copyright (2019) Wiley-VCH) ---	44
Figure III-3: Detailed structure of a hybrid helix-----	45
Figure III-4: Evolution of absorption and CD upon addition of hybrid helices bromide in MO solution (Reprinted with permission from Ryu, N. et al., Chem. Comm., 2016 , 52, 5800-5803. Copyright (2019) Royal Society of Chemistry) -----	46
Figure III-5: Highlighting of chiral induction on mono-atomic anions ⁴ (Reprinted with permission from Okazaki Y. et al., Chem. Comm., 2018 , 54, 10244-10247. Copyright (2019) Royal Society of Chemistry) -----	47
Figure III-6: Chiral induction on I ₂ (left) and CuI (right) ⁴ (Reprinted with permission from Okazaki Y. et al., Chem. Comm., 2018 , 54, 10244-10247. Copyright (2019) Royal Society of Chemistry)-	48

Figure III-7: CD (top) and absorption (bottom) spectra upon addition of hybrid helices (170 μ M) in a solution of PAA (50 μ M) -----	49
Figure III-8: Time dependency of dissymmetry factor in a solution of hybrid helices (100 μ M) upon addition of PAA (100 μ M) after 5min (scan at 282nm) -----	50
Figure III-9: Evolution of the dissymmetry factor at 2 different wavelength (283nm and 327nm) with the ratio PAA to gemini ([gemini]=100 μ M except for ratio of 5:1 where [gemini]=40 μ M) 2 hours after mixing -----	51
Figure III-10: Fluorescence spectra of 200 μ M PAA + 100 μ M hybrid helices under excitation at 340nm -----	51
Figure III-11: CD (top) and absorption (bottom) spectra upon addition of hybrid helices (100 μ M) in a solution of PSA (50 μ M) in comparison with PAA -----	52
Figure III-12: Evolution CD (top) and absorption (bottom) of the mix PSA (50 μ M) with right hybrid helices (100 μ M) with time-----	54
Figure III-13: Evolution of the dissymmetry factor of a solution of hybrid helices (150 μ M) upon addition of PSA at 351.8nm and 285.4nm -----	55
Figure III-14: Fluorescence spectroscopy of PSA (150 μ M) with and without hybrid helices (150 μ M) upon excitation at 340nm -----	56
Figure III-15: Evolution of fluorescence intensity (at 465nm and 376nm) upon addition of PSA in a solution of hybrid helices (150 μ M) upon excitation at 340nm -----	56
Figure III-16: CPL (top) and fluorescence (bottom) of a 30 μ M PSA solution in presence of 150 μ M hybrid helices upon excitation at 340nm -----	57
Figure III-17: CD (top) and absorbance (bottom) of PTCTK solution upon addition of hybrid helices -----	59
Figure III-18: Evolution of the dissymmetry factor at 2 different wavelengths (438nm and 484nm) with the ratio PTCTK to gemini (with [gemini]=100 μ M) -----	59
Figure III-19: Fluorescence spectra of PTCTK in hybrid helices with different ratios upon excitation at 430nm-----	60

Figure III-20: CPL (top) and fluorescence (bottom) spectra of PTCTK in hybrid helices upon excitation at 430nm-----	61
Figure III-21: CD spectra of silica nano-helices before (4) and after (5) POM grafting ⁶² (Reprinted with permission from Attoui, M. et al., Chem. Eur. J. 2018 , 24, 11344-11353. Copyright (2019) Wiley-VCH)-----	63
Figure III-22: Non-aromatic part of the HSQC NMR after making react activated ABA with ethanol-----	64
Figure III-23: TEM image of silica nano-particles after grafting of 9-chloroacridine (120kV / scale bars: 200nm)-----	65
Figure III-24: CD (top) and absorption (bottom) spectra of silica nano-helices grafted by AHA in ethanol-----	65
Figure III-25: Forced dimer of AHA by addition of tartaric acid-----	66
Figure III-26: CD (top) and absorption (bottom) spectra of silica nano-helices grafted by AHA in water with 10 μ M of tartaric acid sodium salt -----	66
Figure III-27: Absorption of PAA alone (50 μ M) and after grafting on the surface of silica nano-helices -----	67
Figure III-28: TEM pictures of right silica nano-helices before and after calcination at 900°C (120kV / scale bars: 50nm)-----	68
Figure III-29: CD (top) and absorption (bottom) spectra of PAA grafted nano-helices. -----	68
Figure III-30: CD (top) and absorption (bottom) spectra of PAA grafted on nano-helices (5mM solution)-----	69
Figure III-31: Fluorescence spectra of PAA grafted on nano-helices upon excitation at 340nm	70
Figure III-32: CD (top) and absorption (bottom) spectra of DPBI-OPh grafted on silica nano-helices -----	71
Figure III-33: The two enantiomers of general asymmetric perylene -----	72
Figure III-34: TEM pictures of left and right handed helices after grafting of DPBI-OPh (5kV / scale bars: 100nm)-----	73

Figure III-35: CPL (top) and fluorescence (bottom) spectroscopy of DPBI-OPh grafted on nano-helices under excitation at 550nm -----	73
Figure III-36: CD (top left), CPL (top right), absorption (bottom left) and fluorescence (bottom right) spectra of DPBI-Cl grafted on silica nano-helices -----	74
Figure III-37: CD (top) and absorbance (bottom) spectra of PTCTK grafted silica nano-helices -----	75
Figure III-38: TEM pictures of left handed helices after PTCTK grafting (5kV / scale bars: 200nm) -----	76
Figure IV-1: CD (top left), CPL (top right), absorbance (bottom left) and fluorescence (bottom right) spectra of a 1mM CSA solution (excitation wavelength for CPL and fluorescence is 291nm) -----	80
Figure IV-2: CD (top) and absorbance (bottom) spectra of CSA (50 μ M) upon addition of hybrid helices (from clear to dark, 21 μ M addition, [Hybrid] _{final} = 168 μ M) -----	81
Figure IV-3: CPL (top) and emission (bottom) spectra of CSA (estimated at 500 μ M) in hybrid helices (1680 μ M) upon excitation at 291nm -----	83
Figure IV-4: CD (top) and absorption (bottom) spectra of solutions containing either CSA (1mM) or hybrid helices (210 μ M) -----	84
Figure IV-5: Effect of the addition of hybrid helices (210 μ M) in CSA solution (1mM), dotted line are the sum of the signals before mixing while solid line are measured spectra -----	84
Figure IV-6: CPL (top) and fluorescence (bottom) spectra of CSA in hybrid helices with synergetic (left) and antagonist (right) enantiomers with raw data in dotted and fit in solid line upon excitation at 291nm -----	85
Figure IV-7: CD (top) and absorption (bottom) spectra of L-PBPA in water after 0, 2 and 6 days -----	87
Figure IV-8: Left: Evolution of the CD signal (top) and absorption (bottom) upon addition of right-handed hybrid helices in a 100 μ M solution of L-PBPA (2 days after mix) / Right: Evolution of the dissymmetry factor depending of the ratio of right-handed helices to L-PBPA at several wavelength -----	88

Figure IV-9: Comparison of CD (top) and absorption (bottom) spectra upon addition of left-handed (blue) or right-handed (red) hybrid helices in a 100 μ M solution of L-PBPA (2 days after mixing)	89
Figure IV-10: CPL (top) and fluorescence (bottom) spectra of L-PBPA with and without hybrid helices ([PBPA]=100 μ M and [gemini]=50 μ M) upon excitation at 470nm	89
Figure IV-11: Fluorescence spectra of N-hydrosuccinimide based carbon dots in water at various excitation wavelength ⁷⁹ and emission wavelength dependency in function of the size of graphitic sheet ⁸⁴ (Reprinted with permission from Stan C. S. et al., <i>J. Matt. Chem. C</i> , 2015 , 3, 789-795 and Sk M. A. et al., <i>J. Matt. Chem. C</i> , 2014 , 2, 6954-6960. Copyright (2019) Royal Society of Chemistry)	91
Figure IV-12: 2D fluorescence spectra of carbon dots formed at 290 $^{\circ}$ C (top) and fluorescence of carbon dots form at various temperatures upon excitation at 350nm (bottom)	92
Figure IV-13: CD (top) and absorption (bottom) spectra of carbon dots form from left (blue) and right (red) handed helices at 290 $^{\circ}$ C	93
Figure IV-14: TEM image of left (A) and right (B) handed helices after formation of carbo dots at 290 $^{\circ}$ C and of the dots after destruction of the silica membrane using NaOH solution (C) (120kV / scale bars : 100nm)	93
Figure IV-15: CD (top) and absorbance (bottom) spectra of hybrid helices before (left) and after (right) graphitization	94
Figure IV-16: CPL (top) and fluorescence (bottom) spectra of carbon dots after graphitization of hybrid helices upon excitation at 330nm	95
Figure IV-17: CD (top left), absorbance (bottom left), CPL (top right) and florescence (bottom right) spectra of carbon dots from hybrid helices after 10min desorption upon excitation at 320nm	96
Figure VI-1: 16-2-16 bromide reaction scheme	104
Figure VI-2: Ion exchange to 16-2-16 acetate	105
Figure VI-3: Ion exchange to 16-2-16 L-tartrate	106

Figure VI-4: Left: Scheme of the aging effect on the formation of nano-structures / Right: TEM picture of nano-helices formed after self-assembling of 16-2-16 D-tartrate using uranyl acetate as contrasting agent (120kV / scale bar: 200nm)-----	107
Figure VI-5: TEOS pre-hydrolysis reaction-----	107
Figure VI-6: Polycondensation reaction, negatively charged part of the molecule interact with gemini part of 16-2-16 tartrate-----	108
Figure VI-7: Synthetic pathway to PTCTK -----	110
Figure VI-8: Synthetic pathway leading to PBPA -----	111
Figure VI-9: Activation of acridanone by POCl ₃ -----	112
Figure VI-10: Nucleophilic substitution leading to ABA-----	113
Figure VI-11: Activation using ethyl chloroformate and reaction with amine group (R is the chromophore and R' is attached to the helix)-----	114
Figure VI-12: Two possible conformations of gemini moiety of 16-2-16-----	115
Figure VI-13: Molecular structure of L (on left) and D (on right) 16-2-16 gemini tartrate with the gemini part in the corresponding conformation. The “backward-Z” and “Z” part are shown in bold red-----	115
Figure VI-14: Schematic representation of multiple bilayer formation in the cases of racemic mixture and enantiopure solution of 16-2-16 tartrate ⁵⁵ -----	116
Figure VI-15: Evolution of the supramolecular morphology of 16-2-16 L-tartrate solution ⁸⁹ --	117

REFERENCES

1. Kelvin, W. T. *Molecular Tactics of a Cristal*. 70 (1894).
2. Petitjean, M. Chirality in metric spaces: In memoriam Michel Deza. *Optim. Lett.* (2017) doi:10.1007/s11590-017-1189-7.
3. Bartik, K., Haouaj, M. E., Luhmer, M., Collet, A. & Reisse, J. Can Monoatomic Xenon Become Chiral? *ChemPhysChem* **1**, 221–224 (2000).
4. Okazaki, Y. *et al.* Induced circular dichroism of monoatomic anions: silica-assisted the transfer of chiral environment from molecular assembled nanohelices to halide ions. *Chem. Commun.* **54**, 10244–10247 (2018).
5. Fresnel, A. Mémoire sur la double réfraction que les rayons lumineux éprouvent en traversant les aiguilles de cristal de roche suivant des directions parallèles à l'axe. in *Oeuvres complètes d'Augustin Fresnel* vol. 1 731–747 (1866).
6. Bailey, J. Circular Polarization in Star- Formation Regions: Implications for Biomolecular Homochirality. *Science* **281**, 672–674 (1998).
7. Chiou, T.-H. *et al.* Circular Polarization Vision in a Stomatopod Crustacean. *Curr. Biol.* **18**, 429–434 (2008).
8. Wynberg, H. *et al.* Circular polarization observed in bioluminescence. *Nature* **286**, 641 (1980).
9. Cross, L. C. & Klyne, W. IUPAC Commission on Nomenclature of Organic Chemistry. in *Rules for the Nomenclature of Organic Chemistry* 13–30 (Elsevier, 1976). doi:10.1016/B978-0-08-021019-3.50003-1.
10. Cahn, R. S., Ingold, C. & Prelog, V. Specification of Molecular Chirality. *Angew. Chem. Int. Edit.* **5**, 385–415 (1966).
11. Allenmark, S. Induced circular dichroism by chiral molecular interaction. *Chirality* **15**, 409–422 (2003).

12. Kikuchi, Y., Kobayashi, K. & Aoyama, Y. Molecular recognition. 18. Complexation of chiral glycols, steroidal polyols, and sugars with a multibenzenoid, achiral host as studied by induced circular dichroism spectroscopy: exciton chirality induction in resorcinol-aldehyde cyclotetramer and its use as a supramolecular probe for the assignments of stereochemistry of chiral guests. *J. Am. Chem. Soc.* **114**, 1351–1358 (1992).
13. Mizutani, T., Takagi, H., Hara, O., Horiguchi, T. & Ogoshi, H. Axial chirality induction in flexible biphenols by hydrogen bonding and steric interactions. *Tetrahedron Lett.* **38**, 1991–1994 (1997).
14. Kamboj, S., Saini, V., Magon, N., Bala, S. & Jhawar, V. Vesicular drug delivery systems: A novel approach for drug targeting. *IJDD* **5**, 121–130 (2013).
15. Ratner, B. D. & Bryant, S. J. Biomaterials: Where We Have Been and Where We Are Going. *Annu. Rev. Biomed. Eng.* **6**, 41–75 (2004).
16. Kawasaki, T., Tokunishi, M., Kimizuka, N. & Kunitake, T. Hierarchical Self-Assembly of Chiral Complementary Hydrogen-Bond Networks in Water: Reconstitution of Supramolecular Membranes. *J. Am. Chem. Soc.* **123**, 6792–6800 (2001).
17. Fuhrhop, J. H., Schnieder, P., Rosenberg, J. & Boekema, E. The chiral bilayer effect stabilizes micellar fibers. *J. Am. Chem. Soc.* **109**, 3387–3390 (1987).
18. Nakashima, N., Asakuma, S. & Kunitake, T. Optical microscopic study of helical superstructures of chiral bilayer membranes. *J. Am. Chem. Soc.* **107**, 509–510 (1985).
19. Ihara, H., Takafuji, M., Hirayama, C. & O'Brien, D. F. Effect of photopolymerization on the morphology of helical supramolecular assemblies. *Langmuir* **8**, 1548–1553 (1992).
20. Okazaki, Y., Jintoku, H., Takafuji, M., Oda, R. & Ihara, H. Creation of a polymer backbone in lipid bilayer membrane-based nanotubes for morphological and microenvironmental stabilization. *RSC Adv.* **4**, 33194–33197 (2014).

21. Beinert, H., Kennedy, M. C. & Stout, C. D. Aconitase as Iron–Sulfur Protein, Enzyme, and Iron-Regulatory Protein. *Chem. Rev.* **96**, 2335–2374 (1996).
22. Lloyd, S. J., Lauble, H., Prasad, G. S. & Stout, C. D. The mechanism of aconitase: 1.8 Å resolution crystal structure of the S642A:citrate complex. *Protein Sci.* **8**, 2655–2662 (1999).
23. Schoonheydt, R., Johnston, C. T. & Bergaya, F. *Surface and Interface Chemistry of Clay Minerals*. (Elsevier, 2018).
24. Fraser, D. G., Fitz, D., Jakschitz, T. & Rode, B. M. Selective adsorption and chiral amplification of amino acids in vermiculite clay-implications for the origin of biochirality. *Phys. Chem. Chem. Phys.* **13**, 831–838 (2011).
25. Klán, P. & Wirz, J. *Photochemistry of Organic Compounds*. (John Wiley & Sons, Ltd, 2009). doi:10.1002/9781444300017.
26. Porrès, L. *et al.* Absolute Measurements of Photoluminescence Quantum Yields of Solutions Using an Integrating Sphere. *J. Fluoresc.* **16**, 267–273 (2006).
27. Herschel, J. F. W. On a Case of Superficial Colour presented by an homogeneous liquid internally colourless. *Royal Society* **135**, 143–145 (1845).
28. Kasha, M. Characterization of electronic transitions in complex molecules. *Discuss. Faraday Soc.* **9**, 14 (1950).
29. Boudin, S. Phosphorescence des solutions glycériques d'éosine influence des iodures. *J. Chim. Phys.* **27**, 285–290 (1930).
30. Mukherjee, S. & Thilagar, P. Recent advances in purely organic phosphorescent materials. *Chem. Commun.* **51**, 10988–11003 (2015).
31. Würthner, F., Kaiser, T. E. & Saha-Möller, C. R. J-Aggregates: From Serendipitous Discovery to Supramolecular Engineering of Functional Dye Materials. *Angew. Chem. Int. Edit.* **50**, 3376–3410 (2011).

32. Franck, J. & Teller, E. Migration and Photochemical Action of Excitation Energy in Crystals. *J. Chem. Phys.* **6**, 861–872 (1938).
33. Condon, E. U. Theories of Optical Rotatory Power. *Rev. Mod. Phys.* **9**, 432–457 (1937).
34. Naaman, R., Autschbach, J. & Waldeck, D. *Electronic and magnetic properties of chiral molecules and supramolecular architectures*. (Springer, 2011).
35. Riehl, J. P. Circularly Polarized Luminescence Spectroscopy. *Chem. Rev.* **86**, 16 (1986).
36. Imai, Y. *et al.* Control of circularly polarized luminescence (CPL) properties by supramolecular complexation. *New J. Chem.* **32**, 1110 (2008).
37. Li, H. *et al.* Aggregation-induced chirality, circularly polarized luminescence, and helical self-assembly of a leucine-containing AIE luminogen. *J. Mater. Chem. C* **3**, 2399–2404 (2015).
38. Nakamura, M., Ota, F., Takada, T., Akagi, K. & Yamana, K. Circularly polarized luminescence of helically assembled pyrene π -stacks on RNA and DNA duplexes. *Chirality* **30**, 602–608 (2018).
39. Jiang, Q. *et al.* Circularly Polarized Luminescence of Achiral Cyanine Molecules Assembled on DNA Templates. *J. Am. Chem. Soc.* **141**, 9490–9494 (2019).
40. Oda, R., Huc, I., Schmutz, M., Candau, S. J. & MacKintosh, F. C. Tuning bilayer twist using chiral counterions. *Nature* **399**, 4 (1999).
41. Ryu, N. *et al.* Memorized chiral arrangement of gemini surfactant assemblies in nanometric hybrid organic–silica helices. *Chem. Commun.* **52**, 5800–5803 (2016).
42. Cheng, J. *et al.* GoldHelix: Gold Nanoparticles Forming 3D Helical Superstructures with Controlled Morphology and Strong Chiroptical Property. *ACS Nano* **11**, 3806–3818 (2017).
43. Kumar, J., Tsumatori, H., Yuasa, J., Kawai, T. & Nakashima, T. Self-Discriminating Termination of Chiral Supramolecular Polymerization: Tuning the Length of Nanofibers. *Angew. Chem. Int. Edit.* **54**, 5943–5947 (2015).

44. Okazaki, Y. *et al.* Facile and Versatile Approach for Generating Circularly Polarized Luminescence by Non-chiral, Low-molecular Dye-on-nanotemplate Composite System. *Chem. Lett.* **45**, 448–450 (2016).
45. Oda, R., Huc, I. & Candau, S. J. Gemini surfactants, the effect of hydrophobic chain length and dissymmetry. *Chem. Commun.* 2105–2106 (1997) doi:10.1039/a704069e.
46. Sugiyasu, K. *et al.* Double helical silica fibrils by sol–gel transcription of chiral aggregates of gemini surfactants. *Chem. Commun.* 1212–1213 (2002) doi:10.1039/b202799m.
47. Ono, Y. *et al.* Organic gels are useful as a template for the preparation of hollow fiber silica. *Chem. Commun.* 1477–1478 (1998) doi:10.1039/a802829j.
48. Okazaki, Y. *et al.* Chiral Colloids: Homogeneous Suspension of Individualized SiO₂ Helical and Twisted Nanoribbons. *ACS Nano* **8**, 6863–6872 (2014).
49. Osswald, P. & Würthner, F. Effects of Bay Substituents on the Racemization Barriers of Perylene Bisimides: Resolution of Atropo-Enantiomers. *J. Am. Chem. Soc.* **129**, 14319–14326 (2007).
50. Chen, W. *et al.* Water-induced formation of a chiral phenylalanine derivative supramolecule. *Phys. Chem. Chem. Phys.* **20**, 4144–4148 (2018).
51. Crucho, C. I. C., Baleizão, C. & Farinha, J. P. S. Functional Group Coverage and Conversion Quantification in Nanostructured Silica by ¹H NMR. *Anal. Chem.* **89**, 681–687 (2017).
52. Berova, N., Nakanishi, K. & Woody, R. *Circular Dichroism. Principles and Applications 2nd Edition.* (2000).
53. Han, J. *et al.* Enhanced Circularly Polarized Luminescence in Emissive Charge-Transfer Complexes. *Angew. Chem. Int. Edit.* **58**, 7013–7019 (2019).
54. Sugimoto, M. *et al.* Circularly Polarized Luminescence from Inorganic Materials: Encapsulating Guest Lanthanide Oxides in Chiral Silica Hosts. *Chem. Eur. J.* **24**, 6519–6524 (2018).

55. Oda, R., Artzner, F., Laguerre, M. & Huc, I. Molecular Structure of Self-Assembled Chiral Nanoribbons and Nanotubules Revealed in the Hydrated State. *J. Am. Chem. Soc.* **130**, 14705–14712 (2008).
56. Metcalf, D. H., Ghirardelli, R. G. & Palmer, R. A. Crown ether-lanthanide complexes studied using CPL and TL. I. The solution stoichiometry of europium and terbium nitrate complexes of (2R,3R,11R,12R)-2,3,11,12-tetramethyl-18-crown-6. *Inorg. Chem.* **24**, 634–636 (1985).
57. Flink, S., van Veggel, F. C. J. M. & Reinhoudt, D. N. Functionalization of self-assembled monolayers on glass and oxidized silicon wafers by surface reactions. *J. Phys. Org. Chem.* **14**, 407–415 (2001).
58. Asenath Smith, E. & Chen, W. How To Prevent the Loss of Surface Functionality Derived from Aminosilanes. *Langmuir* **24**, 12405–12409 (2008).
59. Prathap Chandran, S., Hotha, S. & Blv, P. Tunable surface modification of silica nanoparticles through ‘click’ chemistry. *Curr. Sci. India* **95**, (2008).
60. Price, M. B. *et al.* Inter-ligand energy transfer in dye chromophores attached to high bandgap SiO₂ nanoparticles. *Chem. Commun.* **55**, 8804–8807 (2019).
61. Gorman, J. *et al.* Excimer Formation in Carboxylic Acid-Functionalized Perylene Diimides Attached to Silicon Dioxide Nanoparticles. *J. Phys. Chem. C* **123**, 3433–3440 (2019).
62. Attoui, M. *et al.* Optically Active Polyoxometalate-Based Silica Nanohelices: Induced Chirality from Inorganic Nanohelices to Achiral POM Clusters. *Chem. Eur. J.* (2018) doi:10.1002/chem.201801905.
63. Banfi, D. & Patiny, L. *www.nmrdb.org*: Resurrecting and Processing NMR Spectra On-line. *CHIMIA* **62**, 280–281 (2008).
64. Castillo, A. M., Patiny, L. & Wist, J. Fast and accurate algorithm for the simulation of NMR spectra of large spin systems. *J. Magn. Reson.* **209**, 123–130 (2011).

65. Okazaki, Y. *et al.* Direct Observation of Siloxane Chirality on Twisted and Helical Nanometric Amorphous Silica. *Nano Lett.* **16**, 6411–6415 (2016).
66. Yagai, S. Supramolecularly Engineered Functional π -Assemblies Based on Complementary Hydrogen-Bonding Interactions. *BCSJ* **88**, 28–58 (2015).
67. Finlayson, C. E. *et al.* Electronic Transport Properties of Ensembles of Perylene-Substituted Polyisocyanopeptide Arrays. *Adv. Funct. Mater.* **18**, 3947–3955 (2008).
68. Würthner, F. *et al.* Perylene Bisimide Dye Assemblies as Archetype Functional Supramolecular Materials. *Chem. Rev.* **116**, 962–1052 (2016).
69. Kuronuma, M. *et al.* Transient Circular Dichroism Measurement of the Excited Triplet State of Pristine Hexahelicene in Solution at Room Temperature. *Chem. Lett.* **48**, 357–360 (2019).
70. Sánchez-Carnerero, E. M. *et al.* Circularly Polarized Luminescence from Simple Organic Molecules. *Chem. Eur. J.* **21**, 13488–13500 (2015).
71. Zinna, F. *et al.* Circularly polarized luminescence under near-UV excitation and structural elucidation of a Eu complex. *Chem. Commun.* **51**, 11903–11906 (2015).
72. Harada, T. *et al.* Nona-Coordinated Chiral Eu(III) Complexes with Stereoselective Ligand–Ligand Noncovalent Interactions for Enhanced Circularly Polarized Luminescence. *Inorg. Chem.* **51**, 6476–6485 (2012).
73. Huo, S., Duan, P., Jiao, T., Peng, Q. & Liu, M. Self-Assembled Luminescent Quantum Dots To Generate Full-Color and White Circularly Polarized Light. *Angew. Chem. Int. Edit.* **56**, 12174–12178 (2017).
74. Yang, D., Duan, P., Zhang, L. & Liu, M. Chirality and energy transfer amplified circularly polarized luminescence in composite nanohelix. *Nat. Commun.* **8**, 15727 (2017).
75. Longhi, G., Castiglioni, E., Abbate, S., Lebon, F. & Lightner, D. A. Experimental and Calculated CPL Spectra and Related Spectroscopic Data of Camphor and Other Simple Chiral Bicyclic

- Ketones: EXPERIMENTAL AND CALCULATED CD AND CPL SPECTRA OF BICYCLIC KETONES. *Chirality* **25**, 589–599 (2013).
76. Ma, Y. *et al.* Synthesis and properties of amino acid functionalized water-soluble perylene diimides. *Korean J. Chem. Eng.* **32**, 1427–1433 (2015).
77. Farooqi, M. J., Penick, M. A., Burch, J., Negrete, G. R. & Brancaleon, L. Characterization of novel perylene diimides containing aromatic amino acid side chains. *Spectroc. Acta A* **153**, 124–131 (2016).
78. Das, P., Ganguly, S., Banerjee, S. & Das, N. C. Graphene based emergent nanolights: a short review on the synthesis, properties and application. *Res. Chem. Intermediat.* **45**, 3823–3853 (2019).
79. Stan, C. S., Albu, C., Coroaba, A., Popa, M. & Sutiman, D. One step synthesis of fluorescent carbon dots through pyrolysis of N-hydroxysuccinimide. *J. Mater. Chem. C* **3**, 789–795 (2015).
80. Choi, Y. *et al.* Microwave-assisted synthesis of luminescent and biocompatible lysine-based carbon quantum dots. *J. Ind. Eng. Chem.* **47**, 329–335 (2017).
81. Wang, D. *et al.* Fluorescent carbon dots from milk by microwave cooking. *RSC Adv.* **6**, 41516–41521 (2016).
82. Shen, J., Zhu, Y., Chen, C., Yang, X. & Li, C. Facile preparation and upconversion luminescence of graphene quantum dots. *Chem. Commun.* **3** (2011).
83. Lu, W. *et al.* Comparative study for N and S doped carbon dots: Synthesis, characterization and applications for Fe³⁺ probe and cellular imaging. *Anal. Chim. Acta* **898**, 116–127 (2015).
84. Sk, M. A., Ananthanarayanan, A., Huang, L., Lim, K. H. & Chen, P. Revealing the tunable photoluminescence properties of graphene quantum dots. *J. Mater. Chem. C* **2**, 6954–6960 (2014).
85. Wei, Y. *et al.* Investigation on the chirality mechanism of chiral carbon quantum dots derived from tryptophan. *RSC Adv.* **9**, 3208–3214 (2019).

86. Hu, L. *et al.* Chiral evolution of carbon dots and the tuning of laccase activity. *Nanoscale* **10**, 2333–2340 (2018).
87. Suzuki, N. *et al.* Chiral Graphene Quantum Dots. *ACS Nano* **10**, 1744–1755 (2016).
88. Zou, C. *et al.* Bacterial Cellulose: A Versatile Chiral Host for Circularly Polarized Luminescence. *Molecules* **24**, 1008 (2019).
89. Brizard, A. *et al.* Counterion, Temperature, and Time Modulation of Nanometric Chiral Ribbons from Gemini-Tartrate Amphiphiles. *J. Am. Chem. Soc.* **129**, 3754–3762 (2007).

In the field of nano-science, chiral materials attract increasing attention due to their wide possibilities of application. Among these, the interaction between light and matter is closely followed as it may lead to new technological developments. Numerous studies have focused on chiral chromophore aggregates endowed with chiroptical properties, including circular dichroism and circularly polarized light (CPL). However, these systems are strongly dependent of their environment, and often need long synthesis with difficult purification steps. In this project, we investigated the possibility to impose the aggregation of chromophores into chiral hybrid nanostructures or on the surface of chiral silica helices. The nano-objects obtained show induction of the chirality from the host to the non-chiral chromophore as demonstrated by the appearance of chiroptical properties. The structures thus obtained can resist to different environments without significant change on their morphology. Additionally, chiroptical properties of chiral chromophores were modified upon their containment in helical nanostructures. Finally, the hybrid nano-helices incorporating organic amphiphiles were used as chiral reactors for the production of carbon based quantum dots possessing chiroptical properties.

Keywords: Circularly polarized luminescence, Chirality induction, Supramolecular chemistry, Nano-objects

Dans le domaine des nano-sciences, les matériaux chiraux attirent attention grandissante due à leur large champ d'applications, au sein desquelles se trouve la création de nouvelles technologies. Des études se sont déjà concentrées sur l'agrégation chirale de pigments pour leur conférer des propriétés chiro-optiques dont, dichroïsme circulaire et la luminescence circulairement polarisée (CPL). Cependant ces systèmes sont fortement dépendants de leur environnement, et nécessitent généralement de longues synthèses ainsi que des étapes purifications complexes. Dans ce projet, nous avons étudié la possibilité d'imposer une agrégation chirale des pigments au sein des nanostructures hybrides ou à la surface de nano-hélices de silice. Les nano-objets obtenus montrent une induction de chiralité, depuis les structures aux chromophores non-chiraux, par l'apparition de propriétés chiro-optiques. De plus, ces matériaux peuvent résister à différents environnements sans changement notable de leur morphologie. Les propriétés chiro-optiques de chromophores chiraux ont également été ajustées via leur confinement au sein des nano-structures hélicoïdales. Enfin, les nano-hélices hybrides contenant des amphiphiles organiques ont été utilisées en tant que réacteurs chiraux pour la production de quantum-dots à base carbonée possédant des propriétés chiro-optiques.

Mots-clés : Luminescence circulairement polarisée, Induction de chiralité, Chimie supramoléculaire, Nano-objets